

Investigation of MoS₂ Nanosheets in supercapacitor & Nanofluid applications

*A thesis submitted towards the partial fulfillment
of the requirements for the degree of*

**Master of Technology in
Nano Science and Technology**

Submitted by

SUMIT KUMAR BERA

ROLLNO: M4NST19004

Under the guidance of

**Prof. Kalyan Kumar Chattopadhyay
SCHOOL OF MATERIALS SCIENCE AND NANOTECHNOLOGY
Jadavpur University
Kolkata-700032**

Course affiliated to
**Faculty of Engineering and Technology
Jadavpur University
Kolkata-700032,
India,2018**

Mtech in nanoscience and technology

Course affiliated to
Faculty of Engineering and Technology

Jadavpur University

Certificate of Recommendation

This is to certify that the thesis entitled “**Investigation of MoS₂ Nanosheets in supercapacitor & Nanofluid applications**” has been carried out under our guidance by *Sumit Kumar Bera* during the academic session **2017–19** in partial fulfillment of requirements for the award of degree of *Master of Technology in Nano Science and Technology at School of Material Science and Nanotechnology*, Jadavpur University, Kolkata- 700032. In our opinion the work fulfills the requirement for which it is submitted.

It is further certified that the materials obtained from other sources have been acknowledged in the thesis.

Prof. Chandan Kumar Ghosh
Director
School of Materials Science and Nanotechnology
Jadavpur University,
Kolkata-700 032

THESIS ADVISOR
Prof. Kalyan Kumar Chattopadhyay
School of Materials Science and Nanotechnology
Jadavpur University,
Kolkata-700 032

DEAN
Faculty Council of Interdisciplinary Studies, Law and Management
Jadavpur University,
Kolkata-700 032

Mtech in nanoscience and technology

**Course affiliated to
Faculty of Engineering and Technology**

Jadavpur University

Certificate of Approval

The forgoing thesis is hereby approved as credible study of an engineering subject carried out and represented in a manner satisfactorily to warrant its acceptance as a prerequisite to the degree for which it has been submitted.

It is to be understood that by this approval the undersigned does not necessarily endorse or approve any statement made, opinion expressed or conclusion drawn therein but approved the thesis only for the purpose for which it has been submitted.

**Final Examiners for
Evaluation of thesis**

Signature of the Examiners

1. _____

2. _____

3. _____

Date _____

Dedicated
to
My beloved Parents
and
Family

Declaration of originality and compliance of academic ethics

I hereby declare that this thesis contains literature survey and original research work by the undersigned candidate, as a part of M.Tech degree. All information in this document have been obtained and presented in accordance with the academic rules and ethical conduct. I also declare that, as required by these rules and conduct, I have fully cited and referenced all materials and results that are not original to this work.

Name: SUMIT KUMAR BERA

Roll No: M4NST19004

Thesis Title: Investigation of MoS₂ Nanosheets in supercapacitor & Nanofluid applications

Date:

Signature

Acknowledgements

The work described in this thesis entitled “**Investigation of MoS₂ Nanosheets in supercapacitor & Nanofluid applications**” was started in the Thin Film & Nanoscience Laboratory, Jadavpur University in June 2018 and would not have been what it is today without the support and advice of others.

First of all, I would like to thank from deep inside of my heart to **Prof. Kalyan Kumar Chattopadhyay** for the opportunity he has given me to work in his research group to perform the above mentioned work. His ideas and guidance have been invaluable. His father like affection and immense faith on his students is what makes him unique from any other professors. His kindness and simplicity is unforgettable. I am also very grateful for the autonomy of decision I was provided during my research work in his laboratory.

I also pay my sincere thanks to Dr. M. G. Chowdhury, Prof. G. C. Das and Prof. C. K. Ghosh, Dr. Sourav Sarkar for their encouragement during the course.

I extend my heartiest thanks to Suvankar Da, Koushik Sardar Da, Koushik Chanda Da, Subhasish Da, Saikat Da, Nripen Da, Tufan Da, Antika Di, Missi Di and other lab mates for extending their helping hands to me and making my project a really fulfilling experience.

Pratik, Pulok, Debnath, Sourav, Ankit, Ankita and all other batch mates you all have given the mental support and helped a lot to inculcate my knowledge in several fields of my project.

Finally, I would like to express my whole-hearted thanks to **Karamjyoti Da and dipayan da** who are guided me from the very first day as his Brother. They were always there to encourage and give me a clear vision of the project. Theirs simplicity and kindness touched my heart. Without theirs full support, I would not have completed my whole work so easily. they are my deepest gratitude.

Last but not the least, I would like to express my gratitude to my family members who are always with me in every situation. Their presence provides me courage to overcome all the obstacles in my path to achieve the desired success.

ABSTRACT

Molybdenum di-sulfide (MoS_2), a layered transition metal dichalcogenide with an analogous structure to graphene, has attracted enormous attention worldwide owing to its use in a variety of applications such as energy storage, energy conversion, environmental remediation and sensors. MoS_2 and graphene have almost similar functional properties such as high charge carrier transport, high wear resistance and good mechanical strength and friction. However, MoS_2 is advantageous over graphene due to its low-cost, abundance, tailorable morphologies and tuneable band gap with good visible light absorption properties. Among the various morphologies particularly sheet morphology attracts great attention due its 2D nature with enhanced surface area which plays a significant role in the electrochemistry. Nevertheless, the sheet also considered to be highly effective for transformer oil (TO) based nanofluid applications. Keeping these above-mentioned advantages in this work at first by a facile hydrothermal technique using bottom up approach MoS_2 nanosheets were synthesized. X-ray diffraction and RAMAN confirms the formation of Nanosheets by stacking layers. Further High-resolution Transmission electron microscope (HRTEM) image confirms the formation of ultrathin nanosheets. The synthesized nanosheets the electrode material attains a specific capacitance of 265.67 F/g at 2 mV/s scan rate ($968. \text{mF}/\text{cm}^2$) and 482.43 F/g at 1 A/g current density. The obtained high value was attributed to the sheet like morphology which enhance the interaction with the electrolyte ions. Especially for MoS_2 have superior electrochemical properties, making them promising electrode materials for practical applications like symmetric/asymmetric supercapacitor devices. Additionally, the synthesized MoS_2 nanosheets also used to prepare TO based nanofluids. The calculated breakdown voltage enhancement was around 5.32% in the weight percentage (wt%) 0.005%. It drops down to 1.6 % enhancement when the wt% reaches to 0.0075 due to self-agglomeration among the sheets which increases the charge movement rate leading to reduction of breakdown voltage. Moreover, the thermal conductivity value increases up to 17.55% at 40°C in the same Wt%. 0.005 due to high surface area of the filler. Besides, the efficiency of the sheets is further validated by performance in Ethylene Glycol (EG) which vividly used as coolant. In case of EG the observed enhancement was 25.53% at wt% 0.0075. The above indicated result proves the efficiency of the 2D morphology of layered transition metal dichalcogenide in multifunctional applications.

Contents

- **Title Page**
- **Certificate by the Supervisors**
- **Certificate of Approval**
- **Declaration**
- **Acknowledgement**
- **Abstract**
- **Contents**

Chapter 1: Introduction to Nanotechnology 1-25

1.1. Nano Science & Technology.....

1.2. A Brief History of Nanotechnology.....

1.3. Synthesis of Nano Materials

1.4. Current Applications of Nanotechnology

1.5.Future uses of Nano Technology.....

1.6.The Perils & Risks of Nanotechnology.....

References.....

Chapter 2: Overview of Supercapacitors And Nanofluids.....26-51

2.1. Introduction of Supercapacitor.....

2.2. Background of Supercapacitor

2.3. Classification of Supercapacitor.....

2.4. The Electrolytes.....

2.5 Application of Supercapacitor

2.6 Over view of Nanofluids.....

References.....

Chapter 3: Review of Past Works..... 52-71

3.1. Introduction.....

3.2. Literature Review of Past works.....
References.....

Chapter 4: Instruments and Apparatus 72-96

4.1. X-Ray Diffraction.....
4.2. Field Emission Scanning Electron Microscope (FESEM).....
4.3. Raman Spectroscopy.....
4.4. Cyclic Voltammetry
4.5. UV-Spectroscopy.....
4.6. TEM
4.7. XPS.....

Chapter-5: Synthesis and Electrochemical studies of sheet like MOS₂ Nanostructures for Potential Application in Supercapacitors.....97-112

5.1. Introduction
5.2. Sample preparation.....
5.3. Characterization.....
5.4. Result and discussion.....
5.5. conclusion.....
References.....

Chapter 6: Synthesis and studies of sheet like MOS₂ Nanostructures for Application in nanofluid.....113-123

6.1. Introduction.....
6.2. Experimental details.....
6.3. Characterization.....
6.4. Result and Discussion.....
6.5. Conclusion.....
6.6. Reference.....

Chapter 7: Final Conclusion & Future Scope.....124-125

Chapter-1:

Introduction to Nanotechnology



1.1 INTRODUCTION TO NANOTECHNOLOGY:

1.1.1. What is Nanotechnology?

Nanotechnology is science, engineering, and technology conducted at the nanoscale, which is about 1 to 100 nanometers. Nanoscience and nanotechnology are the study and application of extremely small things and can be used across all the other science fields, such as chemistry, biology, physics, materials science, and engineering.

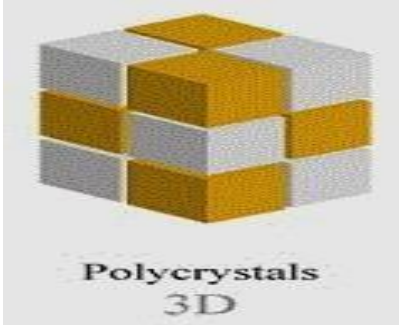
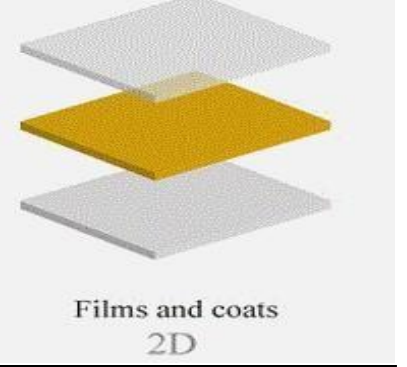
On Dec. 29, 1959, at the California Institute of Technology, Nobel Laureate Richard P. Feynman gave a talk at the annual meeting of the American Physical Society that has become one of the twentieth century's classic science lectures, titled "There's Plenty of Room at the Bottom". He presented a technological vision of extreme miniaturization several years before the word "chip" became part of the lexicon. He talked about the problem of manipulating and controlling things on a small scale. Extrapolating from known physical laws, Feynman envisioned a technology using the ultimate toolbox of nature, building nano objects atom by atom or molecule by molecule.

Nanotechnology literally means any technology performed on a nanoscale that has applications in the real world. It's one billionth of meter or 10^{-9} m. The word "nanoscience" itself is a combination of nano, from the Greek "Nanos" (or Latin "nanus"), meaning "Dwarf", and the word "Science" meaning knowledge. Our naked eyes can see up to 75-80 μm , we are unable to see anything in nano range without any microscope. Nanotechnology is explained by a wide spectrum of various technologies which are based on various physical, chemical, biological processes realized on nano level. Nanotechnology is likely to have a profound impact on our economy and society in the early twenty-first century, comparable to that of semiconductor technology, information technology, or cellular and molecular biology. Science and technology research in nanotechnology promises breakthroughs in such areas as materials and manufacturing, nanoelectronics, medicine and healthcare, energy, biotechnology, information technology, and national security[1-4].

1.1.2. What is a Nanomaterial?

A nanomaterial is an object that has at least one dimension in the nanometre scale (approximately 1-100nm). Nanomaterials are categorized according to their dimensions as shown in **Table1.1**.

A very important concept is to distinctly specify “**the smallness of nano**”. Nanomaterials are larger than single atoms but smaller than bacteria and cells. It uses a scale like that shown in **Fig.1.1** which can easily explain the relationship between bulk materials, like a tennis ball, and nanomaterials.

Nanomaterial Dimension	Nanomaterial Type	Example
All three dimensions < 100nm	Nanoparticles, Quantum dots, nanoshells, nanorings, microcapsules	 <p>Polycrystals 3D</p>
Two dimensions < 100 nm	Thin films, layers and coatings	 <p>Films and coats 2D</p>

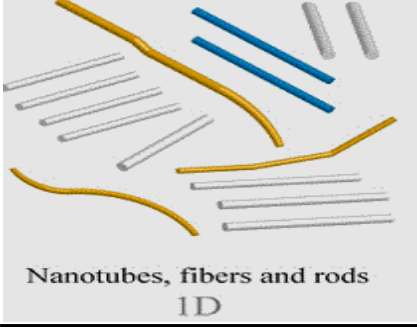
One dimension < 100nm	Nanotubes, nanofibres, nanowires	 <p>Nanotubes, fibers and rods 1D</p>
-----------------------	----------------------------------	--

Table 1.1: Classification of Nano-materials According to the Dimensions

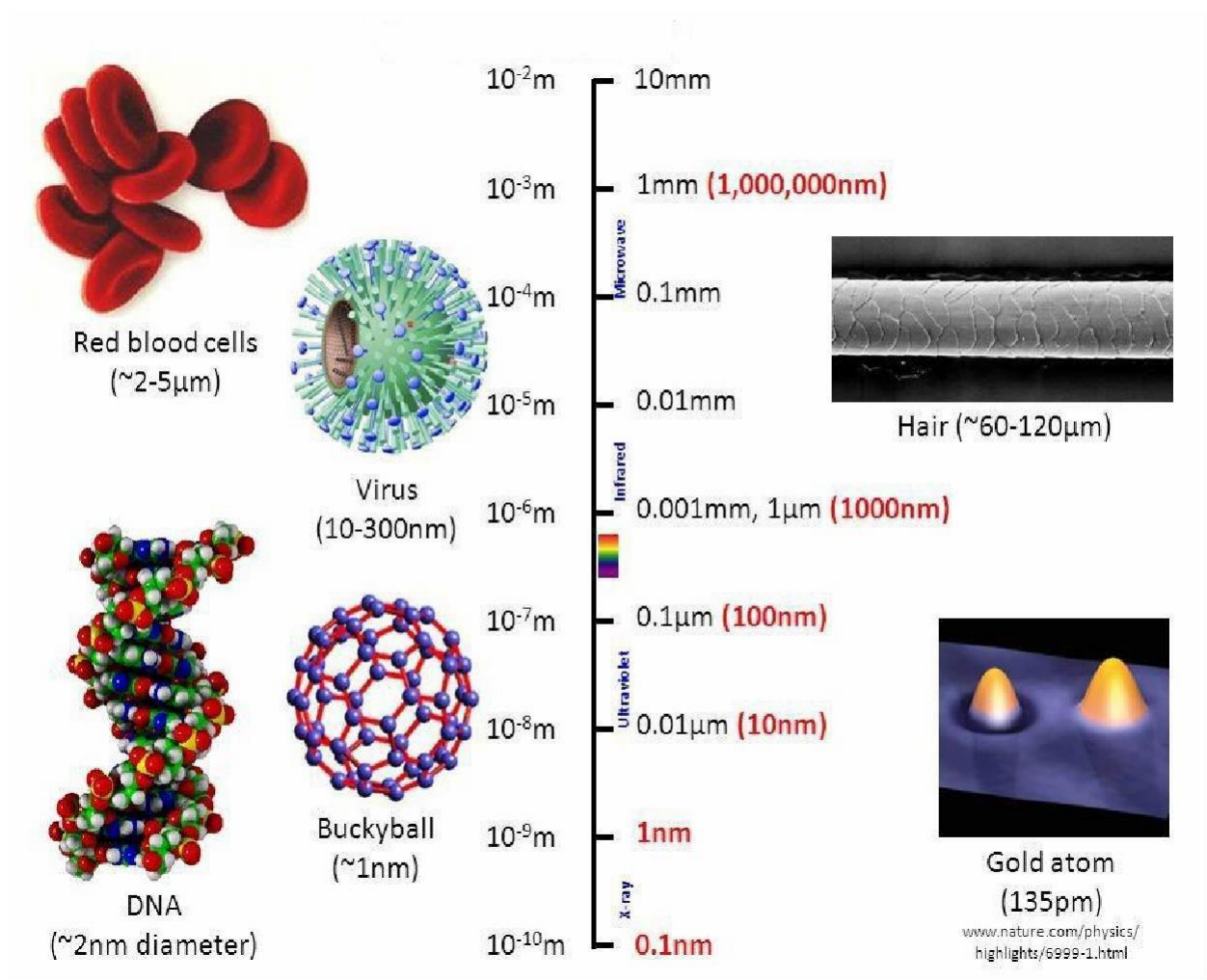


Fig.1.1: From macro-materials to atoms. Nanomaterials and Nano devices that are of interest in nanotechnologies are in the lower end of the scale (1-100nm). (Image credit: adopted from: —A snapshot of nanotechnology, National Cancer Institute)

Some noticeable examples of the nano regime:

- Our **finger nails** grow at the rate of **1nm per second**.
- The **head of a pin** is about **1 million nanometers** across.
- A **human hair** is about **80,000 nm** in diameter.
- A **red blood cell** is **2,500 nanometers**
- A **DNA molecule** is about **1-2 nm** wide.
- The **transistor** of a last-generation Pentium Core Duo Processor is **45nm**.

1.1.3 What Makes “nano” Special:

Nanoscale particles are not new in either nature or science. However, the recent leaps in areas such as microscopy have given scientists new tools to understand and take advantage of phenomena that occur naturally when matter is organized at the nanoscale. In essence, these phenomena are based on "quantum effects" and other simple physical effects such as expanded surface area (more on these below). In addition, the fact that a majority of biological processes occur at the nanoscale gives scientists models and templates to imagine and construct new processes that can enhance their work in medicine, imaging, computing, printing, chemical catalysis, materials synthesis, and many other fields. Nanotechnology is not simply working at ever smaller dimensions; rather, working at the nanoscale enables scientists to utilize the unique physical, chemical, mechanical, and optical properties of materials that naturally occur at that scale.

Scale at which Quantum Effect Dominate Properties Of Materials:

When particle sizes of solid matter in the visible scale are compared to what can be seen in a regular optical microscope, there is little difference in the properties of the particles. But when particles are created with dimensions of about 1–100 nanometers (where the particles can be seen only with powerful specialized microscopes), the materials' properties change significantly from those at larger scales. This is the size scale where so-called quantum effects

rule the behavior and properties of particles. Properties of materials are size-dependent in this scale range. Thus, when particle size is made to be nanoscale, properties such as melting point, fluorescence, electrical conductivity, magnetic permeability, and chemical reactivity change as a function of the size of the particle.

Nanoscale gold illustrates the unique properties that occur at the nanoscale. Nanoscale gold particles are not the yellow color with which we are familiar; nanoscale gold can appear red or purple. At the nanoscale, the motion of the gold's electrons is confined. Because this movement is restricted, gold nanoparticles react differently with light compared to larger-scale gold particles. Their size and optical properties can be put to practical use: nanoscale gold particles selectively accumulate in tumors, where they can enable both precise imaging and targeted laser destruction of the tumor by means that avoid harming healthy cells.

A fascinating and powerful result of the quantum effects of the nanoscale is the concept of tunability of properties. That is, by changing the size of the particle, a scientist can literally fine-tune a material property of interest (e.g., changing fluorescence color; in turn, the fluorescence color of a particle can be used to identify the particle, and various materials can be labeled with

fluorescent markers for various purposes). Another potent quantum effect of the nanoscale is known as tunneling, which is a phenomenon that enables the scanning tunneling microscope and flash memory for computing.

Scale at Which Much of Biology Occurs:

Over millennia, nature has perfected the art of biology at the nanoscale. Many of the inner workings of cells naturally occur at the nanoscale. For example, hemoglobin, the protein that



Fig.1.2: Computer simulation of electron motions within a nanowire that has a diameter in the nanoscale range. (Image: NSF multimedia/ Eric Heller Gallery)

carries oxygen through the body, is 5.5 nanometers in diameter. A strand of DNA, one of the building blocks of human life, is only about 2 nanometers in diameter.

Drawing on the natural nanoscale of biology, many medical researchers are working on designing tools, treatments, and therapies that are more precise and personalized than conventional ones and that can be applied earlier in the course of a disease and lead to fewer adverse side-effects. One medical example of nanotechnology is the bio-barcode assay, a relatively low-cost method of detecting disease-specific biomarkers in the blood, even when there are very few of them in a sample. The basic process, which attaches -recognition particles and DNA amplifiers to gold nanoparticles, was originally demonstrated at Northwestern University for a prostate cancer biomarker following prostatectomy. The bio-barcode assay has proven to be considerably more sensitive than conventional assays for the same target biomarkers, and it can be adapted to detect almost any molecular target.

Growing understanding of nanoscale biomolecular structures is impacting other fields than medicine. Some scientists are looking at ways to use nanoscale biological principles of molecular self-assembly, self-organization, and quantum mechanics to create novel computing platforms. Other researchers have discovered that in photosynthesis, the energy that plants harvest from sunlight is nearly instantly transferred to plant reaction centers by quantum mechanical processes with nearly 100% efficiency (little energy wasted as heat). They are investigating photosynthesis as a model for green energy nanosystems for inexpensive production and storage of nonpolluting solar power.

Scale at Which Surfaces and Interfaces Play a Large Role in Materials Properties and Interactions:

Nanoscale materials have far larger surface areas than similar masses of larger-scale materials. As surface area per mass of a material increases, a greater amount of the material can come into contact with surrounding materials, thus affecting reactivity.

A simple thought experiment shows why nanoparticles have phenomenally high surface areas. A solid cube of a material 1 cm on a side has 6 square centimeters of surface area, about equal to one side of half a stick of gum. But if that volume of 1 cubic centimeter were filled with cubes 1 mm on a side, that would be 1,000 millimeter-sized cubes (10 x 10 x 10), each one of which has

a surface area of 6 square millimeters, for a total surface area of 60 square centimeters about the same as one side of two-thirds of a 3½ x 5½ note card. When the 1 cubic centimeter is filled with micrometer-sized cubes a trillion (10^{12}) of them, each with a surface area of 6 square micrometers the total surface area amounts to 6 square meters, or about the area of the main bathroom in an average house. And when that single cubic centimeter of volume is filled with 1-nanometer-sized cubes 10^{21} of them, each with an area of 6 square nanometers their total surface area comes to 6,000 square meters. In other words, a single cubic centimeter of cubic nanoparticles has a total surface area one-third larger than a football field!

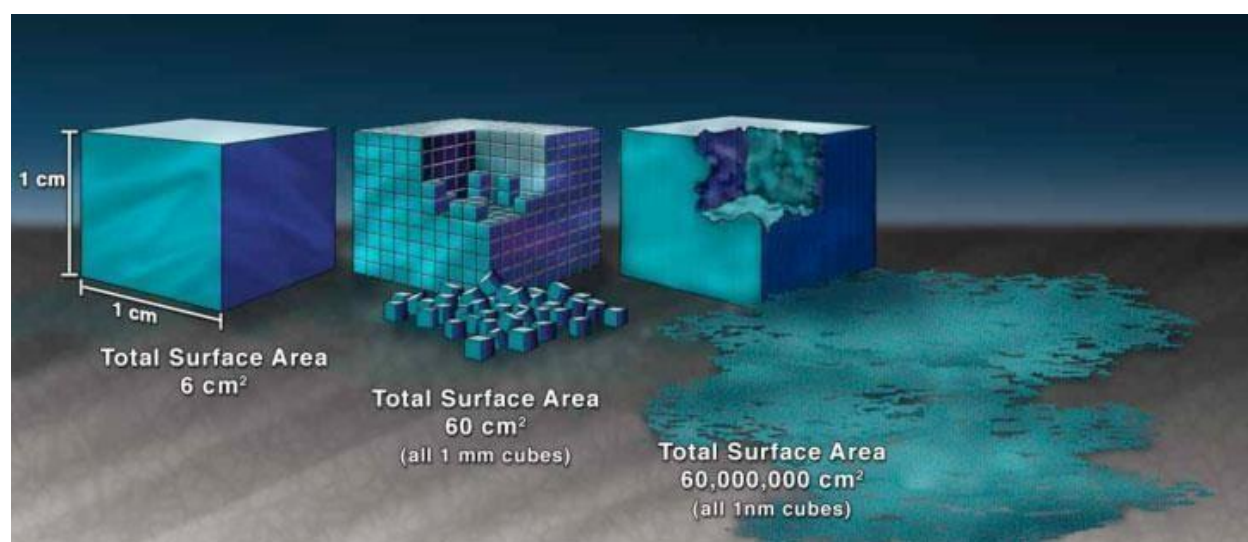


Fig.1.3: Illustration demonstrating the effect of the increased surface area provided by nanostructured materials

One benefit of greater surface area and improved reactivity in nanostructured materials is that they have helped create better catalysts. As a result, catalysis by engineered nanostructured materials already impacts about one-third of the huge U.S. and global catalyst markets, affecting billions of dollars of revenue in the oil and chemical industries. An everyday example of catalysis is the catalytic converter in a car, which reduces the toxicity of the engine's fumes. Nanoengineered batteries, fuel cells, and catalysts can potentially use enhanced reactivity at the nanoscale to produce cleaner, safer, and more affordable modes of producing and storing energy. Large surface area also makes nanostructured membranes and materials ideal candidates for water treatment and desalination, among other uses. It also helps support functionalization of nanoscale material surfaces (adding particles for specific purposes), for applications ranging from drug delivery to clothing insulation.

1.2 A Brief History of Nanotechnology:

- Mr. R Feynman, the Professor of Californian Institute of Technology, delivered lecture on There is Plenty of Room at the Bottom in 1959.
- In 1968, Molecular Beam Epitaxy was developed by Arthur and Cho.
- The word -nanotechnology was introduced for the first time into a scientific world by N. Taniguchi in an international conference on industrial production in Tokyo University in 1974 to describe the super thin processing of materials with nanometer accuracy and also the creation of nanosized mechanism.
- In 1981, Rohrer and Binnig developed Scanning Tunneling Microscope.
- In 1985, C₆₀ and fullerenes were discovered by Harry Kroto, Richard Smalley and Robert Curl.
- In 1985, Top Newman wrote the first page of Charles Dickens's novel A tale of Two Cities with a reduction factor of 25000 using Electron Beam Lithography (EBL).
- In 1986, AFM was developed by Binning and Co-workers.
- In 1986, ideas of nanotechnologies were developed by E. Drexler in his book Vehicles of Creation: the arrival of nanotechnology era.
- In 1987, Magnetic Force Microscope was discovered by Martin and Wickramasinghe.
- In the second half of 80's to the early 90's a number of important discoveries and inventions were made, which created an essential impact on the further development of nanotechnology.
- In 1990, D.M Eigler and E.K Schweizer used an STM to demonstrate atomic scale positioning of individual Xe atoms on a Ni surface at a low temperature (4K) to write IBM.
- In 1991, Sumio Ijima discovered Carbon Nanotube.
- In 1991, USA started first nano technological program of -National Scientific Fundl.
- In 1993, Ijima and Ichihashi grew single walled carbon nanotubes.
- During 1996-98, a special committee of the American Centre for Global Technology Assesment monitored and analyzed the development of Nanotechnology in all countries

and published the survey newsletter on basic trends of development and achievements for scientific, technical and administrative experts in USA.

- In 1996, Cuberes, Schilitter and Gimzewski demonstrated room temperature positioning of individual C₆₀ fullerenes with an STM to produce the C₆₀ abacus.
- In 1997, Steve Lamoreaux measured the Casimir force at submicron distances.
- Umar Mohideen and Anusree Roy measured the Casimir force using AFM at distances scales down to 90 nm.
- In 1999, the session of inter branch group on nanoscience, nanoengineering and nanotechnology took place, the result of which was the forecast on research in nanotechnology for the next 10 years.
- In 1999, IWGN conclusions and recommendations were supported by Presidential Council on Science and Technology (PCAST).
- In 2000, the Japanese Economic Association organized a special department on nanotechnology under the auspices of the Industrial and Technical Committee.
- In 2001, the framework plan of nanotechnology research was developed.
- In 2001, National Nanotechnological Initiative of the USA was approved. The principal idea of the program: NNI defined the strategy of interaction between federal departments of USA for the purpose of prioritizing nanotechnology development, which should become a basis for the economy and national security of the USA in the first half of the 21st century.
- In 2001, Postma and coworkers demonstrated single electron transistor operation using CNT.
- In 2002, Brusentov and co-workers achieved regression of tumor in mouse using magnetic nanoparticle thermia.
- In 2007, Johansen and co-workers made first human clinical trials of magnetic nanoparticle hypothermic treatment of cancer.
- Countries of Western Europe carried out research in nanotechnology within the framework of national programs.
- In Germany research in nanotechnology was supported by Ministry of Science, Education, Research and Technology.

- In England, nanotechnology development was supervised by the Council of Physics and Technology and by National Physics Laboratory.
- In France the nanotechnology development was defined by National Society of Scientific Research.

Thus the nanotechnology paradigm was formed at the turns of 1960's, while the 1980's and 1990's were the start of development of nanotechnology in its own right.

1.3 Synthesis of Nanomaterials:

Goal of any synthesis method for nanomaterials is to yield a material that exhibits properties that are a result of their characteristic length scale being in the nanometer range (~1 – 100 nm). Accordingly, the synthesis method should exhibit control of size in this range so that one property or another can be attained. Often the methods are divided into two main types "Bottom Up approach" and "Top Down approach".

There are two approaches for synthesis of nanomaterials and the fabrication of nanostructures. Top down approach refers to slicing or successive cutting of a bulk material to get nanosized particle. Bottom up approach refers to the buildup of a material from the bottom: atom by atom, molecule by molecule or cluster by cluster. Both approaches play very important role in modern industry and most likely in nanotechnology as well. There are advantages and disadvantages in both approaches.

Attrition or Milling is a typical top down method in making nanoparticles, whereas the colloidal dispersion is a good example of bottom up approach in the synthesis of nano particles. The biggest problem with top down approach is the imperfection of surface structure and significant crystallographic damage to the processed patterns. These imperfection leads to extra challenges in the device design and fabrication. But this approach leads to the bulk production of nanomaterial. Regardless of the defects produced by top down approach, they will continue to play an important role in the synthesis of nanostructures. Though the bottom up approach often referred in nanotechnology, it is not a newer concept. All the living beings in nature observe growth by this approach only and also it has been in industrial use for over a century. Examples include the production of salt and nitrate in chemical industry.

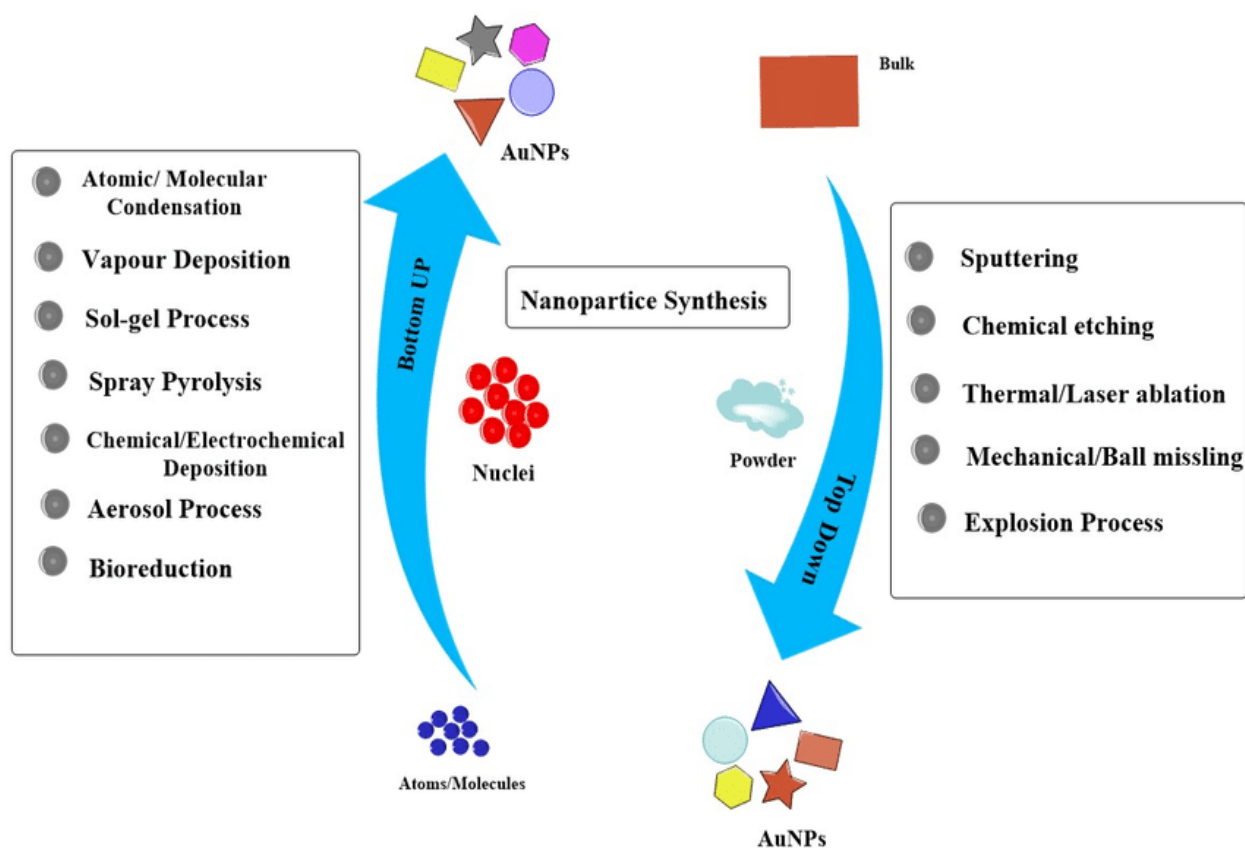


Fig.1.4: Top down and bottom up approach for nanomaterial synthesis and respective synthesis processes (adopted from webpage).

Attrition or Milling is a typical top down method in making nanoparticles, whereas the colloidal dispersion is a good example of bottom up approach in the synthesis of nano particles. The biggest problem with top down approach is the imperfection of surface structure and significant crystallographic damage to the processed patterns. These imperfection leads to extra challenges in the device design and fabrication. But this approach leads to the bulk production of nanomaterial. Regardless of the defects produced by top down approach, they will continue to play an important role in the synthesis of nanostructures. Though the bottom up approach often referred in nanotechnology, it is not a newer concept. All the living beings in nature observe growth by this approach only and also it has been in industrial use for over a century. Examples include the production of salt and nitrate in chemical industry.

Although the bottom up approach is nothing new, it plays an important role in the fabrication and processing of nanostructures. There are several reasons for this and explained as below. When structures fall into a nanometer scale, there is a little chance for top down approach. All the tools we have possessed are too big to deal with such tiny subjects. Bottom up approach also promises a better chance to obtain nanostructures with less defects, more homogeneous chemical composition. On the contrary, top down approach most likely introduces internal stress, in addition to surface defects and contaminations.

1.4 Current Applications of Nanotechnology:

Nano systems are expected to find various unique applications in almost all the field we face in our daily life. Nanostructured materials can be made with unique nanostructures and properties with compare to micro structured one. This field is expected to open new venues in science and technology. Due to the enabling nature of these systems, and because of the significant impact they can have on the commercial and defense applications, venture capitalists, industries, government have taken a special interest in nurturing growth in this field. It will not be wrong to say that micro and nano systems are going to be the next logical step in the –silicon revolution. When a particle is shrunk to nano scale, several properties of the material change in accordance with size. So it gives new applications in several fields. As the size the surface to volume ratio increases, it gives more surface area to react. Several optical as well as mechanical properties are also dependent on the diameter or the size of particles.

Different vast areas of application of Nano Technology are:

- In Medical Science
- Environment Application
- Energy
- Information and Communication
- Heavy Industries
- Consumer Goods

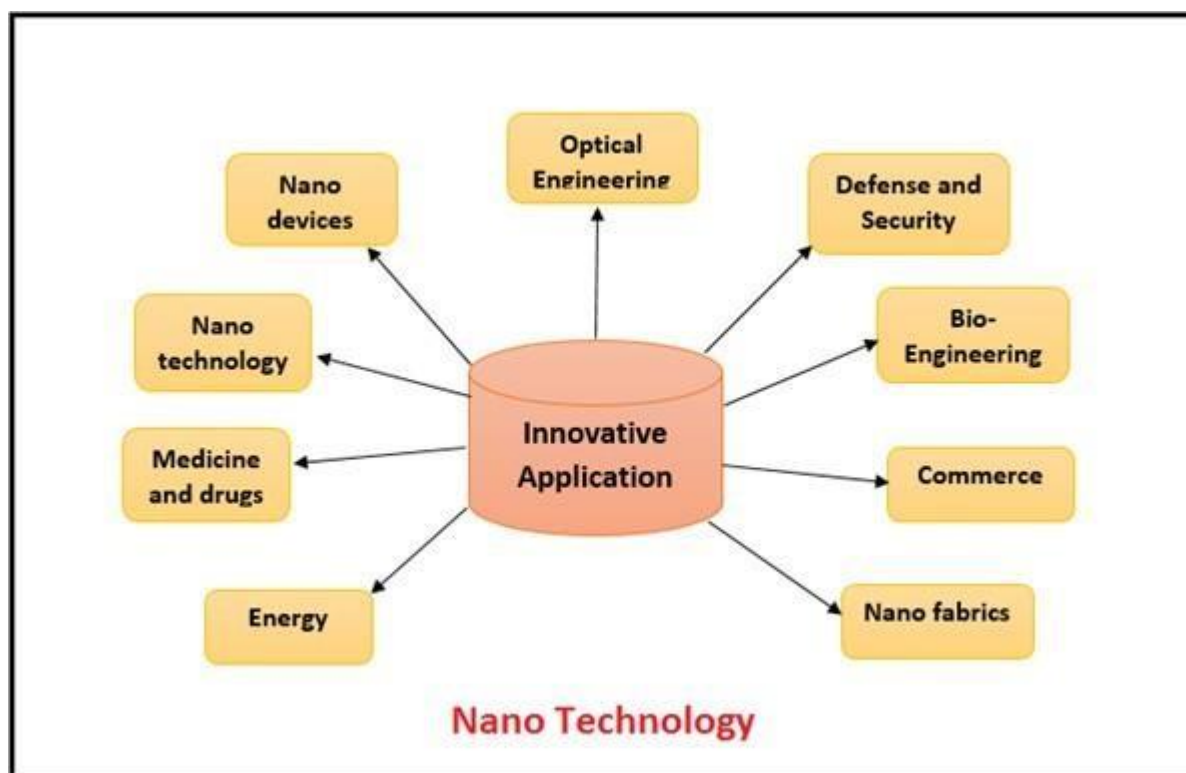


Fig.1.5: Different application field of Nano Technology (adopted from webpage)

❖ In Medical Science:

One of the vast and innovative application area of nanotechnology is medical science. Nanotechnology has opened many new doors in the area of diagnosis of severe diseases like cancer etc. It is nanotechnology only due to which we can think of detection of diseases in DNA levels. It has many applications in biomedical nanotechnology, nano biotechnology, and nano medicine. The size of the nanomaterial is similar to that of most biological molecules and structures, therefore nanomaterial can be useful in vivo and in vitro medical research and applications. The integration of nanotechnology with biology has resulted in development of diagnostic devices, contrast agents, analytical tools, physical therapy applications and drug delivery vehicles[7-10].

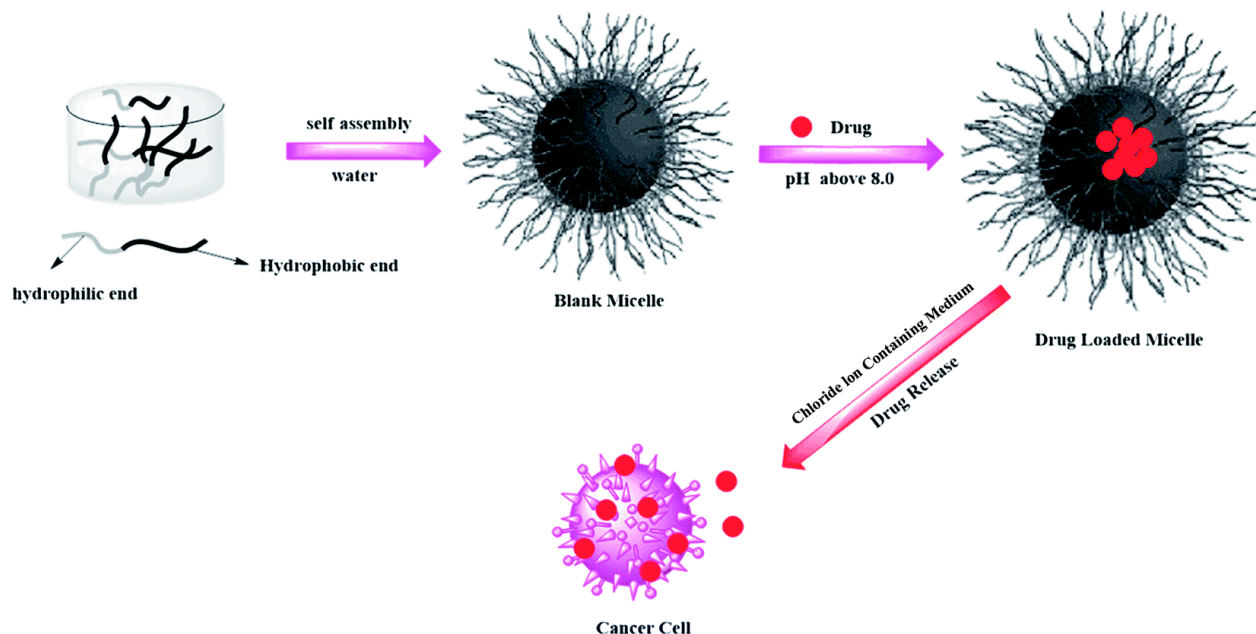


Fig.1.6: Drug Delivery to the Cancer cell (Adopted from Webpage)[9]

➤ **Diagnostic:**

Nanotechnology-on-a-chip gives one more dimension to lab-on-a-chip technology. Gold nanoparticles, tagged with short segments of DNA, can be used for detection of genetic sequence in a biological sample. Multicolor optical coding for biological assays has been achieved by embedding different-sized quantum dots into polymeric micro beads. Nano pore technology converts strings of nucleotides directly into electronic signatures for analysis of nucleic acids.

➤ **Drug Delivery:**

Nanotechnology has become a new path for the medical field by delivering drugs to desired cells using nanoparticles. An example of drug delivery can be found in nanoporous materials. Another example is to use block co-polymers which form micelles for drug encapsulations. They can hold small drug molecules for transporting them to the desired location.

➤ **Tissue Engineering:**

Nanotechnology helps to reproduce and repair damaged cell. -Tissue engineering can form artificially stimulated cell proliferation by using suitable nano material-based scaffolds and growth factors. For example, bones can be grown artificially on carbon nanotube scaffolds. Tissue engineering might replace today's conventional treatments like organ transplants or artificial implants.

➤ **Environment applications:**

➤ **Filtration:**

A strong influence of photochemistry on waste-water treatment, air purification is there. One class of filtration techniques is the use of membranes with suitable holes, whereby the liquid is pressed through the membrane. Nanoporous membranes are suitable for mechanical filtration with pores smaller than 10 nm. Magnetic nanoparticles also offer an effective and reliable method to remove heavy metal contaminants from waste water by using magnetic separation techniques.

➤ **Energy:**

The most advanced nanotechnology related works are on storage, conversion, manufacturing improvements, process rate, energy saving and enhancement of renewable energy sources.

Solar cells have layers of several semiconductors stacked to absorb light at different energies but they can manage only 40 % of solar energy. Nanotechnology can increase the energy efficiency of light conversion by using nano structured material with a continuum of band-gap.



In 2005, scientists from University of Toronto developed **Fig.1.7: adopted from webpage** spray-on nano particle substance, when it is applied to a surface it's transferred to solar collector.

Information and Communication:

The critical length scale of integrated circuits is already within 50 nm and below regarding the gate length of transistors of CPU and memory device.

➤ **Memory Storage:**

Electronic memory design is dependent on transistors. However, crossbar switch dependent electronics have offered an alternative using reconfigurable between vertical and horizontal wiring arrays to create ultra-high density memory.

➤ **Novel Semiconductor Device:**

In 1999, the ultimate CMOS device was developed by the laboratory of Electronics and Information Technology in Grenoble of France. They tested the limits principles of MOSFET transistor with diameter of 18 nm means approximately 70 atoms placed side by side. This was almost one tenth size of the smallest industrial transistor.

➤ **Novel Optoelectronic Device:**

Nowadays, traditional electrical devices are replaced by optical or optoelectronic devices due to their bandwidth and capacity. Photonic crystal and quantum dot are examples of this kind of material. Photonic crystals have periodic variation of refractive index with lattice constant. They generally offer selectable band gap for propagation of certain wavelength i.e. they resemble semiconductor but electrons are replaced by photon or light. Quantum dot is an object in nano scale with 3-D structure. It has impact application on laser. The difference between this laser and traditional laser is their emitted wavelength depends upon the diameter of the dot. Quantum laser offers high quality of beam and also cheaper than conventional laser diode.

➤ **Display Technology:**

In display system low energy consumption can be achieved by using CNT (Carbon Nano Tube). It is conductive and due to their small diameter, they can be used as field emitters. So it has an effective use in Field Emitter Display. The working principle is same as CRT display but it's in a small length scale.

➤ **Quantum Computers:**

It's a new approach in the industry of computer. It has quantum bit memory which is

called qubit for several computations at the same time. It improves the facility of the older system.

Heavy Industries:

➤ **Aerospace:**

Lighter and stronger materials have immense use in aircraft manufacturing. Spacecraft will be beneficial, where weight is a major factor. Nanotechnology helps to reduce the size of equipment and decreases fuel consumption required to get it airborne.

➤ **Catalysis:**

In nano range, chemical catalysis has an adverse effect due to its high surface to volume ratio. The application of this catalyst is from fuel cell to catalytic converters and photo catalytic devices. Catalysis is also important for the production of chemicals. Nano filtration may be an important application in this field though toxicity should be taken as a part of this investigation.

➤ **Construction:**

Nanotechnology has potential to construct faster, cheaper and safer construction materials. Nanotechnology has an adverse effect in the field of steel, glass, coatings, fire protection and detection, vehicle manufacturing etc.

Consumer Goods:

Nanotechnology has a great impact in the field of consumer goods from easy to clean to scratch resistant surfaces. Modern textiles are wrinkle resistant and stain repellent. Clothes have become smart and embedded with wearable electronics. In the field of cosmetics also, nanotechnology has a huge effect.

➤ **Foods:**

Few examples of nanotechnology in this field are bacteria identification and food quality monitoring using biosensors, intelligent, smart and advance food packaging systems, nano encapsulation of bio active food compounds. Nano composite coating improves the

food packaging by placing anti-microbial agent directly on the surface of coating. They can improve the mechanical and heat resistant property and lower the oxygen transmission rate.

➤ **Textiles:**

The incorporation of engineered nano fiber in clothes makes the clothes water and strain repellent and wrinkle free. Nano technological finished textiles can be washed less frequently at lower temperatures.

➤ **Cosmetics:**

Mainly sunscreen cosmetics are made of nanoparticles. Traditional chemicals used in sun screens have poor long term stability. Sunscreen based on mineral nanoparticles such as titanium oxide offers more UV protection.

➤ **Agriculture:**

Applications of nanotechnology have the potential to change the entire agriculture sector and food industry from production to conservation, processing, packaging, transportation, and even waste treatment.

➤ **Sports:**

Nanotechnology has applications in the field of sports like soccer, football, baseball etc. Baseball bats are made of carbon nanotubes which reinforce the resin and also improve its performance by making it lighter. Other items such as sport towels, yoga mats, exercise mats use antimicrobial nanotechnology to prevent illnesses caused by bacteria such as Methicillin-resistant *Staphylococcus aureus* (commonly known as MRSA).

1.5 Future uses of Nano Technology:

As projected by the *Foresight Institute*, the everyday benefits of an increased availability of nanofactories would include the following:

- **Medical Nanorobots That Cure Disease and Reverse Aging.** Robert Freitas, Senior Research Fellow at the *Institute for Molecular Manufacturing*, projects in his *Nanomedicine Book Series* a future where medical nanorobots are introduced into the human body to perform cellular and microscopic surgeries, repair specific injuries, and patrol the body to identify and resist disease. On the website for the *Institute for Ethics & Emerging Technologies*, Burch described a scenario where an ingested pill would supply

molecular materials with instructions for nanobots to form new neurons to replace damaged or dying brain cells. These new brain cells would process information much faster than a biological brain, just as an artificial limb can be stronger than a human arm or leg.

- **Reduced Cost of Manufactured Products.** Basic costs will fall to the value of raw materials such as carbon, nitrogen, and oxygen and the energy required to operate nanofactory. Imagine an automobile built of carbon fibers and created in nanofactories rather than with materials that require mining, processing, and configuration. Theoretically, virtually any material or object can be assembled bottom-up by a combination of nanofactories. Large-scale results occur when simultaneous and synergistic nanoscale processes are combined. Eric Drexler, an American engineer known for popularizing nanotechnology, predicts a future of desk-top factories making large, useful products, similar to the replicator of Star Trek fame. In fact, in June 2014, *Nestle's Institute of Health Sciences* announced a new project that may eventually lead to a kitchen machine that can create tailored supplements – or even food.
- **Development of Artificial General Intelligence (AGI).** According to *Foresight Institute*, nanofactories will include machine systems for engineering and technical work which, in turn, will manufacture computers that are thousands of times more powerful and inexpensive than current computers. As machines learn and transfer knowledge from one application or environment to another, rapid advances become probable. However, there is some question as to how quickly AGI can be achieved. Since 1990, a prize of \$100,000 has been available to anyone whose machine can fool independent judges into thinking it is human while engaged in freeform conversation. The prize has yet to be awarded.
- **Elimination of Industrial Chemical Pollution.** Since every atom in organic food stock is used in the final product, or directed into properly packaged waste, no polluting atoms are released into the environment. For example, natural coal produces pollutants such as sulfur dioxide, nitrogen oxides, airborne physical particles, and mercury when burned. Building an artificial fuel that eliminates by-products, or converts them into non-harmful form, would be healthier and less expensive.

1.6. The Perils & Risks of Nanotechnology:

Even proponents of nanotechnology, such as Burch and Drexler, recognize its potential to harm and possibly annihilate the human race if the technology is uncontrolled or misdirected. These potentially harmful effects include the following:

- **Overpopulation.** The mortality rate for humans over 80 years of age has decreased about 1.5% per year since the 1960s. Robert Freitas, Jr. suggests that advances in nanotechnology will eliminate all genetic diseases and slow aging, –augmenting human healthspan at least tenfold. If increases in longevity do not reduce births, the human race would expand exponentially, exacerbating societal tensions and potentially exhausting resources.
- **Increase in Crime and Terrorism.** Chemical and biological weapons could become more deadly and easier to conceal or track, especially if they become available on the black market or can be constructed in a home factory. Nanofactories theoretically could produce an intelligent anti-personnel weapon the size of an insect capable of carrying a lethal dose of botulism. The number of such weapons capable of killing every human being on the planet could be packed into a single suitcase.
- **Disparity Between Haves and Have-Nots.** Nanotechnology developments are likely to be initially expensive and consequently protected by layers of patents, laws, and anti-competitive barriers. Accordingly, the benefits of lower costs are likely to be limited to the owners of the technology. Poverty and income disparity could become more exaggerated, thus generating social unrest.
- **Conflicts Over Religious Beliefs and Lifestyles.** Throughout the world, products are banned or restricted based upon religious or moral principles not necessarily shared by the majority. Examples include guns in Britain, alcohol in Muslim societies, and recreational drugs in various countries. The ability to produce banned products in personal nanofactories could cause disruption in those societies.
- **Appearance of “Grey Goo”** Some scientists are concerned that self-replicating nano factories may run amok, eating the biosphere in a frenzied effort to make unlimited copies of themselves. Just as anti-social behavior is irresistible to a certain percentage of the

population as evidenced by the number of computer viruses in existence irresponsible people and groups are likely to make self-replicating nano factories, thereby increasing the possibility of disaster.

References:

1. Klabunde, Kenneth J. "Introduction to nanotechnology." *Nanoscale Materials in Chemistry* (2001): 1-13.
2. Owens, Frank J., and C. P. Poole. "Introduction to nanotechnology." (2003).
3. Poole, C. P., and J. F. J. Owens. "Introduction to nanotechnology." *New Delhi* (2005).
4. Gordon, Assaf T., et al. "Introduction to nanotechnology: potential applications in physical medicine and rehabilitation." *American journal of physical medicine & rehabilitation* 86.3 (2007): 225-241.
5. Poel, I. "The introduction of nanotechnology as a societal experiment." *Technoscience in progress. Managing the uncertainty of nanotechnology* (2009):129.

6. Campbell, Colin K. "Applications of surface acoustic and shallow bulk acoustic wave devices." *Proceedings of the IEEE* 77.10 (1989): 1453-1484.
7. Singhal, Sunil, Shuming Nie, and May D. Wang. "Nanotechnology applications in surgical oncology." *Annual review of medicine* 61 (2010): 359.
8. Duncan, Timothy V. "Applications of nanotechnology in food packaging and food safety: Barrier materials, antimicrobials and sensors." *Journal of colloid and interface science* 363.1 (2011): 1-24.
9. Cai, Weibo, et al. "Applications of gold nanoparticles in cancer nanotechnology." *Nanotechnology, science and applications* 2008.1 (2008).
10. Mitra, Sumita B., Dong Wu, and Brian N. Holmes. "An application of nanotechnology in advanced dental materials." *The Journal of the American Dental Association* 134.10 (2003): 1382-1390.
11. Jain, Kewal K. "Nanodiagnosics: application of nanotechnology in molecular diagnostics." *Expert Review of Molecular Diagnostics* 3.2 (2003): 153-161.
12. Wang, Xu, et al. "Application of nanotechnology in cancer therapy and imaging." *CA: a cancer journal for clinicians* 58.2 (2008): 97-110.
13. Seeman, Nadrian C. "DNA engineering and its application to nanotechnology." *Trends in biotechnology* 17.11 (1999): 437-443.
14. Misra, Ranjita, Sarbari Acharya, and Sanjeeb K. Sahoo. "Cancer nanotechnology: application of nanotechnology in cancer therapy." *Drug Discovery Today* 15.19 (2010): 842-850.
15. Gilardi, Gianfranco, and Andrea Fantuzzi. "Manipulating redox systems: application to nanotechnology." *Trends in Biotechnology* 19.11 (2001): 468-476.

16. Sahaym, Uttara, and M. Grant Norton. "Advances in the application of nanotechnology in enabling a 'hydrogen economy'." *Journal of Materials Science* 43.16 (2008): 5395-5429.
17. Zhu, W., P. J. M. Bartos, and A. Porro. "Application of nanotechnology in construction." *Materials and Structures* 37.9 (2004): 649-658.
18. Mu, Li, and Robert L. Sprando. "Application of nanotechnology in cosmetics." *Pharmaceutical research* 27.8 (2010): 1746-1749.
19. Artan, Reha, and Ayşegül Tepe. "The initial values method for buckling of nonlocal bars with application in nanotechnology." *European Journal of Mechanics-A/Solids* 27.3 (2008): 469-477.
20. Navalakhe, Rajshri M., and Tarala D. Nandedkar. "Application of nanotechnology in biomedicine." *Indian journal of experimental biology* 45.2 (2007): 160.
21. Hu, A. W., and Z. H. Fu. "Nanotechnology and its application in packaging and packaging machinery." *Packaging Engineering* 24 (2003): 22-24.
22. Ehdaie, Beeta. "Application of nanotechnology in cancer research: review of progress in the National Cancer Institute's Alliance for Nanotechnology." *Int J Biol Sci* 3.2 (2007): 108-110.
23. Evans, Philip, Hiroshi Matsunaga, and Makoto Kiguchi. "Large-scale application of nanotechnology for wood protection." *Nature nanotechnology* 3.10 (2008): 577-577.
24. Nassar, Nashaat N., Azfar Hassan, and Pedro Pereira-Almao. "Application of nanotechnology for heavy oil upgrading: Catalytic steam gasification/cracking of asphaltenes." *Energy & Fuels* 25.4 (2011): 1566-1570.
25. Postek, Michael T., and Andras E. Vladár. "Helium ion microscopy and its application to nanotechnology and nanometrology." *Scanning* 30.6 (2008): 457-462.

26. Cuixing, Meng. "APPLICATION OF NANOTECHNOLOGY IN MODIFICATION OF POLYMER [J]." *New Chemical Materials* 2 (2001): 000.
27. For example, see C.S. Thaxton, R. Elghanian, A.D. Thomas, S.I. Stoeva, J.S. Lee, N.D. Smith, A.J. Schaeffer, H. Klocker, W. Horninger, G. Bartsch, and C.A. Mirkin. Nanoparticle-based bio-barcode assay redefines -undetectable PSA and biochemical recurrence after radical prostatectomy. *Proc. Nat. Acad. Sci. U. S. A.* 106(44):18437– 18442, 2009, doi:10.1073/pnas.0904719106.
28. For more detail, see <http://newscenter.lbl.gov/feature-stories/2010/05/10/untangling-quantum-entanglement/> and associated links.
29. As of 2003, catalyst technologies accounted for over \$1 trillion of revenue in the U.S. economy and about a third of the material GDP (M.E. Davis and D. Tilley, *Future Directions in Catalysis Research, Structures that Function on the Nanoscale*, NSF Workshop, Caltech, June 19-20, 2003; <http://www.che.caltech.edu/nsfcatalworkshop/#Reports>).
30. <https://www.moneycrashers.com/nanotechnology-examples-future-applications-risks/>

Chapter 2:

Overview of Supercapacitors And Nanofluids



2.1. Introduction of Supercapacitor:

In today's energy-dependent world, electrochemical devices for energy storage and conversion such as batteries, fuel cells, and electrochemical supercapacitors (ESs) have been recognized as the most important inventions among all energy storage and conversion technologies. The electrochemical supercapacitor, also known as a supercapacitor, ultracapacitor, or electrochemical double-layer capacitor, is a special type of capacitor that can store relatively high energy density compared to storage capabilities of conventional capacitors. ES devices possess several high-impact characteristics such as fast charging capabilities, long charge–discharge cycles, and broad operating temperature ranges. As a result, their use in hybrid and electrical vehicles, electronics, aircraft, and smart grids is widespread. Although ES systems still face some challenges, such as relatively low energy density and high cost, further development will allow ESs to work as power devices in tandem with batteries and fuel cells and also function as stand-alone high energy storage devices. For energy storage devices, energy density and power density are very important parameters for characterizing the performance of the devices. Energy density defines the amount of energy that can be stored in a given volume or weight of the material. Power density defines the total energy per unit time which can be stored into the device. So the ideal storage device should have both of high energy density and high power density. To compare the power and energy capabilities, a representation known as the Ragone plot or diagram has been developed, it is shown in figure. Batteries have high energy density, but poor power density. Fuel cells have the highest energy density, and lowest power density. By contrast with them, supercapacitors could possess high power density and notable increased high energy density.

With the expert's progressive research, numerous noble characteristics about capacitors are come to notice. In 1957, the first patent for electrochemical capacitor was registered by General Electric in America. In 1971, Nippon Electric Company (NEC) in Japan is the earliest one to make true commercial devices with these techniques, called them supercapacitor. Nowadays, people put batteries and capacitors into one category. Both of them are named after Electrochemical Energy Storage (EES) devices.

The present energy crisis has created a growing demand for efficient, portable, and high-power energy storage devices. Supercapacitors are fast emerging as a promising potential solution to this problem.

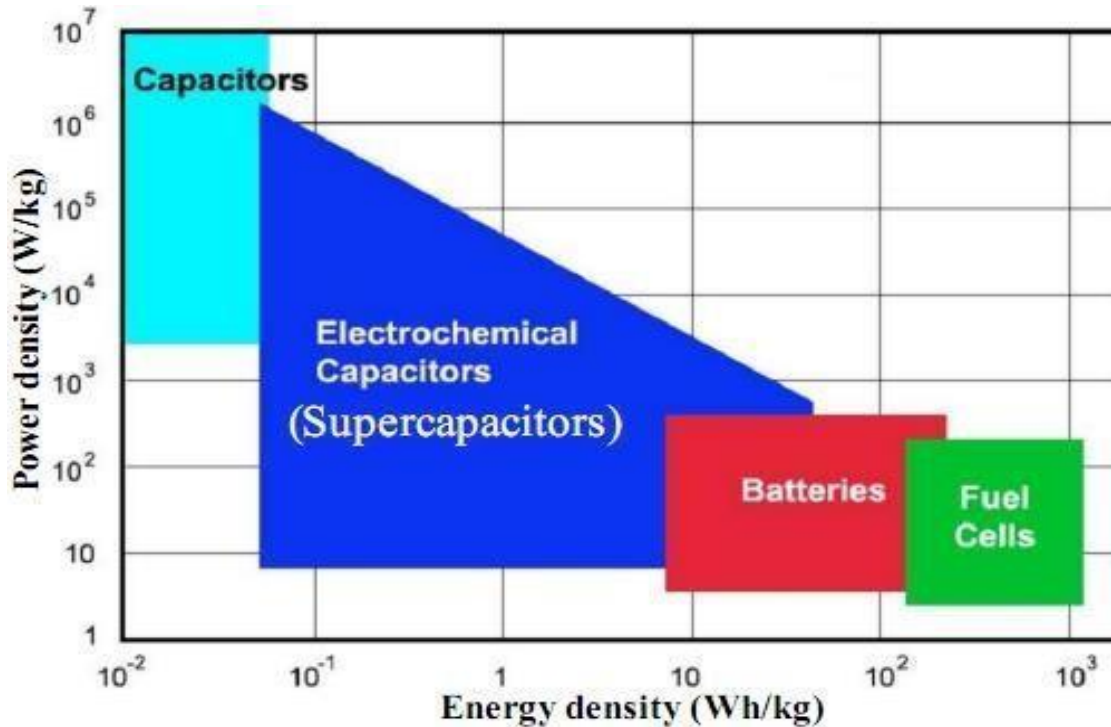


Fig. 2.1 Ragone plot of various energy storage devices

Supercapacitor also known as electric double-layer capacitor (EDLC), super condenser, pseudo capacitor, electrochemical double layer capacitor or ultracapacitors is an electrochemical capacitor with relatively high energy density.

Compared to conventional electrolytic capacitors the energy density is typically on the order of hundreds of times greater. In comparison with conventional batteries or fuel cells, EDLCs also have a much higher power density.

2.2. Background of Supercapacitor

Conventional capacitors consist of two conducting electrodes separated by an insulating dielectric material. When a voltage is applied to a capacitor, opposite charges accumulate on the surfaces of each electrode. The charges are kept separate by the dielectric, thus producing an electric field that allows the capacitor to store energy. This is illustrated in the Diagram of conventional capacitor. Capacitance C is defined as the ratio of stored (positive) charge Q to the applied voltage V .

$$C = \frac{Q}{V} \quad \dots\dots\dots (2.1)$$

For a conventional capacitor, C is directly proportional to the surface area A of each electrode and inversely proportional to the distance D between the electrodes.

$$C = \epsilon \frac{A}{d} = \epsilon_0 \epsilon_r \frac{A}{d} \quad \dots\dots\dots (2.2)$$

Where ϵ is the dielectric constant.

The two primary attributes of a capacitor are its energy density and power density. For either measure, the density can be calculated as a quantity per unit mass or per unit volume. The energy E stored in a capacitor is directly proportional to its capacitance:

$$E = \frac{1}{2} CV^2 \quad \dots\dots\dots (2.3)$$

In general, the power P is the energy expended per unit time. To determine P for a capacitor one must consider that capacitors are generally represented as a circuit in series with an external —load|| resistance R .

The internal components of the capacitor (e.g., current collectors, electrodes, and dielectric material) also contribute to the resistance, which is measured in aggregate by a quantity known as the equivalent series resistance (ESR). The voltage during discharge is determined by these resistances. When measured at matched impedance ($R = \text{ESR}$), the maximum power P_{max} for a capacitor is given by:

$$P_{\max} = \frac{V^2}{4} \times \text{ESR} \quad \dots\dots\dots (2.4)$$

This relationship shows how the ESR can limit the maximum power of a capacitor. Conventional capacitors have relatively high power densities, but relatively low energy densities when compared to electrochemical batteries and to fuel cells. That is, a battery can store more total energy than a capacitor, but it cannot deliver it very quickly, which means its power density is low. Capacitors, on the other hand, store relatively less energy per unit mass or volume, but what electrical energy they do store can be discharged rapidly to produce a lot of power, so their power density is usually high. Supercapacitors are governed by the same basic principles as conventional capacitors. However, they incorporate electrodes with much higher surface areas A and much thinner dielectrics that decrease the distance d between the electrodes. Thus from Eq. 2 and 3, this leads to an increase in both capacitance and energy. Furthermore, by maintaining the low ESR characteristic of conventional capacitors, supercapacitors also are able to achieve comparable power densities. Additionally, supercapacitors have several advantages over electrochemical batteries and fuel cells, including higher power density, shorter charging times, and longer cycle life and shelf life.

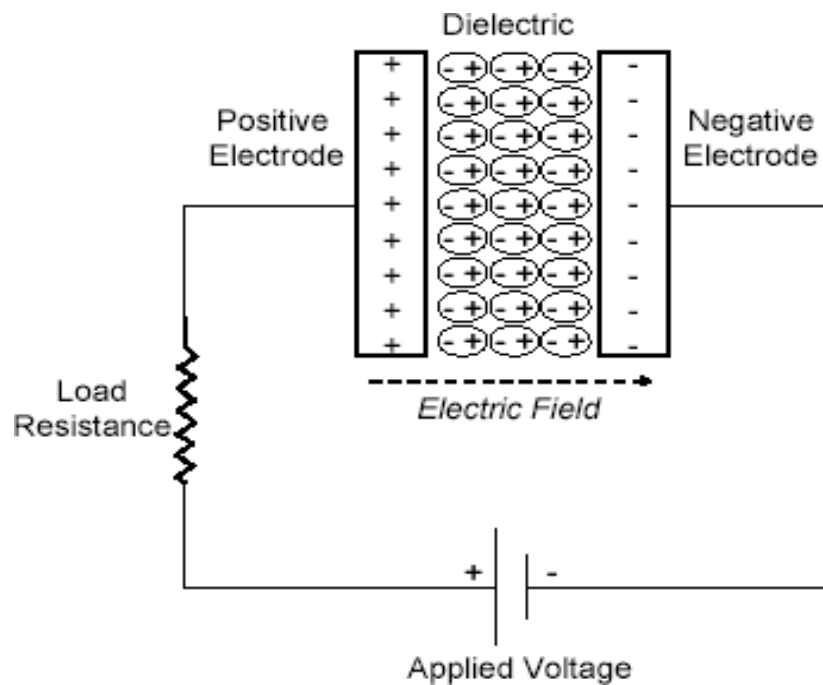


Fig 2.2: Diagram of conventional capacitor (adopted from webpage).

2.3. Classification of Supercapacitor:

Based upon current supercapacitors can be divided into three general classes: electrochemical double-layer capacitors, pseudocapacitors, and hybrid capacitors. Each class is characterized by its unique mechanism for storing charge. These are, respectively, non-Faradaic, Faradaic, and a combination of the two. Faradaic processes, such as oxidation- reduction reactions, involve the transfer of charge between electrode and electrolyte. A non-Faradaic mechanism, by contrast, does not use a chemical mechanism. Rather, charges are distributed on surfaces by physical processes that do not involve the making or breaking of chemical bonds. A graphical taxonomy of the different classes and subclasses of supercapacitors is presented in this figure.

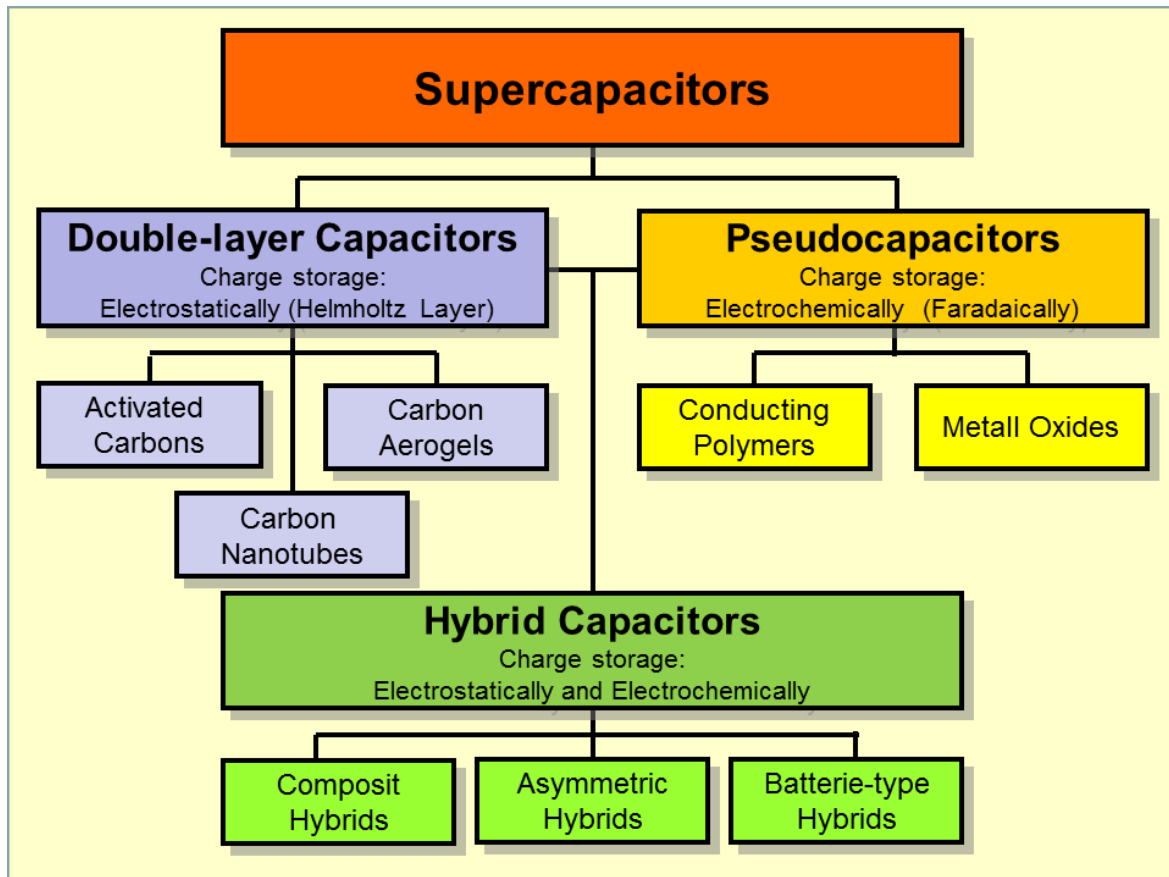


Fig.2.3: Classification of supercapacitors (adopted from webpage)

(I) Electrochemical Double Layer Capacitor (EDLC):

Electrochemical double-layer capacitors (EDLCs) are constructed from two carbon-based electrodes, an electrolyte, and a separator. Fig. 2 provides a schematic of a typical EDLC. Like conventional capacitors, EDLCs store charge electrostatically, or non-faradaically, and there is no transfer of charge between electrode and electrolyte. EDLCs utilize an electrochemical double-layer of charge to store energy. As voltage is applied, charge accumulates on the electrode surfaces. Following the natural attraction of unlike charges, ions in the electrolyte diffuse across the separator into the pores of the electrode of opposite charge. However, the electrodes are engineered to prevent the recombination of the ions. Thus, a double-layer of charge is produced at each electrode. These double-layers, coupled with an increase in surface area and a decrease in the distance between electrodes, allow EDLCs to achieve higher energy densities than conventional capacitors. Because there is no transfer of charge between electrolyte and electrode, there are no chemical or composition changes associated with non-Faradaic processes. For this reason, charge storage in EDLCs is highly reversible, which allows them to achieve very high cycling stabilities. EDLCs generally operate with stable performance characteristics for a great many charge-discharge cycles, sometimes as many as 10³ cycles. On the other hand, electrochemical batteries are generally limited to only about 10³ cycles. Because of their cycling stability, EDLCs are well suited for applications that involve non-user serviceable locations, such as deep sea or mountain environments.

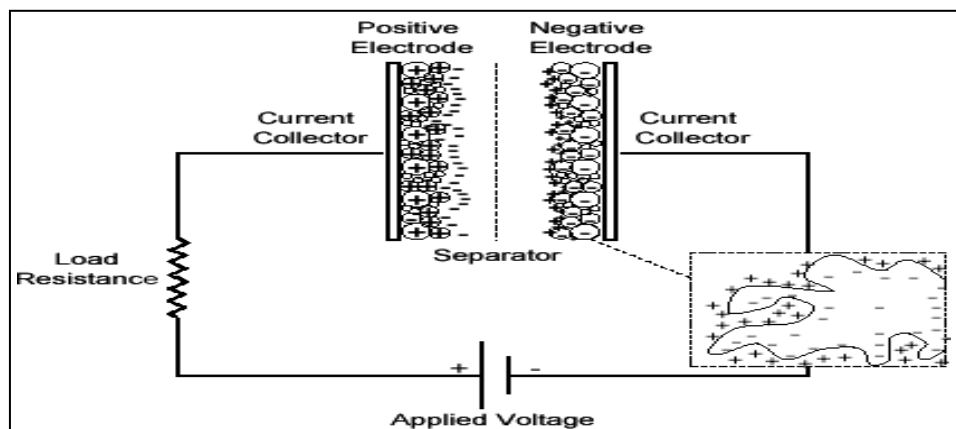


Fig 2.4: Diagram of EDLC (adopted from webpage)

The performance characteristics of an EDLC can be adjusted by changing the nature of its electrolyte. An EDLC can utilize either an aqueous or organic electrolyte. Aqueous electrolytes, such as H₂SO₄ and KOH, generally have lower ESR and lower minimum pore size requirements compared to organic electrolytes, such as acetonitrile. However, aqueous electrolytes also have lower breakdown voltages. Therefore, in choosing between an aqueous or organic electrolyte, one must consider the tradeoffs between capacitance, ESR, and voltage. Because of these tradeoffs, the choice of electrolyte often depends on the intended application of the supercapacitor. While the nature of the electrolyte is of great importance in supercapacitor design, the subclasses of EDLCs are distinguished primarily by the form of carbon they use as an electrode material. Carbon electrode materials generally have higher surface area, lower cost, and more established fabrication techniques than other materials, such as conducting polymers and metal oxides. Different forms of carbon materials that can be used to store charge in EDLC electrodes are activated carbons, carbon aerogels, and carbon nanotubes.

(II) Pseudocapacitor:

In contrast to EDLCs, which store charge electrostatically, pseudocapacitors store charge faradaically through the transfer of charge between electrode and electrolyte. This is accomplished through electrosorption, reduction-oxidation reactions, and intercalation processes. These Faradaic processes may allow pseudocapacitors to achieve greater capacitances and energy densities than EDLCs.

There are many electrode materials that are used to store charge in pseudocapacitors, conducting polymers, metal oxides, chalcogenides, nitrides etc. The charge transfer that takes place in these reactions is voltage dependent, so a capacitive phenomenon occurs. There are two types of reactions that can involve a charge transfer that is voltage dependent. One is redox reaction and another is adsorption of ions.

(III) Hybrid Capacitor:

Hybrid capacitors attempt to exploit the relative advantages and mitigate the relative disadvantages of EDLCs and pseudocapacitors to realize better performance characteristics. Utilizing both Faradaic and non-Faradaic processes to store charge, hybrid capacitors have achieved energy and power densities greater than EDLCs without the sacrifices in cycling stability and affordability that have limited the success of pseudocapacitors. Research has focused on three different types of hybrid capacitors, distinguished by their electrode configuration: composite, asymmetric, and battery-type respectively.

2.4. The Electrolytes:

The performance of a supercapacitor is not only dependent on the electrode materials, but is also strongly affected by the electrolytes employed. A high cell operating voltage provides both high energy density and power density, but is limited by the stability of the electrolyte in the applied potential. The current trend in supercapacitor development involves the switch from an aqueous electrolyte, which has a low operating voltage of 1 V (due to the thermodynamic decomposition of water) to a non-aqueous medium which allows a much higher voltage window of about 2.5 V. The most recent supercapacitors available in the market use electrolytes based on aprotic solvents, typically acetonitrile or carbonate-based solvents (i.e. propylene carbonate). The advantages of a higher energy density when using aprotic electrolyte rather than aqueous electrolyte. However, there are other considerations on the use of non-aqueous electrolytes such as high cost, low conductivity compared to aqueous electrolyte leading to power deterioration, low dielectric constant resulting in smaller capacitance, complex purification procedure as well as safety concerns due to the flammability and toxicity of the organic solvent. Ionic liquids (ILs), which are known as room temperature molten salts, are under considerable research for use as next generation electrolytes. They are attractive candidates for electrolytes used in energy storage because of their good chemical and physical properties, such as high thermal stability, high electrochemical stability over a wide potential window, non-toxicity, non-flammability, variety of combination choices of cations and anions, acceptable conductivity at elevated temperature, etc. ILs are liquids at ambient or even lower temperatures and are composed entirely of ions, making them attractive solvent free green electrolytes,. But they are typically high viscosity liquids and have low ionic conductivity at room temperature, which inevitably affect their performance.

2.5. Application of Supercapacitor

Automobile:

Some of the most popular applications of supercapacitor include automotive vehicle incorporation. Hybrid Electric Vehicles (HEV) and Pure Electric vehicles (PEV) were gradually popularized over recent years. With much research efforts spent into improving the fuel economy of vehicles, both HEV and PEV represent the one of the important trends of vehicle development. Both the HEV and PEV contain an electrical machine onboard for propulsion. When the vehicle starts to move off, the initial power required by the motor can be several times that of the average power demand. Deprivation of electrical power during this instant simply implies sluggish pickup performance. This is a highly challenging task as batteries with high energy density, e.g., lithium battery, are limited in output power capability. Comparatively, supercapacitor has both superior output and input power capability. The optimization of regenerative braking in vehicles is of much concern, for doing so allows the vehicle's kinetic energy to be saved and utilized at a later moment, reducing energy that is otherwise wasted as heat. As the power delivered during regenerative braking is vast, the high input power capability of supercapacitor makes it exceptionally suitable to achieve significant energy saving and carbon reduction. Therefore, supercapacitor has the potential to play an important role in automobile applications.

Mobile Devices:

Supercapacitors can take on many different physical forms. Cap-XX has been active in promoting thin and small supercapacitor which can be applied in applications which had severe space constraint. Some recent mobile phones have high quality xenon flash inbuilt into the phone to enable good photo quality when light is scarce. Xenon flash has traditionally been used on cameras, and consumes much power in an instant. Should the mobile phone have to cater to the power requirement, it would have added unnecessary bulk and weight to the battery, failing which would result in severely shortened battery life. Some mobile manufacturers have incorporated a supercapacitor into the mobile phone to ease the temporary high power demand. In this application, the supercapacitor performs peak load shaving. It is shown that with peak load shaving, the battery current is suppressed at a maximum of 0.2A even though the camera flash current may be as high as 4A. Although the battery supplies the entire energy requirement, it does not see high power demand. The supercapacitor voltage experiences a significant fall as a

result of supplying energy to the flash. As a result, the battery does not have to be large to cater to temporal high power demands.

Micro-Grid:

The micro-grid is labeled as a possible next-generation energy network. It comprises of electrical power generation units as well as electrical energy storage components. Popular electrical power generator includes photovoltaic cell, wind turbine, fuel cell and micro turbine while commonly used electrical energy storage units would be the supercapacitor and battery. As the micro-grids can be inter-connected to the power grid, it is able to supply or demand power from the power grid. At times, this configuration is known as the smart grid. The micro-grid has the capability of reducing carbon emission through green energy harnessing as well as having the potential of providing self-sustainable energy. Thus, it is regarded as a contender for the next generation energy network.

2.6 Overview of Nanofluids:

1. Introduction of nanofluid:

Nanofluids are two phase mixtures engineered by dispersing nanometer sized particles with sizes ranging below 100 nm in base fluids (Sarit K. Das et al. 2008). The nanometer sized particles which are used for the dispersion in base fluids are nanoparticles, nanofibers, nanotubes, nanowires and nanorods. Materials generally used as nanoparticles include metal oxides (e.g., alumina, silica, zirconia, titania), oxide ceramics (e.g. Al_2O_3 , CuO), chemically stable metals (e.g. gold, copper), carbon in various forms (e.g., diamond, graphite, carbon nanotubes, fullerene) metal carbides (e.g. SiC) and functionalized nanoparticles. The base fluid types include oils, water, organic liquids such as glycols, refrigerants, polymeric solutions, bio fluids, lubricants and other common liquids.

The fluids with nano sized solid particles suspended in them are called “nanofluids.” The suspended metallic or nonmetallic nanoparticles change the transport properties and heat transfer characteristics of the base fluid. Nanofluids are the new generation heat transfer fluids for various industrial and automotive applications because of their excellent thermal performance and the word was which was coined at Argonne National Laboratory of USA by Choi in 1995 [28], which showed that the conventional liquid thermal performance could be remarkably improved using nanoparticles.

Nanofluids can be used for a wide variety of engineering applications like transportation, thermal management of electronics, medical, food, defence, nuclear, space, and manufacturing of many types [29].

2. Benefits of using nanofluid:

- ❖ The nanoparticles have a very small particle size with a very large surface area, which result in a significant increase in the heat capacity of the nanofluid as well as the absorption of the solar energy.
- ❖ The optical characteristics of nanofluids are better than that of the base fluid (higher absorption and extinction coefficients). They show high absorption and low emittance in both solar spectrum range and in infrared spectrum range, respectively.
- ❖ The thermal conductivity of the nanofluids is significantly high compared to the base fluid due to the presence of nanoparticles.
- ❖ The good stability of nanofluids under wide range of temperature gradients combined with high absorption coefficient make nanofluids as an excellent absorbing medium.
- ❖ Use of nanofluids avoids the sedimentation, clogging, fouling of pipes and pumps due to its extremely small size compared with micro or millimeter sized particles, which is a useful property in many solar applications.
- ❖ Nanofluids reduce the required heat transfer area of the thermal devices and as a result reduce the total cost of the SESs.
- ❖ Nanofluids, in general, have high density and high convective heat transfer coefficient (HTC) with a low specific heat of nanoparticles which result in increasing the efficiency of the thermal devices.
- ❖ Due to nano size particles, pressure drop is minimum.
- ❖ Higher thermal conductivity of nanoparticles will increase the heat transfer rate.
- ❖ Successful employment of nanofluid will lead to lighter and smaller heat exchanger.
- ❖ Heat transfer rate increases due to large surface area of the nanoparticles in the base fluid.
- ❖ Nanofluids are most suitable for rapid heating and cooling systems.
- ❖ Due to nano size particles, fluid is considered as integral fluid
- ❖ Good mixture nanofluids will give better heat transfer.
- ❖ Micro channel cooling without clogging. Nanofluids are not only a better medium for heat transfer in general but they are also ideal for micro channel applications where high heat loads are needed.

3. Preparation Methods for Nanofluids:

Various methods have been tried to produce different kinds of nanoparticles and nano suspensions. There are two primary methods to prepare nanofluids: A two-step method in which nanoparticles or nanotubes are first produced as a dry powder. The resulting nanoparticles are then dispersed into a fluid in a second step and Single-step nanofluid processing method have also been developed and there are a novel methods also mentioned in this section.

3.1. Two-Step Method:

This method is the most widely used for preparing nanofluids. Nanoparticles, nanofibers, nanotubes, or other nanomaterials used in this method are first produced as dry powders by chemical or physical methods. Then, the nano-sized powder will be dispersed into a fluid in the second processing step with the help of intensive magnetic force agitation, ultrasonic agitation, high-shear mixing, homogenizing, and ball milling. Two-step method is the most economic method to produce nanofluids in large scale, because nanopowder synthesis techniques have already been scaled up to industrial production levels. Due to the high surface area and surface activity, nanoparticles have the tendency to aggregate. The important technique to enhance the stability of nanoparticles in fluids is the use of surfactants. However, the functionality of the surfactants under high temperature is also a big concern, especially for high-temperature applications. Due to the difficulty in preparing stable nanofluids by two-step method, several advanced techniques are developed to produce nanofluids, including one-step method. In the following part, we will introduce single-step method.

3.2. One-Step Method:

The nanoparticles may agglomerate during the drying storage, and transportation process, leading to difficulties in the following dispersion stage of two-step method. Consequently, the stability and thermal conductivity of nanofluid are not ideal. In addition, the production cost is high. To reduce the agglomeration of the nanoparticles, one-step methods have been developed. There are some ways for preparing nanofluids using this method including direct evaporation condensation [30,31], chemical vapour condensation [32], and single-step chemical synthesis.

3.3. Other Novel Methods:

Wei et al developed a continuous flow micro fluidic micro reactor to synthesize copper nanofluids. By this method, copper nanofluids can be continuously synthesized, and their microstructure and properties can be varied by adjusting parameters such as reactant concentration, flow rate, and additive. CuO nanofluids with high solid volume fraction (up to 10 vol%) can be synthesized through a novel precursor transformation method with the help of ultrasonic and microwave irradiation.

The precursor $\text{Cu}(\text{OH})_2$ is completely transformed to CuO nanoparticle in water under microwave irradiation. The ammonium citrate prevents the growth and aggregation of nanoparticles, resulting in a stable CuO aqueous nanofluid with higher thermal conductivity than those prepared by other dispersing methods. Phase-transfer method is also a facile way to obtain monodisperse noble metal colloids. Phase transfer method is also applied for preparing stable kerosene based Fe_3O_4 nanofluids. Oleic acid is successfully grafted onto the surface of Fe_3O_4 nanoparticles by chemisorbed mode, which lets Fe_3O_4 nanoparticles have good compatibility with kerosene. In a water cyclohexane two-phase system, aqueous formaldehyde is transferred to cyclohexane phase via reaction with dodecylamine to form reductive intermediates in cyclohexane. The intermediates are capable of reducing silver or gold ions in aqueous solution to form dodecylamine-protected silver and gold nanoparticles in cyclohexane solution at room temperature. Feng et al. used the aqueous organic phase transfer method for preparing gold, silver, and platinum nanoparticles on the basis of the decrease of the PVP's solubility in water with the temperature increase [30,31,32].

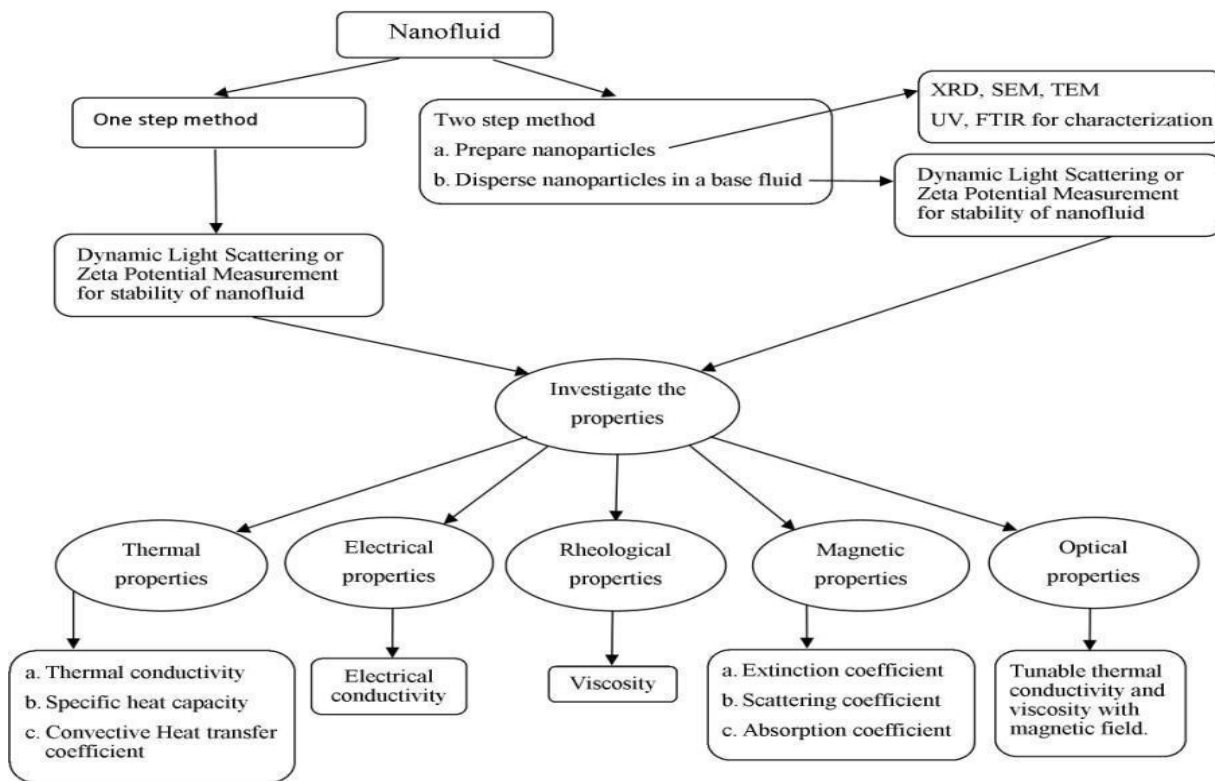


Fig. 1. Preparation, characterization and Investigated properties of nanofluid.

4. Properties of nanofluid:

The concept of adding small solid particles into a base fluid to increase the thermal conductivity of the suspension has been practiced for a long time. The Properties of nanofluids are Viscosity, Specific heat, Thermal Conductivity and Stability. These properties play a very important role in preparation of Nanofluids. The Properties are discussed below:

4.1 Viscosity:

Even though the literature on heat convection in nanofluids is limited compared to that in thermal conductivity, the results and approaches in the field are quite diverse, and worth mentioning. However, the understanding of the issues of convection is strictly related to the viscosity of the nanofluids.

In first place we need to understand that whether nanofluids are Newtonian or shear thinning is important. This question was addressed by the first work ever done on heat convection in nanofluids in 1998, by Pak and Cho[1]. They reported that the nanofluids behaved as Newtonian when 13 and 27 nm nanoparticles of $\gamma\text{Al}_2\text{O}_3$ and TiO_2 were suspended in water, but only for very low particle volume fractions. Shear thinning behavior was, however, detected with an increase of particle volume fraction. In particular, the Al_2O_3 -water nanofluid started showing shear thinning behavior at 3% particle volume fraction onward, while TiO_2 -water behaved as Newtonian up to 10%. Pak and Cho also observed a large increase in the viscosity of both nanofluids, and showed that this behavior was not predicted by standard empirical models for suspension viscosities, such as the one developed by Batchelor in 1977 [17,47]. In 1999, Lee et al. [29] reported similar substantial increase in viscosity for water- and ethylene glycol-based nanofluids with Al_2O_3 nanoparticles. They also mentioned that the confirmation of this finding might offset the enhanced heat transfer observed in nanofluids.

In 2003, however, Das et al. [30] conducted a similar study for a water- Al_2O_3 nanofluid, but reported no observation of shear thinning behavior. In particular, they confirmed Newtonian behavior of the nanofluid with 1% to 4% concentrations by volume. They also showed a linear trend of viscosity versus shear rate, even though viscosity values are still higher than the ones of pure water. Viscosity is also reported to increase with nanoparticle loading, but remains Newtonian in nature.

4.2 Specific Heat:

The specific heat for each nanofluid was measured in a Differential Scanning Calorimeter (DSC), model DSC1 (Mettler Toledo, USA). The calculation of the specific heat capacity is based in the DIN standard (DIN 51007), The sequence used in the determination was as follows: isotherm of 5 minutes at 25 0C, dynamic segment from 25°C to 95°C at heating rate of 10 0C/min and isotherm of 5 minutes

at 95 °C. Literature on experimental specific heats of nanofluids is very limited, In 2009, Namburu [14] reported that several ethylene glycol based nanofluids exhibit lower specific heat than their respective base fluids. Similarly, Bergman [15] reported experimental evidences that a water-alumina nanofluid appeared to have enhanced thermal conductivity, but lower specific heat, relative to the base fluid. Vajjha and Das studied nanofluids with 2–10% by volume of Al_2O_3 , SiO_2 , and ZnO nanoparticles in a 60:40 ethylene glycol-water mixture. They reported that the specific heat of all their nanofluids decreases substantially as the volumetric concentration of nanoparticles increases, and it increases moderately with temperature. Lower specific heat has also been reported in the numerical work of Puliti et al. [17]. In one case, no anomalous specific heat was observed, and classic theories were able to predict the nanofluid density and specific heat within a 10% deviation.

Conflicting results to the ones mentioned above, however, have also been reported. Nelson et al. Observed that the specific heat of polyalphaolefin is increased by 50% with a dispersion of exfoliated graphite nanoparticles at a concentration of 0.6% by weight. Similarly, Shin and Banerjee reported a 26% enhancement of the specific heat of a molten salt (eutectic of 62% lithium carbonate and 38% potassium carbonate) with a suspension of silica nanoparticles at a concentration of 1% by weight. However, other contradictory results were reported by Zhou and Ni [20]; they observed that the specific heat of an alumina-water nanofluid decreased by 40–50% at a concentration of 21.7% by volume of nanoparticles. Shin and Banerjee [21] commented on the results by Zhou and Ni, pointing out that alumina nanoparticles tend to cluster, and the authors did not report if the nanoparticles were well dispersed. In fact, agglomerated alumina nanoparticles tend to precipitate out of the water solution; consequently degrading the thermal properties of the nanofluid. More recently, Shin and Banerjee reported a 14.5% enhancement in the specific heat of a chloride salt eutectic, using a dispersion of 1% by weight of silica nanoparticles (20–30 nm nominal diameter). In this case, the dispersion behavior of the nanoparticles was confirmed by scanning electron microscopy.

Shin and Banerjee proposed three independent thermal transport mechanisms to explain the unusual enhancement of the specific heat they observed:

- (1) Mode 1: the specific heat is enhanced due to higher specific surface energy of the surface atoms of the nanoparticles, as compared to the bulk material. The surface energy is higher because of the low vibration frequency and higher amplitudes of the vibrations at the surface of the nanoparticles.
- (2) Mode 2: the enhancement of the specific heat can also be due to additional thermal storage mechanisms due to interfacial interactions between nanoparticles and the liquid molecules, which act as virtual spring-mass systems. This interfacial effect is present due to the extremely high specific surface area of the nanoparticles.

(3) Mode 3: a third mechanism potentially involved is liquid layering, already discussed earlier with regards to the thermal conductivity enhancement. Solidlike liquid layers adhering to the nanoparticles are more likely to have an enhanced specific heat due to a shorter intermolecular mean free path compared to the bulk fluid. Because the specific heat is a key thermal property for many engineering applications, there is a great need for additional experimental results on this fundamental property for nanofluids.

4.3 Thermal conductivity:

One of the important aspects of heat transfer characteristics of cooling fluid is the thermal conductivity. Thermal conductivity of nanofluids varies dependent on different parameters, such as particle volume fraction, particle material, particle size, particle shape, type of base fluid, and temperature. Each of the parameters is discussed separately in the later sections.

4.3.1 Effect of particle volume fraction:

For the past research conducted on nanofluids it is observed that the enhancement in thermal conductivity increases with particle volume fraction. Ding et al [23] produced CNT–water nanofluids with 0.25 wt% of gum arabic (GA) as dispersant. Results show an increased thermal conductivity ratio of 1–1.8 at 0–1 wt% of CNT concentration. Wen and Ding[24] prepared CNT–water nanofluids and observed a 25% enhancement in thermal conductivity at 0.8 wt%. Linear independence of thermal conductivity was obtained up to 0.2 vol.%, but saturation begins to occur at this point. Assael et al performed studies using MWCNT–water nanofluids, and an enhancement of 34–36% was observed at a particle volume of 0.6 vol.%. Liu et al [25] observed a thermal conductivity enhancement of 12.4–30.0% with 1–2 vol.% of CNT nanoparticles in EG and engine oil (EO), respectively. Hwang et al[26] performed studies using different types of nanoparticle such as MWCNTs, CuO and SiO₂ in water and EG The highest thermal conductivity enhancement was observed for an MWCNT–water nanofluid: 11.3% at 1 vol.%. A similar study was performed by Choi et al[27] using a CNT in oil mixture. An enhancement ratio of greater than 2.5 or 160% was observed in 1 vol.% of nanofluid

3.3.2. Effect of particle material:

Various studies conducted in the past concluded that particle material also greatly contributes towards the thermal conductivity enhancement of nanofluids. The difference in thermal conductivities of

particle material and particle type could be the factor that affects the thermal conductivities of nanofluids. Studies performed by Hwang et al using different type enhancement was observed for an MWCNT–water nanofluid compared to any other nanoparticles. This is due to the fact that MWCNTs possess the highest thermal conductivity of $3000\text{Wm}^{-1}\text{K}^{-1}$ compared to other nanoparticles. Furthermore, Chopkar et al[33] dispersed Al_2Cu and Ag_2Al nanoparticles into water and EG, and results showed that Ag_2Al nanoparticles enhanced thermal conductivity slightly more when compared to Al_2Cu nanoparticles. Theoretically, Ag_2Al possesses a higher thermal conductivity than Al_2Cu . Similarly, based on studies performed by Lee et al[34], they found that CuO nanoparticles possess higher thermal conductivity enhancement compared to Al_2O_3 nanoparticles. However, Al_2O_3 itself has a higher thermal conductivity than CuO. Justification in both cases above could be obtained from the experimental work done by Lee et al[34]. In their experiments, it was observed that Al_2O_3 nanoparticles formed relatively larger clusters when compared to CuO nanoparticles. According to the theory of Brownian motion of nanoparticles, the effect of Brownian motion reduces at higher particle size. Therefore, enhancement of thermal conductivity could be lower. Recently, Pang et al[35] conducted a study by dispersing Al_2O_3 and SiC in methanol. Enhancement was observed to be 10.74% and 14.29% over base fluid at 0.5 vol.% for Al_2O_3 and SiO_2 nanoparticles, respectively. Similarly, Al_2O_3 has higher thermal conductivity than SiO_2 . The effect of clustering is another factor which explains why SiO_2 nanofluid possesses higher thermal conductivity than Al_2O_3 although Al_2O_3 materials possess higher thermal conductivity than SiO_2 . The thermal conductivities of nanofluids were much higher when CNTs were dispersed in different base fluids. Choi et al[36] studied the enhancement of thermal conductivity by dispersing CNT nanoparticles in oil mixture. A very high enhancement of ratio 2.5 or 160% was observed at 1 vol.%. Such high enhancement could be related to the superior characteristic of CNT nanoparticles. With an L/D ratio of approximately 132 000 000, a large amount of heat can be transported ballistically inside the nanotubes, hence improving the conduction of heat in CNT particles. s of nanoparticle such as MWCNTs, CuO and SiO_2 in water and EG conclude that the highest thermal conductivity

3.3.3 Effect of base fluid:

According to the conventional effective medium theory (Maxwell, 1873), as the base fluid thermal conductivity decreases, the effective thermal conductivity of a nanofluid increases. Most of the experimental reports agree with the theoretical values given by this conventional mean field model. As per Wang *et al.*'s (1999) results on the thermal conductivity of suspensions of Al_2O_3 and CuO nanoparticles in several base fluids such as water, ethylene glycol, vacuum pump oil and engine oil, the highest thermal conductivity ratio was observed when ethylene glycol was used as the base fluid. EG has comparatively low thermal conductivity compared to other base fluids. Engine

oil showed somewhat lower thermal conductivity ratios than Ethylene Glycol. Water and pump oil showed even smaller ratios respectively. However, CuO/EG as well as CuO/water nanofluids showed exactly same thermal conductivity enhancements at the same volume fraction of the nanoparticles. The experimental studies reported by Xie *et al.* (2002b) also supported the values given by the mean field theory.

3.3.4 Effect of particle size:

The advent of nanofluids offers the processing of nanoparticles of various sizes in the range of 5-500 nm. It has been found that the particle sizes of nanoparticles have a significant role in deciding the effective thermal conductivity of nanofluids. There are many studies reported in literature regarding the dependence of nanoparticle size on effective thermal conductivity of nanofluids. Chopkar *et al.* (2006) studied the effect of the size of dispersed nanoparticles for Al₇₀Cu₃₀/EG nanofluids by varying the size of Al₇₀Cu₃₀ nanoparticles in the range from 9 nm to 83 nm. In another study on water and EG based nanofluids consisting of Al₂Cu and Ag₂Al nanoparticles, Chopkar *et al.* (2008) also investigated the effect of particle size on effective thermal conductivity of nanofluids. In all these cases it has been found that the effective thermal conductivity of a nanofluid increases with decreasing nanoparticle size. Also, the results of Eastman *et al.* (2001) and Lee *et al.* (1999) support this conclusion drawn by Chopkar *et al.* (2008) on the particle size effect on the effective thermal conductivity of nanofluids. In another study of the effect of particle size on the thermal conductivity of nanofluids, reported by Beck *et al.* (2009) in water as well as EG based nanofluids consisting of Al₂O₃ nanoparticles, the normalized thermal conductivity of nanofluids vary in such a way that it decreases with decreasing the nanoparticle size. Thus conflicting reports have appeared in literature on the dependence of particle size on the thermal conductivity of nanofluids.

3.3.5 Effect of particle shape:

For experimentation, spherical as well as cylindrical shaped nanoparticles are commonly used for nanofluid synthesis. The cylindrical particles have larger aspect ratio (length to diameter ratio) than spherical particles. The wide differences in the dimensions of these particles do influence the enhancement in effective thermal properties of nanofluids. Xie *et al.* (2002a) measured the thermal conductivity of water as well as EG based nanofluids consisting of both cylindrical as well as spherical SiC nanoparticles. It was observed that in water based nanofluids, the cylindrical suspensions had higher thermal conductivity enhancement of about 22.9% than the spherical particles for the same volume fraction (4.2%). Also the theoretical values based on Hamilton-Crosser model (1962) are found to be in good agreement with this comparatively higher enhancement for cylindrical particle suspensions. Another experimental study reported by Murshed *et al.* (2005) in water based nanofluids

consisting of spherical as well as rod shaped TiO₂ nanoparticles showed a comparatively higher enhancement for rod shaped particles (32.8%) than spherical particles (29.7%) at a volume fraction of 5%. In addition to these experimental results a general observation is that nanotube suspensions show a higher enhancement than the spherical particle suspension due to rapid heat transfer along a larger distance through a cylindrical particle since it has a length of the order of a micrometer. However, the cylindrical particle suspension need higher pumping power due to its enhanced viscosity (Timofeeva *et al.*, 2009) which limits its usage, possible application as a heat transfer fluid.

4.4 Stability of Nanofluids:

The stability of the nanofluids was analysed through the evolution of the amount of light backscattered by the nanofluid from an incident laser beam. A Turbiscan Lab Expert (Formulation SA, France) was used to carry out the tests. Measurements are based on the multiple light scattering theory. This equipment consists of a pulsed near-infrared light source and a detector that measures the light backscattered by the sample. For each nanofluid, the backscattering profiles were obtained along the height cell. To analyse the stability of nanofluids the measurements were carried out at different time intervals up to a total time of 48 hours. Many methods have been developed to evaluate the stability of nanofluids. The simplest method is sedimentation method. The sediment weight or the sediment volume of nanoparticles in a nanofluid under an external force field is an indication of the stability of the characterized nanofluid. The variation of concentration or particle size of supernatant particle with sediment time can be obtained by special apparatus. The nanofluids are considered to be stable when the concentration or particle size of supernatant particles keeps constant. Sedimentation photograph of nanofluids in test tubes taken by a camera is also a usual method for observing the stability of nanofluids. Zhu *et al.* used a sedimentation balance method to measure the stability of the graphite suspension. The tray of sedimentation balance immersed in the fresh graphite suspension. The weight of sediment nanoparticles during a certain period was measured. The suspension fraction of graphite nanoparticles at a certain time could be calculated. For the sedimentation method, long period for observation is the defect. Therefore, centrifugation method is developed to evaluate the stability of nanofluids. Singh *et al.* applied the centrifugation method to observe the stability of silver nanofluids prepared by the microwave synthesis in ethanol by reduction of Ag NO₃ with PVP as stabilizing agent. It has been found that the obtained nanofluids are stable for more than 1 month in the stationary state and more than 10 h under centrifugation at 3,000 rpm without sedimentation. Excellent stability of the obtained nanofluid is due to the protective role of PVP, as it retards the growth and agglomeration of nanoparticles by steric effect. Li prepared the aqueous polyaniline colloids and used the centrifugation method to evaluate the stability of the colloids. Electrostatic repulsive forces between nanofibers enabled the long-term stability of the colloids.

5. APPLICATIONS OF NANOFLUIDS:

5.1 Liquid cooling

Cooling is the major technical challenge facing high tech industries such as microelectronics, metrology, manufacturing and transportation. It is highly desirable for the maintenance of various electronic products at desired operating temperatures for long life time and proper functioning. The cooling performance was significantly enhanced with the aid of nanofluids (Lee and Choi 1996). In the realm of electronics cooling, the industrialists started using nanofluids instead of conventional liquids. In addition, nanofluids could effectively remove hot spots and maintain components at uniform temperatures. Considering the range of efforts to extend liquid cooling technologies and the superior thermal properties, nanofluids would be utilized for hot spot cooling systems for computer, high heat flux, telecom, defence and power electronics uses.

5.2 Crystal Silicon Mirror Cooling

An advanced cooling technology was developed using nanofluids to cool crystal silicon mirrors (Lee and Choi 1996) in high intensity x-ray sources was one among the initial applications in the field of nanofluid research. Lee and Choi performed analysis for the estimation of better performance of microchannel heat exchangers with liquid nitrogen, conventional water and finally nanofluids as working fluids. Their research efforts showed that nanofluids could significantly increase power densities and reduce thermal resistances. Furthermore, the chance of flow induced vibration and thermal distortion were much eliminated by passing nanofluids through microchannels within the silicon mirror. The researchers also investigated that power densities of around 3000 W/cm^2 for high aspect ratio microchannels were accomplished with nanofluids.

5.3 Vehicle Cooling:

Nanoparticles could not only be dispersed in engine oils and coolants, but also in gear oils, lubricants, transmission fluids and other fluids as well. These nanofluids provide better insight into thermal management system and better lubrication. Tzeng et al. (2005) were the pioneers by using nanofluid technology in automatic power transmission system. In their research work, Al_2O_3 and CuO nanoparticles were dispersed in transmission oil to investigate the optimum possible compositions of nanofluid for enhanced heat transfer performance. The temperature distribution of the RBC exterior

were measured at four varying rotating speeds (400, 800, 1200, and 1600 rpm) and the conditions of real car at various rotating speeds were simulated. The investigations revealed that better heat transfer effect was achieved with CuO nanofluids and they have the efficiency of lowest temperature distribution at both low and high rotating speeds. This work is vital since it shows real world application of nanofluids representing a greater step forward for industrial applications of nanofluids.

5.4 Space and Nuclear Systems Cooling :

Vassallo et al. (2004) and You et al. (2003) explained the unprecedented phenomenon that nanofluids could able to increase the critical heat flux (CHF) by triple fold measure in pool boiling. Kim et al. (2006) found that the high surface wettability produced by nanoparticle addition could demonstrate remarkable thermal properties of nanofluids. Experimental investigation is required in developing realistic predictive models of CHF in nanofluids. The upper heat flux limit in nucleate boiling systems and the ability to increase the CHF, is of paramount practical importance to ultrahigh heat flux devices that use nucleate boiling, such as nuclear reactor components and high power lasers. Hence, nanofluids have raised up exciting possibilities for simplifying cooling requirements for space applications and increasing chip power in electronic devices. The Massachusetts Institute of Technology (MIT), United States has established an interdisciplinary centre for nanofluid technology for the nuclear energy industry. The researchers were evaluating the vital impact of the use of nanofluids on the safety, economic and neutronic performance of nuclear systems.

5.5 Defense Applications :

Numerous military systems and devices, such as military vehicle components radars, high powered military electronics, lasers, require high heat flux cooling to the level more than 1000 W/cm^2 . Cooling with conventional heat transfer fluids at this high level is much difficult. Nanofluid technology also provides advanced cooling systems for military combat vehicles, high-power laser diodes and submarines. It seems that nanofluid research in defense applications considers energy harvesting through chemical reactions or multifunctional nanofluids with added thermal energy storage.

5.6 Tribological Applications :

Nanofluid technology was applied in developing better lubricants and oils. Li et al. (2004) reported performance on lubricant nanofluids containing ZrO_2 and IrO_2 nanoparticles. The experimental results showed that nanoparticles decreases friction on the surface of 100 C6 steel. Que et al. (1997) reported that surface modified nanoparticles stably dispersed in mineral oils are very effective in enhancing load-carrying capacity and reducing wear in lubrication application.

5.7 Biomedical Applications :

Nanofluids were also developed for medical treatments, including cancer therapy. Iron-based nanofluids could be used to produce higher temperatures around the tumor cells, by killing cancerous cells without affecting the nearby healthy tissues (Jordan et al. 1999). Nanofluids could also be used for safer surgery by cooling around the surgical region, thereby enhancing a patient's chance of survival and reducing the risk of organ damage.

References:

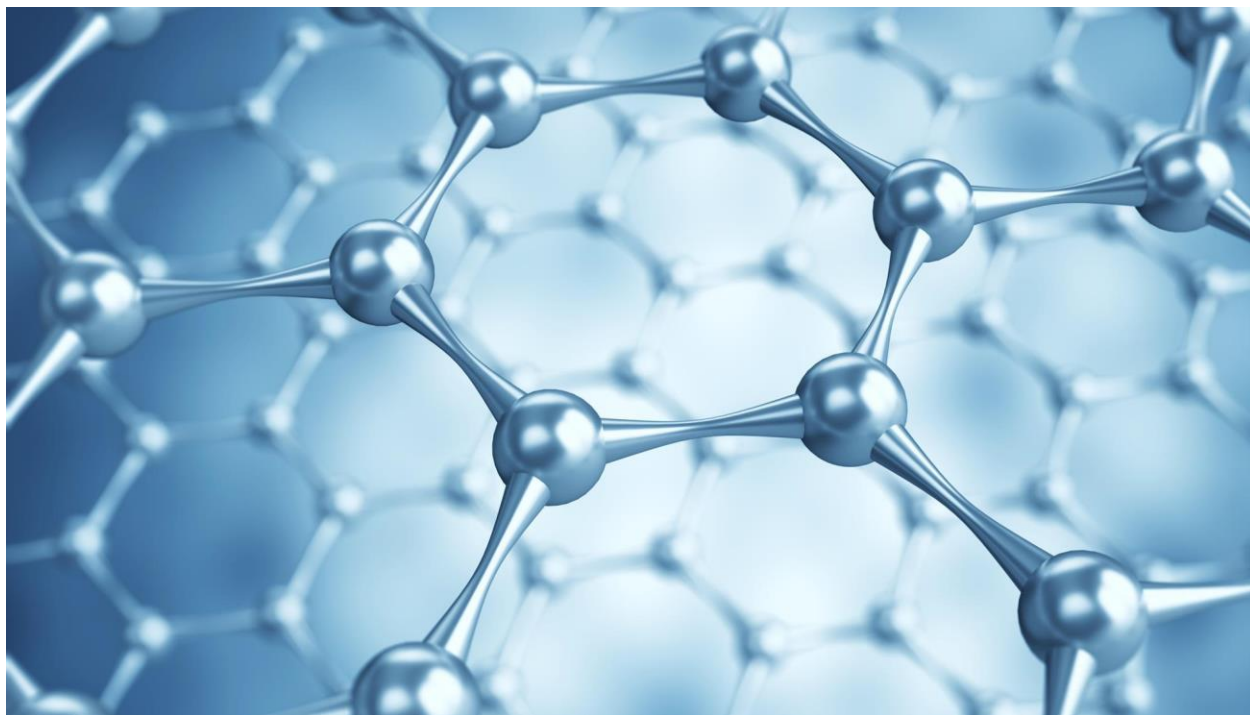
1. Hecht, David. "Printable power using carbon nanotube supercapacitors: Nanotechnology." (2009): 10.
2. Mohapatra, S., A. Acharya, and G. S. Roy. "The role of nanomaterial for the design of supercapacitor." *Lat. Am. J. Phys. Educ. Vol 6.3* (2012): 380.
3. Du, Chunsheng, and Ning Pan. "Carbon nanotube-based supercapacitors." *Nanotech. L. & Bus.* 4 (2007): 3.
4. Meng, Chui-Zhou, Chang-Hong Liu, and Shou-Shan Fan. "Carbon nanotube based supercapacitor." U.S. Patent No. 8,488,300. 16 Jul. 2013.
5. Boyea, J. M., et al. "Carbon nanotube-based supercapacitors: technologies and markets." *Nanotech. L. & Bus.* 4 (2007): 19.
6. Chen, Tao, and Liming Dai. "Carbon nanomaterials for high-performance supercapacitors." *Materials Today* 16.7 (2013): 272-280.
7. Habibi, Y., L. Lucia, and O. J. Rojas. "Carbon nanomaterials for highperformance supercapacitors." *Materials Today* 110 (2010): 3479-3500.
8. Aricò, Antonino Salvatore, et al. "Nanostructured materials for advanced energy conversion and storage devices." *Nature materials* 4.5 (2005): 366-377.
9. Gogotsi, Yury, and Patrice Simon. "True performance metrics in electrochemical energy storage." *Science* 334.6058 (2011): 917-918.
10. Harman, Grant. "Australian university research commercialisation: perceptions of technology transfer specialists and science and technology academics." *Journal of Higher Education Policy and Management* 32.1 (2010): 69-83.
11. Halper, Marin. "Supercapacitors and Other Nano-Enabled Energy Systems." (2006).

12. Yu, Aiping, Victor Chabot, and Jiujun Zhang. Electrochemical supercapacitors
13. Shukla, A. K., and K. Martha. "Electrochemical power sources." *Resonance* 6.8 (2001):
14. Barak, Monty, ed. *Electrochemical power sources: primary and secondary batteries*. No. 1. IET, 1980.
15. Martin Winter, and Ralph J. Brodd, *Chem. Rev.* 2004, 104, 4245–4269
16. Vajjha, R. S., and Das, D. K., 2009, —Specific Heat Measurement of Three Nanofluids and Development of New Correlations, *J. Heat Transf.*, 131(7), p. 071601
17. Puliti, G., Paolucci, S., and Sen, M., 2011, —Thermodynamic Properties of Gold-Water Nanolayer Mixtures Using Molecular Dynamics, *J. Nanopart. Res.*, 13(9), pp. 4277–4293.
18. Nelson, I. C., Banerjee, D., and Ponnappan, R., 2009, —Flow Loop Experiments Using Polyalphaolefin Nanofluids, *J. Thermophys. Heat Transfer*, 23(4), pp. 752–7
19. Shin, D., and Banerjee, D., 2011, —Enhancement of Specific Heat Capacity of High-Temperature Silica-Nanofluids Synthesized in Alkali Chloride Salt Eutectics for Solar Thermal-Energy Storage Applications, *Int. J. Heat Mass Transfer*, 54(5–6), pp. 1064–1070.
20. Zhou, S.-Q., and Ni, R., 2008, —Measurement of the Specific Heat Capacity of Water-. Based Al₂O₃ Nanofluid, *Appl. Phys. Lett.*, 92(9), p. 093123
21. Shin, D., and Banerjee, D., 2011, —Enhanced Specific Heat of Silica Nanofluid, *J. Heat Transfer*, 133(2), p. 024501
22. Ding Y, Alias H, Wen D and Williams R A 2005 Heat transfer of aqueous suspensions of carbon nanotubes (CNT nanofluids) *Int. J. Heat Mass Transfer*
23. Wen D and Ding Y 2004 Effective thermal conductivity of aqueous suspensions of carbon nanotubes (carbon nanotube nanofluids) *J. Thermophys. Heat Transfer*

23. Assael M J, Metaxa I N, Arvanitidis J, Christofilos D and Lioutas C 2005 Thermal conductivity enhancement in aqueous suspensions of carbon multiwalled and double-walled nanotubes in the presence of two different dispersants *Int. J. Thermophys.*
24. Jana S, Salehi-Khojin A and Zhong W H 2007 Enhancement of fluid thermal conductivity by the addition of single and hybrid nano-additives *Thermochimica Acta*
25. Babu K and Kumar P T S 2011 Effect of CNT concentration and agitation on surface heat flux during quenching in CNT nanofluids *Int. J. Heat Mass Transfer* Choi S U S, Zhang Z G, Yu W, Lockwood F E and Grulke E A 2001 Anomalous thermal conductivity enhancement in nano-tube suspensions *Appl. Phys. Lett.*
26. Das S K, Putta N, Thiesen P and Roetzel W 2003 Temperature dependence of thermal conductivity enhancement for nanofluids *ASME Trans. J. Heat Transfer*
27. Choi SUS. Enhancing thermal conductivity of fluids with nanoparticles. *ASME FED-Vol. 231/MD*
28. Wong KV, Leon OD. Applications of nanofluids: current and future. *Advances in Mechanical Engineering* 2010(ID 519659):pp 11.
29. J. A. Eastman, U. S. Choi, S. Li, L. J. Thompson, S. Lee, *Proceedings of the Materials Research (Nanophase and Nanocomposite Materials II)*, 1997.
30. J. A. Eastman, S. U. S. Choi, S. Li, G. Soyez, L. J. Thompson, R. J. DiMelfi, J. Metastab. *Nanocryst.* 2(1998) 629.
31. V. V. Srdic, M. Winterer, A. Miller, G. Miehe, H. Hahn, *J. Am. Ceram. Soc.* 84 (2001) 277.
33. H. T. Zhu, C. Y. Zhang, Y. M. Tang, and J. X. Wang, "Novel synthesis and thermal conductivity of CuO nanofluid," *Journal of Physical Chemistry C*, vol. 111, no. 4, pp. 1646–1650, 2007.

Chapter- 3

Review Of Past Work



Review of Past work

1. Introduction:

The rapid development of human civilization and industrialization has brought serious issues associated to our daily life and universal economy [1,2]. The protection of environment and utilization of energy are currently the most important challenges to our universe. Energy is an important input for the economic growth of a nation and environmental quality. Generally, our major energy sources are non-renewable which include fossil fuels such as coal, oil, natural gas, etc. Over 80% of our current energy usage is provided by fossil fuels. However, the burning of fossil fuels raises the amount of carbon dioxide (CO₂) emission which is a major cause of climate change and global warming. Also, the extensive use of fossil resources contribute to major pollution of the environment [3,4]. Therefore, it is an urgent necessity for the expansion of sanitary renewable energy sources to replace the fossil resources. Renewable energy sources includes sunlight, wind, tides, hydro, geothermal heat and biofuels. Among these, solar energy (sun light) is abundantly available at free of cost and adjustable to numerous applications [5]. For example, solar energy can be utilized by photo-catalysts to degrade organic pollutants, reduce CO₂ into renewable hydrocarbon solar fuels and for the production of hydrogen by water splitting [6–8]. The pollution caused by textile, cosmetics and food industries that use organic dyes which are the primary sources for contaminating aqueous environment due to their toxicity and non-biodegradability. The photocatalytic degradation is considered as an effective way for the removal of such organic pollutants from waste-waters. Therefore, it is necessary to develop highly active catalytic materials to solve critical problems related to energy and environment.

Various electrochemical energy conversion and storage technologies such as solar cells, Li-ion battery, supercapacitor and hydrogen evolution reaction are becoming more useful techniques to overcome the imminent shortage of nature resources and growing environmental pollution [9]. The performance of all these techniques depends on the properties of the materials used. Therefore, it is necessary to develop an appropriate material to solve the critical problems related to energy and environment.

Molybdenum disulfide (MoS_2) is a type of layered transition metal dichalcogenide. Due to its structural similarities to graphene, it has drawn enormous attention for various applications such as dye-sensitized solar cells, supercapacitor, Li-ion battery, hydrogen evolution reaction, photocatalysis for the degradation of organic pollutants, sensors etc. MoS_2 shows similar physical properties to that of graphene that include high charge carrier transport, high wear resistance, etc.

However, MoS_2 has superior properties over graphene such as low cost, more abundant, tuneable band gap with good visible light absorption capacity. In the bulk MoS_2 crystal structures, layers of Mo atoms are sandwiched between two layers of closely packed S atoms forming layered structure in the form of S-Mo-S. Strong covalent bonding characterizes the Mo-S interaction and the interactions between S layers are vander Waals forces [10,11]. Thus, the structure allows introducing other ions or molecules in between S-Mo-S layers. The wide applications of MoS_2 originate from their superior physical/chemical properties, which can be tailored to different morphologies, particle dimensions, and heterostructures.

1.1 Preparation methods of MoS_2 :

In order to enhance desired properties, the selection of an effective fabrication method should be the first and pivotal step. Numerous methods have been employed to prepare MoS_2 , in order to optimize its properties and achieve the superior performance. Examples of materials prepared from a top-down approach have been based on the exfoliation of bulk MoS_2 , [12-14] such as mechanical cleavage, chemical intercalation followed by exfoliation, [14-16] liquid phase exfoliation by direct sonication, and laser thinning techniques. Meanwhile, examples of bottom-up approaches are CVD growth and chemical synthesis.

1.2 Top Down approach:

MoS_2 nanosheets containing tens to hundreds of crystal 2D layers can be achieved via mechanical cleavage from the bulk MoS_2 . Novoselov et al. successfully applied this method to prepare single-layer MoS_2 from the bulk. [17] After a fresh surface of a layered bulk crystal was rubbed against a Si/SiO₂ surface, flakes with various thicknesses of MoS_2 were detached and adsorbed onto the target surface. Single-layer MoS_2 sheets could be further obtained from the thicker flakes, which was confirmed by scanning electron microscopy (SEM).

Although mechanical cleavage can produce 2D MoS₂ with high quality, low throughput limits this method in practical applications. To obtain the large quantities of single-layer MoS₂ sheets, the solution-based exfoliation methods are often used. Recently, some research groups have developed chemical or electrochemical Li-intercalation and exfoliation intercalation methods to produce MoS₂ nanosheets.[18]

For reliable and scaled-up production of atomically thin MoS₂ nanosheets, some studies demonstrated that the exfoliation process can be achieved by sonicating the bulk in various liquid phases, such as N-methylpyrrolidone[19] dimethyl-formamide,[20],[21] or a mixture of ethanol and water.[22] These liquid phases can not only exfoliate MoS₂ but also stabilize the nanosheets to some given extent due to their effect on the surface energy. In addition, liquid-phase exfoliation has been extended to the application of surfactant-containing solutions.[23] Accordingly, these methods hold great promise for scaled-up production of layered MoS₂ in environmentally benign solutions.

1.3 Bottom up approach:

Because of the violent nature of the chemical exfoliation, the crystal structure becomes deformed. However, large-area MoS₂ with mono- or several-layer structures can be prepared by using the chemical vapor deposition (CVD) method. Compared with chemical exfoliation, the CVD method is more efficient in growing MoS₂ monolayer films on substrates (SiO₂ /Si) [24] or Au [25], with high quality and controllable thickness.[26,27] Moreover, the formation of the continuous MoS₂ films by CVD is compatible with the current electronic fabrication processes, making this a promising candidate for building atomically thin layered electrical,[28] photovoltaic, [29] Optical [30]Or HER [31] devices. A two-step thermolysis process was recently reported for deposition of ultrathin MoS₂ nanosheets by dip-coating of ammonium thiomolybdates on Si/SiO₂ foils and converting the films to MoS₂ by annealing at 500^o C followed by sulfurization at 1000^o C under sulphur vapor. Typically, MoO₃ and sulfur powders are used as precursors for deposition of MoS₂ films on acetone and isopropanol-cleaned Si/SiO₂ foils. Upon heating, the reaction of volatile suboxides (MoO_{3-x}) with the sulfur vapor gave MoS₂ layers on the substrate. Using refined CVD, crystalline islands of monolayer molybdenum disulphide with high carrier mobility were grown up to 120 mm lateral size, which had the potential to provide superior optical or electrical properties to those of exfoliated samples.[30]

1.4 Properties of MoS₂:

Crystal properties:

Naturally, MoS₂ can form a phase with trigonal prismatic or an octahedral Mo coordination. 2H and 3R MoS₂ both correspond to trigonal prismatic coordination.

The 2H type, which is dominant and more stable in nature, has two layers per unit cell stacked in the hexagonal symmetry. The 3R-type has three layers per cell in rhombohedral symmetry, and is unstable and easily transforms to 2H upon heating. In most studies, MoS₂ with 2H crystal structure has been used as a precursor to prepare mono- or few-layer MoS₂ nanosheets.

Meanwhile, the

shift of one of the sulfur layers leads to an AbC stacking sequence, resulting in the generation of the 1T crystal phase, which has trigonal symmetry and corresponds to octahedral coordination of the metal atoms (Fig 1). Generally, the filling of Mo d orbitals is directly influenced by the structure of MoS₂. For the trigonal prismatic phase (2H), the d orbital splits into three degenerate states with an energy gap of 1 eV, while the d orbitals degenerate into other forms of orbitals in the tetragonal symmetry of the 1T phase, and up to six electrons can fill the e_g orbital. [31]

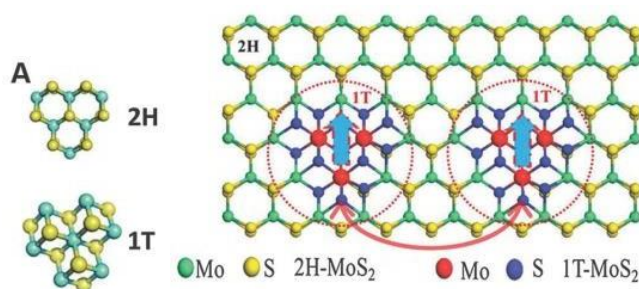


Fig 1 : The 2H and 1T phase of MoS₂, and diagrammatic representation of the phase incorporation of the 1T phase in 2H-MoS₂ nanosheets.

As shown in Fig. 2, because the p orbitals of sulfur are at much lower energy than the Fermi level, the filling of d orbitals determines the nature of the different phases in MoS₂ compounds. Complete filling of orbitals gives rise to semiconducting behaviour (2H) while partial filling results in metallic behaviour (1T).[32] Thus, as orbital occupation varies, the electronic

properties of MoS₂ gradually change from metal, to semiconductor, to topological insulator, and this provides a diversity of physical and chemical properties for a wide variety of applications.

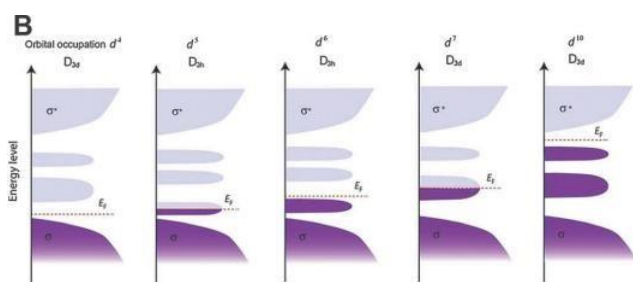


Fig 2: Qualitative schematic illustration showing progressive filling of d orbitals that are located within the bandgap of bonding (s) and anti-bonding states (s*) in group 4, 5, 6, 7 and 10 TMDs. D 3h and D 3d refer to the point groups associated with the trigonal prismatic and octahedral coordination of the transition metals. When an orbital is partially filled (such as in the case of group 5 and 7 TMDs), the Fermi level (E_F) is within the band and the compound exhibits a metallic character. When an orbital is fully filled (such as in group 6 TMDs), the Fermi level is in the energy gap and a semiconducting character is observed. Copyright 2015, American Chemical Society.

1.5 Electrical and optical properties:

The band structures of MoS₂ materials can be calculated based on density functional theory (DFT). When the bulk is reduced to a single layer, it had been predicted that an indirect to direct bandgap transition would occur in the d-electron system. Bulk MoS₂ is an indirect-gap semiconductor having a bandgap of about 1 eV, with a valence band maximum (VBM) at the G point and a conduction band minimum (CBM) at the mid-point along G–K symmetry lines (Fig. 3), while the monolayer form is a direct-gap semiconductor with VBM and CBM coinciding at the K-point. [33] Splendiani et al. reported on the thickness-dependent physical properties of MoS₂. [34] Combined with optical absorption, photoluminescence (PL), and photoconductivity, the evolution of electronic structure and the resulting optical properties of ultrathin MoS₂ crystals were observed as a function of the number of layer numbers. The crossover from an indirect gap material to a direct gap material accounted for the enhancement of luminescence

in the MoS₂ monolayer. The observed dependence of the bandgap on the layer number was in agreement with band calculations. Furthermore, the bandgap transition was derived from quantum confinement effects, resulting in pronounced differences in the emissions from photo-excitation in the bulk and monolayer material. As depicted in Fig. 4, the bulk showed negligible photoluminescence, while thinner exhibited much stronger PL signals.[35,36]

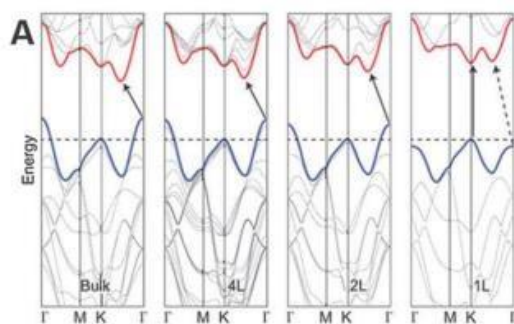


Fig 3: Energy dispersion (energy versus wavevector k) in bulk, quadrilayer (4L), bilayer (2L) and monolayer (1L) MoS₂ from left to right. The horizontal dashed line represents the energy of a band maximum at the K point

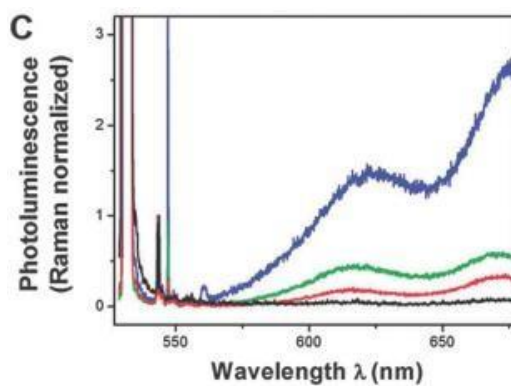


Fig 4 : Photoluminescence spectra normalized by Raman intensity for MoS₂ layers with different thicknesses, showing a dramatic increase of luminescence efficiency in the MoS₂ monolayer. Copyright 2010, American Chemical Society. (C) Raman spectra of thin and bulk MoS₂ films.

2. Review of Supercapacitor works

Metal sulfides are known to be electrochemically active materials for supercapacitor applications due to their high surface area and large in-plane conductivity [37,38]. For example, VS₂ nanosheets have been employed as in plane supercapacitor electrodes and revealed a considerable specific electric capacitance of 4.76 mF cm⁻² with an excellent cycling behavior even after 1000 charge/discharge cycles [39]. Supercapacitor electrodes based on CoS₂ ellipsoids were found to show a high capacitance of 1040 Fg⁻¹ at 0.5 A g⁻¹ [40]. Similarly, Yang et al. [41] demonstrated notable electrochemical performance of hierarchical flower like NiS. The material established a high capacitance of 857.76 F g⁻¹ at 0.5 A g⁻¹ because of their large surface area. Recently a family of two-dimensional (2D) layered materials produced from transition metal dichalcogenides, such as tungsten sulfide (WS₂) and molybdenum disulfide (MoS₂), have attracted much attention in supercapacitors because of their unique chemical and physical properties [42,43]. Particularly, the 2D layered material MoS₂ has received much attention in the field of supercapacitors due to its analogous structure to graphite. MoS₂ composed of three atom layers: a Mo layer sandwiched between two S layers, and the triple layers are stacked and held together by weak van der Waals interactions that allows easy intercalation of foreign ions (H⁺, Li⁺) [44]. MoS₂ is expected to exhibit good pseudocapacitive properties due to its sheet like morphology, which provide large surface area for double-layer charge storage with Mo can exhibiting a range of oxidation states from

+2 to +6 [45]. In addition, MoS₂ has the advantages of higher intrinsic fast ionic conductivity (than oxides) and higher theoretical capacity (than graphite). Charge storage in MoS₂ thin films can potentially occur via three main modes: (i) intersheet double-layer charge storage, (ii) intra sheet double-layer charge storage on individual atomic MoS₂ layers via diffusion into the basal edges, and (iii) faradaic charge transfer process on the Mo transition metal center [46].

Very first work on MoS₂ films as an electrode material for supercapacitor was reported by Soon and Loh [47]. They have demonstrated the presence of double layer charge behavior in edge-oriented MoS₂ nanowall films at alternating current frequencies up to 100 Hz. Supercapacitor performances of MoS₂ films prepared by chemical vapour deposition was comparable to that of carbon nanotube arrays [48]. Cao et al. [49] reported on fabrication of micro-supercapacitors

based on 2D MoS₂ films with a capacitance of 8 mF cm⁻² (volumetric capacitance of 178 F cm⁻³) and excellent cyclic performance through a simple and low-cost spray painting on Si/SiO₂ chip followed by laser patterning. Karthikeyan et al. [50] synthesized MoS₂ nanostructures by one-pot hydrothermal method. The MoS₂ nanostructures showed a specific capacitance of 92.85 F g⁻¹ at a current density of 0.5 mA cm⁻² with an excellent cycling stability (93.8% retention after 1000 cycles) in 1M Na₂SO₄ aqueous electrolyte. Zhou et al. [51] reported a pseudocapacitance performance of flower-like MoS₂ nanospheres prepared by the hydrothermal route which exhibited a specific capacitance of 122 F g⁻¹ at 1 A g⁻¹ in 1 M KCl electrolyte. Yang et al. [52] demonstrated the fabrication of edge-oriented MoS₂ nanoporous films by electrochemical anodization of molybdenum metal in the presence of sulfur vapour. The nanoporous films delivered a capacitance of 14.5 mF cm⁻² with a good cycling performance up to 10000 cycles. Further, mesoporous MoS₂ nanostructures prepared by hydrothermal method had delivered a capacitance of 376 and 403 F g⁻¹ in 1 M Na₂SO₄ and 1 M KCl, respectively [53]. Wang et al. [54] reported a capacitance of 168 F g⁻¹ with 92.6% retained capacitance even after 3000 cycles for three dimensional flower-like MoS₂ nanostructures prepared by hydrothermal route.

The electronic conductivity of 2H-MoS₂ is lower compared to graphite/graphene, and the specific capacitance of MoS₂ is still very limited in alone for energy storage applications. However, MoS₂ is a promising material to increase the energy density of the capacitors, particularly in combination with carbon, graphene, CNTs, reduced graphene oxide and conducting polymers. The composites of MoS₂ - graphene, MoS₂ -rGO and MoS₂ -conducting polymers could provide better electrochemical performances relative to its pristine components. For example, Hu et al. [55] reported a porous tubular C/MoS₂ nanocomposites as a supercapacitor electrode which exhibited a capacitance of 210 F g⁻¹ with excellent long-term cycling stability over 1000 cycles whereas the bulk MoS₂ showed 40 F g⁻¹ at 1 A g⁻¹. Huang et al. [56] demonstrated a maximum specific capacitance of the 243 F g⁻¹ for MoS₂ /graphene composite synthesized by a modified L -cysteine-assisted solution-phase method. The MoS₂ /graphene composite electrode had showed a good long-term cyclic stability (only 7.7% decrease in specific capacitance after 1000 cycles). The enhancement in specific capacitance and cycling stability was believed to be due to the 3D MoS₂ /graphene inter- connected conductive network which promotes not only efficient charge transport and facilitates the electrolyte

diffusion, but also effectively prevents the volume expansion/ contraction and aggregation of electroactive materials during charge/discharge process [57]. Bissett et al. [58] demonstrated on composite membranes made from solution exfoliated dispersions of 2D materials, such as semiconducting MoS₂ and semimetallic graphene that can create a synergistic effect, allowing for high performance electrochemical energy storage devices construction. The high specific capacitance of the MoS₂ /graphene membranes, with only a small mass loading ($\sim 1 \text{ mg cm}^{-2}$), no added binders, and no extra porous charge separators had served as a cost-effective, simple, and scalable electrochemical energy storage cell architecture with an excellent cycle life. It was found that the optimal ratio of the MoS₂ and graphene, in terms of electrochemical performance, was 1:3 (MoS₂ /graphene). The composite membrane was able to achieve a high specific capacitance ($\sim 11 \text{ mF cm}^{-2}$ at 5 mV s^{-1}). MoS₂ nanosheets in different proportions deposited on reduced graphene oxide (RGO) by microwave heating had showed specific capacitance values of 128, 265, and 148 F g^{-1} at 10 mV s^{-1} and the energy density value of 63 W/kg [59].

MoS₂-graphene nanosheets not only prevented the agglomeration of MoS₂ nanosheets but also restricted the growth of MoS₂ during layer-by-layer by the bond formed between MoS₂ nanosheets and graphene. The hybrid film electrode shows a specific capacitance of 282 F g^{-1} at a scan rate of 20 mV s^{-1} with an improved cycle life retaining over 93% of its initial capacitance [60]. Very recently, Clerici et al. [61] reported on a rapid one-pot synthesis of MoS₂ -decorated laser-induced graphene (MoS₂ -LIG) by direct writing of polyimide foils. By covering the polymer surface with a layer of MoS₂ dispersion before processing, it is possible to obtain an in situ decoration of a porous graphene network during laser writing. The micro and nanostructuring of the LIG allow the high-rate transportation of electrolyte ions and electrons throughout the electrode network, while the in situ decoration with MoS₂ flakes permits the comprehensive utilization of pseudo and

double-layer capacitances that resulted in excellent electrochemical performances. Very recently, layered MoS₂ nanosheets/N-doped graphene (MoS₂ /NG) composite was synthesized by one-pot hydrothermal method. By adjusting precursor ratios, flower-like MoS₂ /NG hybrid with nitrogen content of 3.5% on the graphene layers was obtained. Electrochemical characterizations indicated that the maximum specific capacitance of the MoS₂ /NG electrodes reached up to 245 F g^{-1} at 0.25 A g^{-1} (and 146 F g^{-1} at 20 A g^{-1}). In addition, the electrode exhibits superior cyclic stability

with 91.3% capacitance retention after 1000 cycles at 2 A g^{-1} [62]. Similarly, MoS_2 /MWCNT composite exhibited superior electrochemical performance to pure MWCNT and MoS_2 . The composite had showed a high specific capacitance of 452.7 F g^{-1} at a current density of 1 A g^{-1} , as compared to 69.2 F g^{-1} for MWCNT and 149.6 F g^{-1} for MoS_2 .[63] In Table 1, we summarized the electrochemical performances of MoS_2 and its composites. The electrochemical results confirmed that the layered MoS_2 materials composited with the graphene and conducting polymers are potentially suitable candidates for supercapacitor applications.

Table-1: electrochemical performance of MoS_2 and its composites for supercapacitor applications.

MATERIAL	PREPARATION METHOD	ELECTROLYTE	CAPACITANCE	CYCLING STABILITY
MoS_2 film	Chemical vapour deposition	0.5 M H_2SO_4	71 mF cm^{-1} at 1 mV s^{-1}	–
MoS_2 nanosheets	Hydrothermal	KOH	8 mF cm^{-1} at 0.22 A m^{-2}	92% after 1000 cycles
MoS_2 nanosheets	Liquid exfoliation	KOH	3.1 mF cm^{-1} at 0.22 A m^{-2}	–
	Hydrothermal	1M Na_2SO_4	92.85 Fg^{-1} at 0.5 mA cm^{-2}	93.8% after 1000 cycles
MoS_2 nanospheres	Hydrothermal	1M KCl	122 Fg^{-1} at 1 Ag^{-1}	–
MoS_2 nanoporous film	Electrochemical anodization	1M LiOH	14.5 mF cm^{-1} at 1 mA cm^{-2}	Capacitance increased after 1000 cycles
Mesoporous MoS_2 nanostructure	Hydrothermal	1M Na_2SO_4	376 Fg^{-1} at 1 mV s^{-1}	80% after 2000 cycles
		1M KCl	403 Fg^{-1} at 1 mV s^{-1}	80% after 2000 cycles
3D MoS_2	Hydrothermal	1M KCl	168 Fg^{-1} at	92.6% after

nanostructure			1 Ag^{-1}	3000 cycles
Metallic 1T-MoS ₂	Chemical Exfoliation	0.5 M H ₂ SO ₄	650 F cm^{-3} at 20 mV s^{-1}	97% after 5000 cycles
C/MOS ₂	Hydrothermal	3M KOH	210 Fg^{-1} at 1 Ag^{-1}	105% after 1000 cycles
MoS ₂ /G	Hydrothermal	1M Na ₂ SO ₄	243 Fg^{-1} at 1 Ag^{-1}	92.3% after 1000 cycles
MoS ₂ /G	Liquid exfoliation And ultrasonication	1M Na ₂ SO ₄	11 mF cm^{-1} at 5 mV s^{-1}	70% after 5000 cycles
MoS ₂ /G M oS ₂ /G	Microwave Layer by layer	1M HClO ₄ 1M Na ₂ SO ₄	265 Fg^{-1} at 1 mV s^{-1} 282 Fg^{-1} at 20 mV s^{-1}	92% after 1000 cycles 95% after 1000 cyclesS
MoS ₂ /G	Hydrothermal	1M H ₂ SO ₄	416 Fg^{-1} at 1 Ag^{-1}	–
MoS ₂ /N-doped G	Hydrothermal	1M KOH	245 Fg^{-1} at 0.25 Ag^{-1}	91.3% after 1000 cycles
MoS ₂ /MWCNT	Hydrothermal	1M Na ₂ SO ₄	452.7 Fg^{-1} at 1 Ag^{-1}	91% after 1000 cycles
ACFTs/MoS ₂	Hydrothermal	1M Na ₂ SO ₄	308.5 Fg^{-1} at 5 mV s^{-1}	97.38% after 6000 cycles
MoS ₂ /rgo fiber capacitors	Electrochemical exfoliation	PVA H ₂ SO ₄ -	30 F cm^{-3} at $0.1 \mu\text{A}$	1000 cycles
MoS ₂ /PANI	Solvothermal and insitu-oxidative polymerization solvothermal	1M H ₂ SO ₄	496 Fg^{-1} at 1 Ag^{-1}	79% after 6000 cycles

3. Review of nanofluids works

3.1 Introduction

In the past few decades, rapid advances in nanotechnology have led to emerging of new generation of coolants called “nanofluids”. Nanofluids are defined as suspension of nanoparticles in a basefluid. Some typical nanofluids are ethylene glycol based molybdenum nanofluids and water based copper oxide nanofluids, Nanofluids are dilute suspensions of functionalized nanoparticles composite materials developed about a decade ago with the specific aim of increasing the thermal conductivity of heat transfer fluids, which have now evolved into a promising nano technological area. Such thermal nanofluids for heat transfer applications represent a class of its own difference from conventional colloids for other applications.

3.2 Review of Past work

Murshed et al. [71] used a rod-shaped and spherical shaped TiO_2 nanoparticles and prepared nanofluids by dispersing these nanoparticles in de-ionized water. The experimental result showed the improvement in thermal conductivity with an increase in particle loadings (0.5–5 vol%) and is affected by particle size and shape. The results of thermal conductivity for TiO_2 (15 nm)-water nanofluids showed a 29.70% enhancement with 5% particle volume fraction and thermal conductivity for TiO_2 (ϕ 10 nm \times 40 nm)-water nanofluids showed a 32.80% enhancement at same volume fraction. Rod shaped nanoparticles showed more enhancements compared to a sphere shaped. Duangthongsuk and Wong wis observed the thermal conductivity of TiO_2 nanoparticles for 0.2–2 vol% dispersed in water. The thermal conductivity of nanofluids increased as the particle loading and temperature (ranging between 15°C and 35°C) were increased.

Buongiorno et al. [72] carried an International Nanofluid Property Benchmark Exercise (INPBE), measuring the thermal conductivity of matching samples of colloidally stable nanofluids of thirty organizations worldwide, using experimental approaches like transient hot wire method, steady-state and optical methods. They considered nanofluids having an aqueous and non-aqueous base fluid, metal and metal oxide particles, different shapes (near-spherical/elongated particles), and different particle concentrations. It was concluded that the

data from most groups lies within a range $\pm 10\%$ or even less) about the sample average with some outliers. The thermal conductivity showed increase with particle concentration, aspect ratio. The nanofluids tested in this exercise showed that the effective medium theory developed by Maxwell [73] fairly good to predict thermal conductivity. The experiments were for only one metallic nanoparticle and were used at very low concentration. However, the effect of temperature was not considered.

Liu et al. [74] considered the thermal conductivity improvement of synthetic engine oil based multiwalled carbon nanotubes (MWNTs) and ethylene glycol based multiwalled carbon nanotubes with increase in volume concentration of the nanoparticles. For the 1% volume concentration for the CNT–ethylene glycol, the enhancement value of thermal conductivity was up to 12.4%, while for the CNT–synthetic engine oil suspension, the enhancement value of thermal conductivity was up to 30% at volume concentration of 2%.

. Kole and Dey [85] studied the thermal conductivity enhancement of CuO–gear oil nanofluids and studied the factor affecting on thermal conductivity like temperature and volume fraction of nanofluids. Thermal conductivity was measured between the temperature of 5 and 80°C. The experimental investigation showed 10.4% enhancement of thermal conductivity of nanofluids with 0.025- volume fraction of CuO nanoparticles at room temperature, and it increases to 11.9% at 80°C.

H. D Hunag et. al studied that[86] IF–MoS₂ nanoparticles were synthesized by desulphurizing the MoS₃ precursor. The IF–MoS₂ nanoparticles showed the best friction and wear properties use as additives in oil and tested under boundary lubrication, in comparison with base oil and the oil with 2H–MoS₂. From the characterization performed after friction, several phenomena have been proposed to explain these antiwear ability and friction reducing properties: rolling effect, formation of tribofilm, IF–MoS₂ delamination, and third body theory. A combination of all these effects can explain the very good friction and wear properties of IF–MoS₂

Yuan-Xian Zeng et al.[87] studied The heat transfer oil-based MoS₂ nanofluids have been prepared by dispersing stearic acid-modified MoS₂ in heat transfer oil B350. The modified ligand is effective to improve the lipophilic property of MoS₂ nanoparticles. Thermal conductivity

measurements reveal that the thermal conductivity enhancement reaches up to 38.7% at a mass fraction of only 1.0% at 180⁰C. And the thermal conductivities have been determined experimentally as a function of mass fraction and temperature. It has been found that the thermal conductivity increases with the mass fraction of nanoparticles. And the temperature variation has obvious effects on the thermal conductivity enhancement. Interestingly, the measured thermal conductivity enhancement decreases when the temperature is close to the flash point of the base oil. Anyway, the longterm stability and high thermal conductivity clearly identify the lipophilic MoS₂ nanoparticles as a favorable additive in thermal energy engineering.

References :

1. Y.-J. Wang, D. P. Wilkinson and J. Zhang, *Chem. Rev.*, 2011, 111, 7625–7651.
2. N. G. Sahoo, Y. Pan, L. Li and S. H. Chan, *Adv. Mater.*, 2012, 24, 4203–4210.
3. S. E. Habas, H. A. S. Platt, M. F. A. M. van Hest and D. S. Ginley, *Chem. Rev.*, 2010, 110, 6571–6594.
4. A. Kubacka, M. Ferná'ndez-Garci'a and G. Colo'n, *Chem. Rev.*, 2012, 112, 1555–1614.
5. M. Gratzel, *Nature*, 2001, 414, 338–344.
6. H. Li, Z. Wang, L. Chen and X. Huang, *Adv. Mater.*, 2009, 21, 4593–4607.
7. P. G. Bruce, B. Scrosati and J.-M. Tarascon, *Angew. Chem., Int. Ed.*, 2008, 47, 2930–2946.
8. K. Naoi, W. Naoi, S. Aoyagi, J.-i. Miyamoto and T. Kamino, *Acc. Chem. Res.*, 2013, 46, 1075–1083.
9. H. I. Karunadasa, E. Montalvo, Y. Sun, M. Majda, J. R. Long and C. J. Chang, *Science*, 2012, 335, 698–702.

10. C. Zhu, X. Mu, P. A. van Aken, Y. Yu and J. Maier, *Angew. Chem., Int. Ed.*, 2014, 53, 2152–2156.
11. E. Gourmelon, O. Lignier, H. Hadouda, G. Couturier, J. C. Bernède, J. Tedd, J. Pouzet and J. Salardenne, *Sol. Energy Mater. Sol. Cells*, 1997, 46, 115–121.
12. B. Radisavljevic, A. Radenovic, J. Brivio, V. Giacometti and A. Kis, *Nat. Nanotechnol.*, 2011, 6, 147–150.
13. M. Chhowalla, H. S. Shin, G. Eda, L.-J. Li, K. P. Loh and H. Zhang, *Nat. Chem.*, 2013, 5, 263–275.
14. B. Hinnemann, P. G. Moses, J. Bonde, K. P. Jørgensen, J. H. Nielsen, S. Horch, I. Chorkendorff and J. K. Nørskov, *J. Am. Chem. Soc.*, 2005, 127, 5308–5309.
15. D. Kong, H. Wang, J. J. Cha, M. Pasta, K. J. Koski, J. Yao and Y. Cui, *Nano Lett.*, 2013, 13, 1341–1347.
16. X. Huang, Z. Zeng and H. Zhang, *Chem. Soc. Rev.*, 2013, 42, 1934–1946.
17. W. Han, P. Yuan, Y. Fan, G. Shi, H. Liu, D. Bai and X. Bao, *J. Mater. Chem.*, 2012, 22, 25340–25353.
18. A. B. Laursen, S. Kegnaes, S. Dahl and I. Chorkendorff, *Energy Environ. Sci.*, 2012, 5, 5577–5591.
19. M. A. Lukowski, A. S. Daniel, F. Meng, A. Forticaux, L. Li and S. Jin, *J. Am. Chem. Soc.*, 2013, 135, 10274–10277.
20. J. R. McKone, E. L. Warren, M. J. Bierman, S. W. Boettcher, B. S. Brunschwig, N. S. Lewis and H. B. Gray, *Energy Environ. Sci.*, 2011, 4, 3573–3583.
21. T. F. Jaramillo, K. P. Jørgensen, J. Bonde, J. H. Nielsen, S. Horch and I. Chorkendorff, *Science*, 2007, 317, 100–102.
22. S. Z. Butler, S. M. Hollen, L. Cao, Y. Cui, J. A. Gupta, H. R. Gutierrez, T. F. Heinz, S. S. Hong, J. Huang, A. F. Ismach, E. Johnston-Halperin, M. Kuno, V. V. Plashnitsa, R. D. Robinson, R. S. Ruoff, S. Salahuddin, J. Shan, L. Shi, M. G. Spencer, M. Terrones, W. Windl and J. E. Goldberger, *ACS Nano*, 2013, 7, 2898–2926.

23. K. F. Mak, K. He, J. Shan and T. F. Heinz, *Nat. Nanotechnol.*, 2012, 7, 494–498.
24. Y. Li, H. Wang, L. Xie, Y. Liang, G. Hong and H. Dai, *J. Am. Chem. Soc.*, 2011, 133, 7296–7299.
25. X. Hong, J. Kim, S.-F. Shi, Y. Zhang, C. Jin, Y. Sun, S. Tongay, J. Wu, Y. Zhang and F. Wang, *Nat. Nanotechnol.*, 2014, 9, 682–686.
26. K. Roy, M. Padmanabhan, S. Goswami, T. P. Sai, G. Ramalingam, S. Raghavan and A. Ghosh, *Nat. Nanotechnol.*, 2013, 8, 826–830.
27. Y. Gong, J. Lin, X. Wang, G. Shi, S. Lei, Z. Lin, X. Zou, G. Ye, R. Vajtai, B. I. Yakobson, H. Terrones, M. Terrones, B. K. Tay, J. Lou, S. T. Pantelides, Z. Liu, W. Zhou and P. M. Ajayan, *Nat. Mater.*, 2014, 13, 1135–1142.
28. J. Mann, Q. Ma, P. M. Odenthal, M. Isarraraz, D. Le, E. Preciado, D. Barroso, K. Yamaguchi, G. v. S. Palacio, N. Andrew, T. Tai, M. Wurch, N. Ariana, V. Klee, S. Bobek, D. Sun, T. F. Heinz, T. S. Rahman, R. Kawakami and L. Bartels, *Adv. Mater.*, 2014, 26, 1399–1404.
29. K. Chang and W. Chen, *Chem. Commun.*, 2011, 47, 4252–4254.
30. H. Hwang, H. Kim and J. Cho, *Nano Lett.*, 2011, 11, 4826–4830.
31. K. Chang, Z. Mei, T. Wang, Q. Kang, S. Ouyang and J. Ye, *ACS Nano*, 2014, 8, 7078–7087.
32. Y. Liu, Y.-X. Yu and W.-D. Zhang, *J. Phys. Chem. C*, 2013, 117, 12949–12957.
33. B. Cho, A. R. Kim, Y. Park, J. Yoon, Y.-J. Lee, S. Lee, T. J. Yoo, C. G. Kang, B. H. Lee, H. C. Ko, D.-H. Kim and M. G. Hahm, *ACS Appl. Mater. Interfaces*, 2015, 7, 2952–2959.
34. D. Sarkar, W. Liu, X. Xie, A. C. Anselmo, S. Mitragotri and K. Banerjee, *ACS Nano*, 2014, 8, 3992–4003.
35. X. Xie, D. Sarkar, W. Liu, J. Kang, O. Marinov, M. J. Deen and K. Banerjee, *ACS Nano*, 2014, 8, 5633–5640.

36. T. Wang, H. Zhu, J. Zhuo, Z. Zhu, P. Papakonstantinou, G. Lubarsky, J. Lin and M. Li, *Anal. Chem.*, 2013, 85, 10289–10295.
37. Y. Lin, X. Ling, L. Yu, S. Huang, A. L. Hsu, Y.-H. Lee, J. Kong, M. S. Dresselhaus and T. Palacios, *Nano Lett.*, 2014, 14, 5569–5576.
38. X. Zhang, Z. Lai, Z. Liu, C. Tan, Y. Huang, B. Li, M. Zhao, L. Xie, W. Huang and H. Zhang, *Angew. Chem., Int. Ed.*, 2015, 54, 5425–5428.
39. H. Li, G. Lu, Z. Yin, Q. He, H. Li, Q. Zhang and H. Zhang, *Small*, 2012, 8, 682–686.
40. H. Li, G. Lu, Y. Wang, Z. Yin, C. Cong, Q. He, L. Wang, F. Ding, T. Yu and H. Zhang, *Small*, 2013, 9, 1974–1981.
41. P. Joensen, R. F. Frindt and S. R. Morrison, *Mater. Res. Bull.*, 1986, 21, 457–461.
42. Z. Zeng, T. Sun, J. Zhu, X. Huang, Z. Yin, G. Lu, Z. Fan, Q. Yan, H. H. Hng and H. Zhang, *Angew. Chem., Int. Ed.*, 2012, 51, 9052–9056.
43. H. Wang, H. Feng and J. Li, *Small*, 2014, 10, 2165–2181.
44. J. N. Coleman, M. Lotya, A. O'Neill, S. D. Bergin, P. J. King, U. Khan, K. Young, A. Gaucher, S. De, R. J. Smith, I. V. Shvets, S. K. Arora, G. Stanton, H.-Y. Kim, K. Lee, G. T. Kim, G. S. Duesberg, T. Hallam, J. J. Boland, J. J. Wang, J. F. Donegan, J. C. Grunlan, G. Moriarty, A. Shmeliov, R. J. Nicholls, J. M. Perkins, E. M. Grieveson, K. Theuwissen, D. W. McComb, P. D. Nellist and V. Nicolosi, *Science*, 2011, 331, 568–571.
45. W. Zhang, J.-K. Huang, C.-H. Chen, Y.-H. Chang, Y.J. Cheng and L.-J. Li, *Adv. Mater.*, 2013, 25, 3456–3461.
46. H. Schmidt, S. Wang, L. Chu, M. Toh, R. Kumar, W. Zhao, A. H. C. Neto, J. Martin, S. Adam, B. Oezylmaz and G. Eda, *Nano Lett.*, 2014, 14, 1909–1913.
47. H. Luo, C. Xu, D. Zou, L. Wang and T. Ying, *Mater. Lett.*, 2008, 62, 3558–3560.
48. K. S. Novoselov, D. Jiang, F. Schedin, T. J. Booth, V. V. Khotkevich, S. V. Morozov and A. K. Geim, *Proc. Natl. Acad. Sci. U. S. A.*, 2005, 102, 10451–10453.

49. X. Liu, T. Xu, X. Wu, Z. Zhang, J. Yu, H. Qiu, J.-H. Hong, C.H. Jin, J.-X. Li, X.-R. Wang, L.T. Sun and W. Guo, *Nat. Commun.*, 2013, 4, 1776.
50. S. Ghatak, A. N. Pal and A. Ghosh, *ACS Nano*, 2011, 5, 7707–7712.
51. C. Lee, Q. Li, W. Kalb, X.-Z. Liu, H. Berger, R. W. Carpick and J. Hone, *Science*, 2010, 328, 76–80.
52. Z. Zeng, Z. Yin, X. Huang, H. Li, Q. He, G. Lu, F. Boey and H. Zhang, *Angew. Chem., Int. Ed.*, 2011, 50, 11093–11097.
53. A. O'Neill, U. Khan and J. N. Coleman, *Chem. Mater.*, 2012, 24, 2414–2421.
54. J. Z. Ou, A. F. Chrimes, Y. Wang, S.-y. Tang, M. S. Strano and K. Kalantar-zadeh, *Nano Lett.*, 2014, 14, 857–863.
55. K.-G. Zhou, N.-N. Mao, H.-X. Wang, Y. Peng and H.-L. Zhang, *Angew. Chem., Int. Ed.*, 2011, 50, 10839–10842.
56. R. J. Smith, P. J. King, M. Lotya, C. Wirtz, U. Khan, S. De, A. O'Neill, G. S. Duesberg, J. C. Grunlan, G. Moriarty, J. Chen, J. Wang, A. I. Minett, V. Nicolosi and J. N. Coleman, *Adv. Mater.*, 2011, 23, 3944–3948.
57. G. Guan, S. Zhang, S. Liu, Y. Cai, M. Low, C. P. Teng, I. Y. Phang, Y. Cheng, K. L. Duei, B. M. Srinivasan, Y. Zheng, Y.-W. Zhang and M.-Y. Han, *J. Am. Chem. Soc.*, 2015, 137, 6152–6155.
58. Q. Ji, Y. Zhang, T. Gao, Y. Zhang, D. Ma, M. Liu, Y. Chen, X. Qiao, P.-H. Tan, M. Kan, J. Feng, Q. Sun and Z. Liu, *Nano Lett.*, 2013, 13, 3870–3877.
59. J. Shi, D. Ma, G.-F. Han, Y. Zhang, Q. Ji, T. Gao, J. Sun, X. Song, C. Li, Y. Zhang, X.-Y. Lang, Y. Zhang and Z. Liu, *ACS Nano*, 2014, 8, 10196–10204.
60. S. Najmaei, Z. Liu, W. Zhou, X. Zou, G. Shi, S. Lei, B. I. Yakobson, J.-C. Idrobo, P. M. Ajayan and J. Lou, *Nat. Mater.*, 2013, 12, 754–759.
61. Y.-H. Lee, X.-Q. Zhang, W. Zhang, M.-T. Chang, C.-T. Lin, K.-D. Chang, Y.-C. Yu, J. T.-W. Wang, C.-S. Chang, L.-J. Li and T.-W. Lin, *Adv. Mater.*, 2012, 24, 2320–2325.

62. Y. Feldman, E. Wasserman, D. J. Srolovitz and R. Tenne, *Science*, 1995, 267, 222–225.
63. L. Margulis, G. Salitra, R. Tenne and M. Talianker, *Nature*, 1993, 365, 113–114.
64. Mills A, Hunte A J. An overview of semiconductor photocatalysis. *J Photochem Photobiol A Chem*, 1997, 108: 1–35
- 65 Dawson G, Chen W, Zhang T, et al. A study on the effect of starting material phase on the production of trititanate nanotubes. *Solid State Sci*, 2010, 12: 2170–2176
66. Yana J, Fenga S, Lua H, et al. Alcohol induced liquid-phase synthesis of rutile titania nanotubes. *Mat Sci Eng B*, 2010, 172: 114–120
67. Mozia S. Application of temperature modified titanate nanotubes for removal of an azo dye from water in a hybrid photocatalysis-MD process. *Catalysis Today*, 2010, 156: 198–207
68. Pradhan S K, Reucroft P J, Yang F, et al. Growth of TiO₂ nanorods by metalorganic chemical vapor deposition. *J Crystal Growth*, 2003, 256: 83–88
69. H.D. Huang, J.P. Tua*, T.Z. Zoua, L.L. Zhanga and D.N. He DOI: 10.1007/s11249-005-8552-z
70. Yuan-Xian Zeng,¹ Xiu-Wen Zhong, Zhao-Qing Liu,¹ Shuang Chen,² and Nan Li¹
<http://dx.doi.org/10.1155/2013/2704901>
71. Murshed et al, *J nanopart res*(2010)

Chapter 4:

Instruments and Apparatus Used



4. Characterization Techniques:

There are several methods to characterize the sample to determine its phase, morphology, band gap, lattice vibration, crystallite size, interplanar distance, crystal plane etc. Here also these methods and machineries are used to confirm about its phase and several properties. XRD is done first to determine its phase from the reference of JCPDS. It's also possible to confirm about its crystallographic planes, interplanar distance, crystallite size and lattice structure of the prepared samples. Apart from this, FESEM is done to know its proper morphology in micro and nanoscale, EDS confirms about composition, RAMAN spectroscopy is done to determine its vibration spectroscopy, UV-VIS determines several optical properties like absorbance, reflectance, transmittance from which band gap of semiconducting material can be confirmed. Photoluminescence is also used to know whether there are any defect states or the emission spectra determine band gap emission only. All the above methods are on optical spectroscopy.

In this work we have used various characterization techniques for analysing the synthesized samples and their applications. The characterization techniques are as follows:

- 1. XRD**
- 2. FESEM**
- 3. RAMAN**
- 4. Cyclic Voltammetry**
- 5. UV-VIS-NIR Spectroscopy**
- 6. TEM**
- 7. X-Ray Photoelectron Spectroscopy**

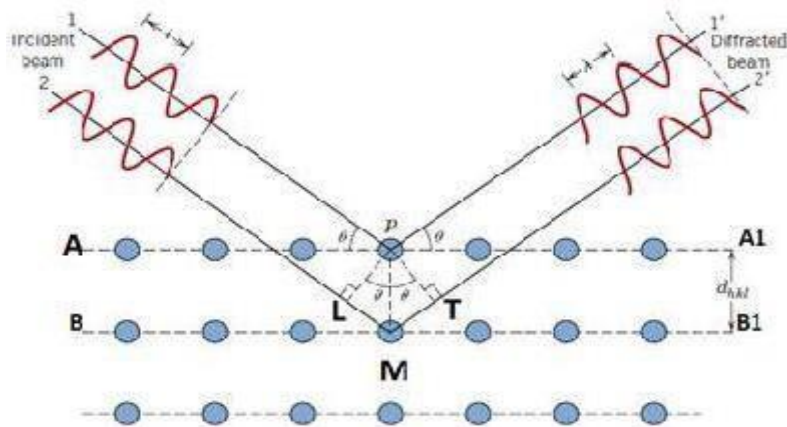
4.1 X-RAY Diffraction:

X-rays are a form of electromagnetic radiation that has high energies and short wavelengths on the order of the atomic spacing for solids. When a beam of x-rays impinges on a solid material, a portion of this beam will be scattered in all directions by the electrons associated with each atom or ion that lies within the beam's path. Let us now examine the necessary conditions for diffraction of x-rays by a periodic arrangement of atoms. Diffraction occurs when a wave encounters a series of regularly spaced obstacles that (1) are capable of scattering the wave, and (2) have spacing that are comparable in magnitude to the wavelength. Furthermore, diffraction is a consequence of specific phase relationships established between two or more waves that have been scattered by the obstacles. The phase relationship between the scattered waves, which will depend upon the difference in path length, is important. One possibility results when this path length difference is an integral number of wavelengths. Considering the two parallel planes of atoms A-A1 and B-B1 in Figure XRD, which have the same h, k, and l Miller indices and are separated by the interplanar spacing d_{hkl} . Now assuming that a parallel, monochromatic, and coherent (in-phase) beam of x-rays of wavelength λ is incident on these two planes at an angle Θ . Two rays in this beam, labeled 1 and 2, are scattered by atoms P and Q. Constructive interference of the scattered rays 1 and 2 occurs also at an angle Θ to the planes, if the path length difference between 1-P-1' and 2-Q-2' (i.e. LM+ST) is equal to a whole number, n, of wavelengths. That is, the condition for diffraction is

$$n\lambda = LM+MT$$

$$\text{or, } n\lambda = d_{hkl} \sin \Theta + d_{hkl} \sin \Theta$$

$$n\lambda = 2 d_{hkl} \sin \Theta \text{ [Bragg's law]}$$

Bragg's Law:**Fig 1.1: Bragg's Law of Diffraction**

4.1.1 Production of X-ray:

X-rays are produced by bombarding a metal target (e.g. Cu, Mo usually) with a beam of electrons emitted from a hot filament (often tungsten). The incident beam will ionize electrons from the K-shell (1s) of the target atom and X-rays are emitted as the resultant vacancies are filled by electrons dropping down from the L (2P) or M (3p) levels. This gives rise to K_{α} and K_{β} lines.

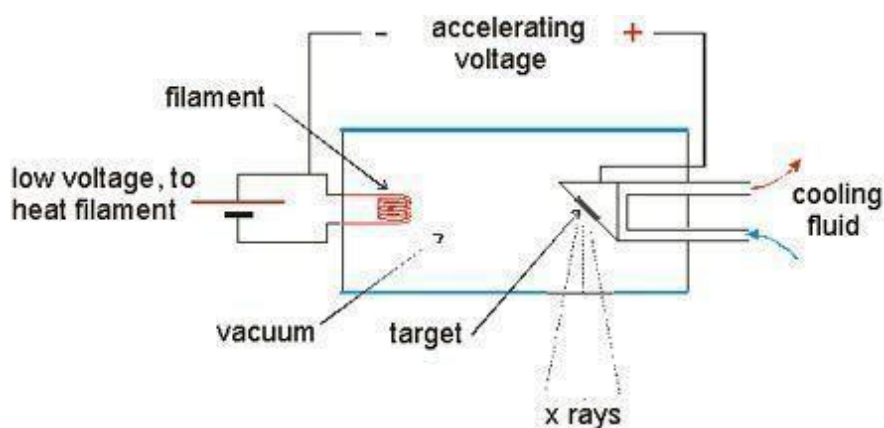


Fig 1.2: Production of X ray

Different method of XRD measurements:

Method	Wavelength(λ)	Incident Angle(θ)
Laue Method	Variable	Fixed
Rotating-crystal	Fixed	variable
Powder Method	Fixed	variable

Table 4.1: Different XRD Methods

4.1.2 Particle Size Determination by Scherrer's Formula:

Experimentally obtained diffraction patterns of the sample are compared with the standard powder diffraction files published by the JCPDS. The average grain size of the samples was calculated using the Scherrer's formula,



Fig 4.2: X-ray Diffractometer (Bruker D8 Advance)

$$D = \frac{0.9\lambda}{\beta \cos \theta}$$

Where, λ is the wavelength of the x-rays,

β is the full width at half maximum intensity in radians.

It is important to realize that the Scherrer formula provides a lower bound on the particle size. The reason for this is that a variety of factors can contribute to the width of a diffraction peak; besides particle size, the most important of these are usually is dependent on the factors like inhomogeneous strain and instrumental effects. If all of these other contributions to the peak width were zero, then the peak width would be determined solely by the particle size and the Scherrer's formula would apply. If the other contributions to the width are non-zero, then the particle size can be larger than that predicted by the Scherrer's formula, with the "extra" peak width coming from the other factors.

4.2 Field Emission Scanning Electron Microscopy (FESEM)

An FESEM is microscope, instead of light it works with electrons, liberated by a field emission source.

4.2.1 Principle:

Under vacuum, electrons generated by a Field Emission Source are accelerated in a field gradient. The beam passes through electromagnetic lenses, focusing onto the specimen. As a result of this bombardment different types of electrons are emitted from the specimen. A detector catches the secondary electrons and an image of the sample surface is constructed by comparing the intensity of these secondary electrons to the scanning primary electron beam. Finally the image is displayed on a monitor. A FESEM is used to visualize very small topographic details on the surface or entire or fractioned objects. Researchers in biology, chemistry and physics apply

this technique to observe structures that may be as small as 1 nanometer. The FESEM may be employed for example to study organelles and DNA material in cells, synthetic polymers, and coatings on microchips.

4.2.2 Preparation:

In order to be observed with a SEM objects are first made conductive for current. This is done by coating them with an extremely thin layer (1.5 - 3.0 nm) of gold or palladium. Further on, objects must be able to sustain the high vacuum and should not alter the vacuum, for example by losing water molecules or gasses. Metals, polymers and crystals are usually little problematic and keep their structure in the SEM. Biological material, however, requires a prefixation, e.g. with cold slush nitrogen (cryo-fixation) or with chemical compounds. This particular microscope is foreseen of a special cryo-unit where frozen objects can be fractured and coated for direct observation in the FESEM. Chemically fixed material needs first to be washed and dried below the critical point to avoid damage of the fine structures due to surface tension. Coating is then performed in a separate device.

4.2.3 Source Electrons:

In standard electron microscopes electrons are mostly generated by heating a tungsten filament by means of a current to a temperature of about 2800°C. Sometimes electrons are produced by a crystal of lanthanum hexaboride (LaB6) that is mounted on a tungsten filament. This modification results in a higher electron density in the beam and a better resolution than with the conventional device. In a field emission (FE) scanning electron microscope no heating but a so-called "cold" source is employed. An extremely thin and sharp tungsten needle (tip diameter 10^{-7} – 10^{-8} m) functions as a cathode in front of a primary and secondary anode. The voltage between cathode and anode is in the order of magnitude of 0.5 to 30 KV. Because the electron beam produced by the FE source is about 1000 times smaller than in a standard microscope, the image quality is markedly better. As field emission necessitates an extreme vacuum (10^{-8} Torr) in the column of the microscope, a device is present that regularly decontaminates the electron source by a current flash. In contrast to a conventional tungsten filament, a FE tip last theoretically for a lifetime, provided the vacuum is maintained stable.

The electron beam is focused by the electro-magnetic lenses (condenser lens, scan coils, stigmator coils and objective lens) and the apertures in the column to a tiny sharp spot.

4.2.4 Condenser Lens:

The current in the condenser determines the diameter of the beam: a low current result in a small diameter, a higher current in a larger beam. A narrow beam has the advantage that the resolution is better, but the disadvantage that the signal to noise ratio is worse. The situation is reversed when the beam has a large diameter. The condenser lens is consisting mostly out of two parts.

4.2.5 Scan Coils:

The scan coils deflect the electron beam over the object according to a zig-zag pattern. The formation of the image on the monitor occurs in synchrony with this scan movement. The scan velocity determines the refreshing rate on the screen and the amount of noise in the image (rapid scan = rapid refreshing = low signal = much noise; see SCANMODE in the virtual FESEM). The smaller the scanned region on the object, the larger the magnification becomes at a constant window size (see MAGNIFICATION in the virtual FESEM). Scan coils often consist of upper and lower coils, which prevent the formation of a circular shadow at low magnification.

4.2.6 The Objective Lens:

The objective lens is the lowest lens in the column. The objective focuses the electron beam on the object (see FOCUS in the virtual FESEM). At a short working distance (= object in a higher position, that is closer to the objective lens) the objective lens needs to apply a greater force to deflect the electron beam. The shortest working distance produces the smallest beam diameter, the best resolution, but also the poorest depth of field. (The depth of field indicates which range in vertical direction in the object can still be visualized sharply).

4.2.7 The Stigmator Coil:

The stigmator coils are utilized to correct irregularities in the x and y deflection of the beam and thus to obtain a perfectly round-shaped beam. When the beam is not circular, but ellipsoidal, the image looks blurred and stretched.

4.2.8 Object Chamber:

After the object has been covered by a conductive layer it is mounted on a special holder. The object is inserted through an exchange chamber into the high vacuum part of the microscope and anchored on a moveable stage. In the virtual FESEM the object can be moved in horizontal and vertical direction on the screen by operating the arrows in the POSITION box. In the real microscope the object can be repositioned in the chamber by means of a joy stick that steers in left right axis, or forward and backward. In addition, the object can be tilted (e.g. for stereo views), rotated and moved in Z direction (= closer or further away to the Objective lens). The —secondary electron emission detector (scintillator) is located at the rear of the object holder in the chamber.

4.2.9 Image Formation:

When the primary probe bombards the object, secondary electrons are emitted from the object surface with a certain velocity that is determined by the levels and angles at the surface of the object. The secondary electrons, which are attracted by the Corona, strike the scintillator (fluorescing mirror) that produces photons. The location and intensity of illumination of the mirror vary depending on the properties of the secondary electrons. The signal produced by the scintillator is amplified and transduced to a video signal that is fed to a cathode ray tube in synchrony with the scan movement of the electron beam. The contrast in the—real time image that appears on the screen reflects the structure on the surface of the object. Parallel to the analog image, a digital image is generated which can be further processed.

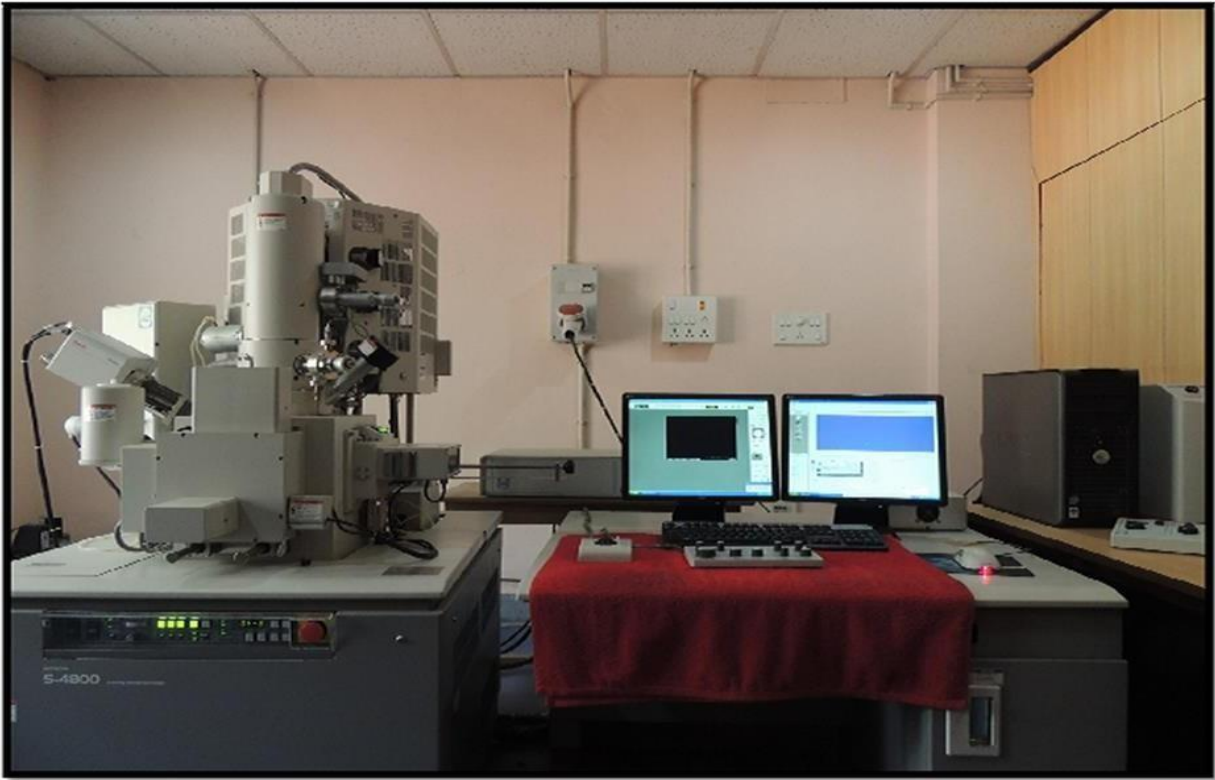


Fig.4.1: FESEM (HITACHI S-4800) Setup



Fig. 4.2: FESEM (ZEISS) Setup

4.3. Cyclic Voltammetry:

Cyclic voltammetry is the most widely used technique for acquiring qualitative information about electrochemical reactions. It offers a rapid location of redox potentials of the electroactive species.



Fig.3.1 :-Cyclic Voltammetry (GAMRY) Setup

Operation

In cyclic voltammetry the voltage is swept between two values at a fixed rate, however now when the voltage reaches V_2 the scan is reversed and the voltage is swept back to V_1 . A typical cyclic voltammogram recorded for a reversible single electrode transfer reaction is shown in below. Again the solution contains only a single electrochemical reactant. For a reversible electrochemical reaction the CV recorded has certain well defined characteristics.

1. The voltage separation between the current peaks is
2. The positions of peak voltage do not alter as a function of voltage scan rate
3. The ratio of the peak currents is equal to one.
4. The peak currents are proportional to the square root of the scan rate The CV for cases where the electron transfer is not reversible show considerably different behaviour from their reversible

counterparts. By analysing the variation of peak position as a function of scan rates it is possible to gain an estimate for the electron transfer rate constants.

4.4. **Raman Spectroscopy:**

Raman scattering was first observed by Dr. C. V. Raman in 1928 and was used to investigate the vibrational states of many molecules.

Raman System:

A typical Raman system consists of the following basic components: (1) Excitation source, usually a laser (2) Optics for sample illumination (3) Double or triple monochromator and (4) Signal processing system consisting of a detector, an amplifier, and an output device. A sample is mounted on the sample chamber and laser light is focused on it with the help of a lens. The scattered light is collected using another lens and is focused at the entrance slit of the monochromator. The monochromator effectively rejects stray light and serves as a dispersing element for incoming radiation. The light leaving the exit slit of the monochromator is collected and focused on the surface of a detector. This optical signal is converted to an electrical signal within the detector and further manipulated using detector electronics. Such a signal is stored in computer memory for each predetermined frequency interval. In a conventional Raman system using a photomultiplier tube (PMT) detector, light intensity at various frequencies is measured by scanning the monochromator. A plot of signal intensity against wavenumber constitutes its Raman spectrum.

Principle

When a sample is irradiated with an intense monochromatic light source (usually a laser), most of the radiation is scattered by the sample and the same wavelength as that of the incoming laser radiation in a process known as Rayleigh scattering. However, a small proportion of the incoming light approximately one photon out of a million is scattered at a wavelength that is shifted from the original laser wavelength.

1. Laser light excites the sample

2. This light is scattered in all directions
3. Some of this scattered light directed to the detector, which records the Raman spectrum
4. This spectrum shows light at the original laser (Rayleigh) frequency and the Raman spectral features unique to the sample.

The same transitions between molecular vibrational states (M) and (M*) in the infrared absorption can also result in Raman scattering. A key difference between the Raman and infrared processes is that, in the former process, the photons involved are not absorbed or emitted but rather shifted in frequency by an amount corresponding to the energy of the particular vibrational transition. In the Stokes process, which is the parallel of absorption, the scattered photons are shifted to lower frequencies as the molecules abstract energy from the exciting photons; in the anti-Stokes process, which is parallel to emission, the scattered photons are shifted to higher frequencies as they pick up the energy released by the molecules in the course of transitions to the ground state.

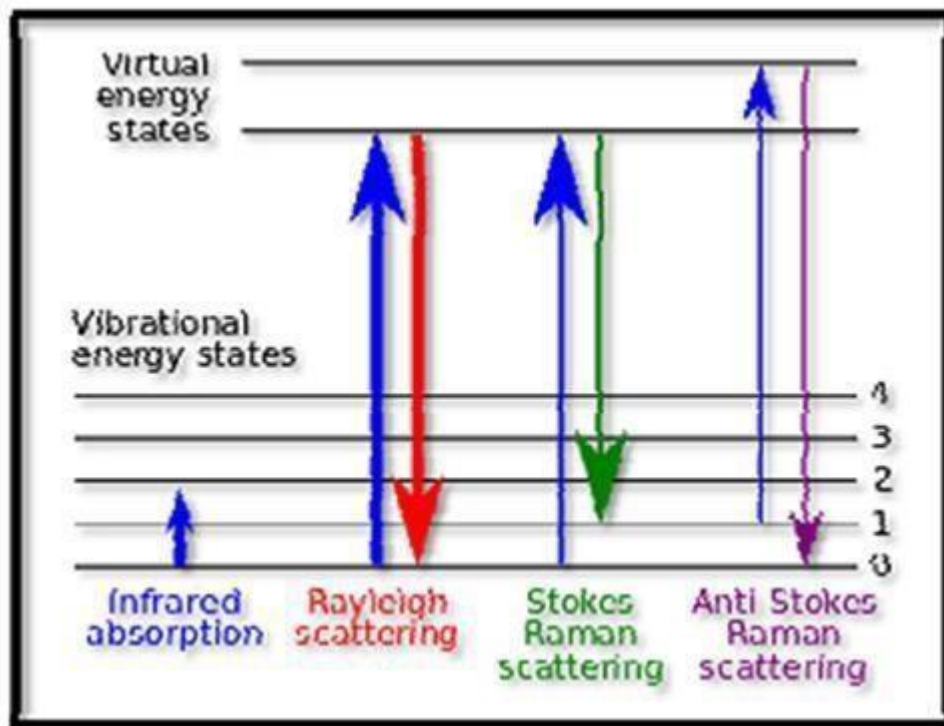


Fig.4.1: Different Types of Scattering

Relaxation from the virtual state occurs almost instantaneously and is predominantly to the initial ground state. This process results in Rayleigh scatter, which is scattered light of the same wavelength as the excitation laser. Relaxation to the first excited vibrational level results in a Stokes-Raman shift. Stokes-Raman shift scattered light is of lower energy (longer wavelength)

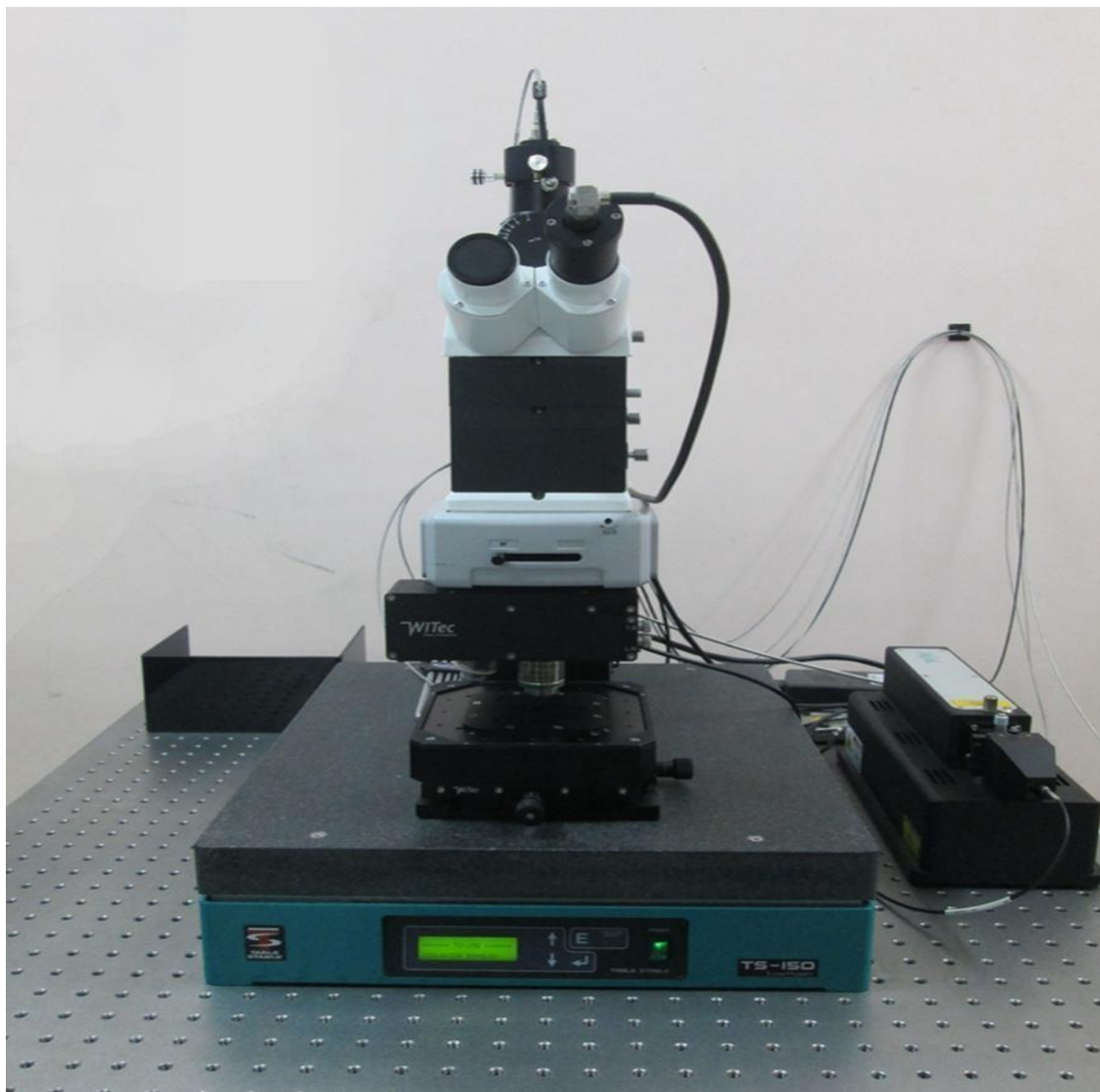


Fig.4.2: Raman Spectrometer

than that of the laser light. In addition, most systems have at least a small population of molecules that are initially in an excited vibrational state. When the Raman process initiates from the excited vibrational level, relaxation to the ground state is possible, producing scatter of higher energy (shorter wavelength) than that of the laser light. This type of scatter is called anti-Stokes Raman scatter. Two molecules can give exactly the same Raman spectrum, and the

intensity of the scattered light is proportional to the amount of material present. Thus Raman provides both qualitative and quantitative information about the sample. The Raman spectra carried out by WITEC alpha 300R - RAMAN spectroscopy.

4.5 UV–Vis–NIR Spectroscopy:

4.3.1 Basic Principle

The instrument used in ultraviolet–visible spectroscopy is called a UV–Vis–NIR Spectrophotometer. Spectrophotometer provides a means for analyzing liquids, gases and solids through the use of radiant energy in the far and near ultraviolet, visible and near infrared regions of the electromagnetic spectrum. Accordingly, the predetermined electromagnetic radiation wavelengths for ultra–violet (UV), visible (Vis) and near infra–red (NIR) radiation are defined as follows:

UV radiation: 300 to 400 nm

Vis radiation: 400 to 765 nm

NIR radiation: 765 to 3200 nm

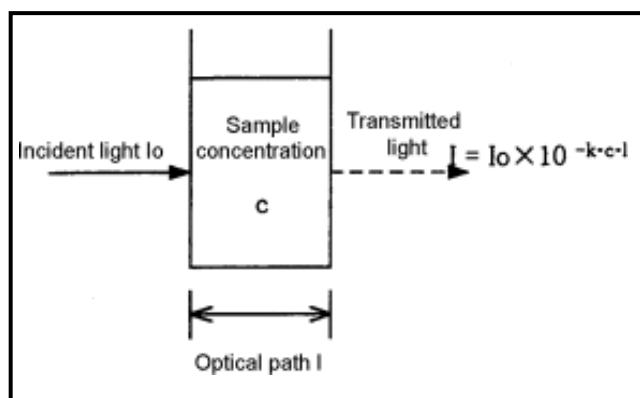


Fig. 5.1 Bouguer–Beer Rule.

The instrument operates by passing a beam of light through a sample and measuring wavelength of light reaching a detector. The wavelength gives valuable information about the chemical structure and the intensity is related to the number of molecules, means quantity or concentration. Analytical information can be revealed in terms of transmittance, absorbance or reflectance of energy in the wavelength range between 160 and 3500 mill microns.

Light is quantized into tiny packets called photons, the energy of which can be transferred to an electron upon collision. However, transfer occurs only when the energy level of the photon equals the energy required for the electron to get promoted onto the next energy state, for example from the ground state to the first excitation state. This process is the basis for absorption spectroscopy. Generally, light of a certain wavelength and energy is illuminated on the sample, which absorbs a certain amount of energy from the incident light. The energy of the light transmitted from the sample afterwards is measured using a photo detector, which registers the absorbance of the sample. A spectrum is a graphical representation of the amount of light absorbed or transmitted by matter as a function of wavelength. A UV–Vis–NIR spectrophotometer measures absorbance or transmittance from the UV range to which the human eye is not sensitive to the visible wavelength range to which the human eye is sensitive. Bouguer–Beer law as shown in **fig. 5.1** is a basic principle of quantitative analysis, is also called the Lambert–Beer rule. The following relationship is established when light with intensity I_0 is directed at a material and light with intensity I is transmitted. In this instance the value I/I_0 is called transmittance (T) and the value $I/I_0 \times 100$ is called transmission rate ($T\%$). The value $\log (1/T) = \log (I_0/I)$ is called absorbance (Abs).

$$T = I/I_0 = 10^{-kcl}$$

$$Abs = \log (1/T) = \log(I_0/I) = -kcl$$

Here k is proportionality constant and l = length of light path through the cuvette in cm. As can be seen from the above formulas, transmittance is not proportional to sample concentration. However, absorbance is proportional to sample concentration (Beer's law) along with optical path (Bouguer's law). In addition, when the optical path is 1cm and the concentration of the target component is 1mol/l, the proportionality constant is called the molar absorption coefficient and expressed using the symbol ϵ . The molar absorption coefficient is a characteristic value of a material under certain, specific conditions. Finally,

stray light, generated light, scattered light, and reflected light must not be present in order for the Bouguer–Beer rule to apply.

Experimental Set Up

Spectrophotometers consist of a number of fundamental components: Light Sources (UV and VIS), monochromator (wavelength selector), sample holder, a detector, signal processor and readout. The radiation source used is often a tungsten filament, a deuterium arc lamp which is continuous over the ultraviolet region, and more recently light emitting diodes (LED) and xenon arc lamps for the visible wavelengths. The detector is typically a photodiode or a CCD. Photodiodes are used with monochromators, which filter the light so that only light of a single wavelength reaches the detector. When measuring absorbance at the UV spectrum, the other lamp has to be turned off. The same goes when measuring visible light absorbance.

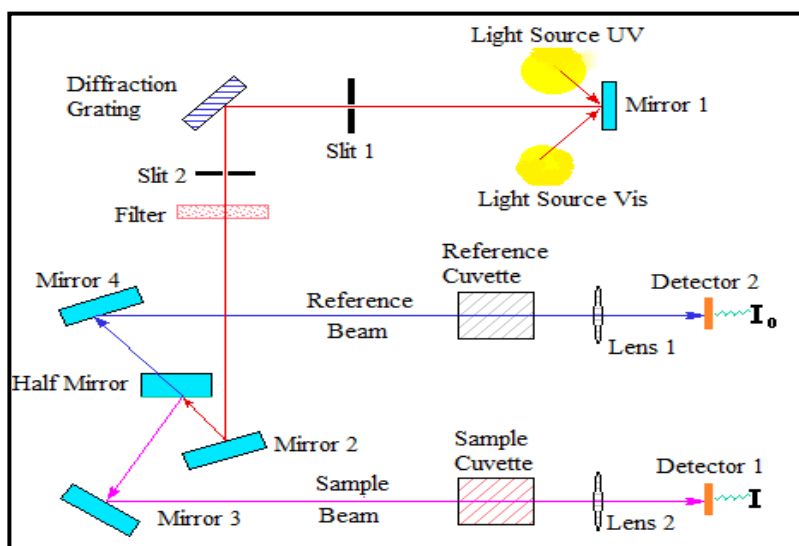


Fig. 5.2 shows schematic diagram of UV–Vis–NIR Spectrophotometer

The light source is a monochromator; the light is split into two equal intensity beams by a half mirrored device before it reaches the sample. One beam, the sample beam, passes through a small transparent container (cuvette) containing a solution of the compound being studied in a transparent solvent. The other beam, the reference, passes through an identical cuvette containing only the solvent. The containers for the sample and reference solution must be transparent to the radiation which will pass through them. Quartz or fused silica cuvettes are required for spectroscopy in the UV–Vis–NIR region. The light sensitive detector follows the sample chamber and measures the intensity of light transmitted from the cuvettes and passes the information to a meter that records and displays the value to the operator on an LCD screen. The intensities of these light beams are then measured by electronic detectors and compared. Some UV–Vis spectrophotometry has two detectors the phototube and the photomultiplier tube. The sample and reference beam are measured at the same time. The intensity of the reference beam, which should have suffered little or no light absorption, is defined as I_0 . The intensity of the sample beam is defined as I . Over a short period of time, the Spectrometer

automatically scans all the component wavelengths in the manner described. The ultraviolet (UV) region scanned is normally from 200 to 400 nm, and the visible portion is from 400 to 800 nm. Therefore, this method is excellent to both determine the concentration and identify the molecular structure or the structural changes. Spectrophotometer is also useful to study the changes in the vibration and conformation energy levels after and before an interaction with a substrate, or another molecule. **Fig. 5.3** shows experimental set-up of UV–Vis–NIR Spectrophotometer.



Fig.5.3 Experimental set up of UV–Vis–NIR Spectrophotometer

Specifications:

Model	: UV–Vis–NIR Spectrometer Perkin Elmer Lambda 19
Lamp	: Deuterium (UV), Tungsten–Halogen (Vis/NIR)
Detectors	: Photomultiplier tube for UV–Vis, Lead–Sulphide cell (PbS) for NIR
Wavelength Range	: 185–3200 nm for Absorbance/transmission and 200–2500 nm for reflectance
Scan Speed	: 0.3 to 1200 nm/min
Wavelength accuracy	: ± 0.15 nm for UV/Vis & ± 0.6 nm for NIR
Base line flatness	: $\pm 0.001\text{\AA}$, 4 nm slit
Ordinate mode	: Scan, time drive, wavelength programming, concentration
Photometric accuracy	: $\pm 0.003\text{\AA}$ or $\pm 0.08\%$ T

4.6 Transmission Electron Microscopy (TEM)

4.3.2 Basic Principle

Transmission electron microscopy (TEM) is a technique used for analyzing the morphology, defects, crystallographic structure, particle size and even composition of a specimen. In this technique a beam of electrons is transmitted through an ultra thin specimen, interacting with the specimen as it passes through. An image is formed from the interaction of the electrons transmitted through the specimen; the image is magnified and focused onto an imaging device, such as a fluorescent screen, on a layer of photographic film, or to be detected by a sensor such as a CCD camera. The transmission electron microscope (TEM) operates on the same basic principles as the light microscope but uses electrons instead of light. What you can see with a light microscope is limited by the wavelength of light. TEM use electrons as "light source" and their much lower wavelength make it possible to get a resolution a thousand times better than with a light microscope.

TEMs are capable of imaging at a significantly higher resolution than light microscopes, owing to the small De Broglie wavelength of electrons. This enables the instrument's user to examine fine detail even as small as a single column of atoms, which

is tens of thousands times smaller than the smallest resolvable object in a light microscope. TEM forms a major analysis method in a range of scientific fields, in both physical and biological sciences. TEMs find application in cancer research, virology, materials science as well as pollution and semiconductor research. At smaller magnifications TEM image contrast is due to absorption of electrons in the material, due to the thickness and composition of the material. At higher magnifications complex wave interactions modulate the intensity of the image, requiring expert analysis of observed images. Alternate modes of use allow for the TEM to observe modulations in chemical identity, crystal orientation, electronic structure and sample induced electron phase shift as well as the regular absorption based imaging.

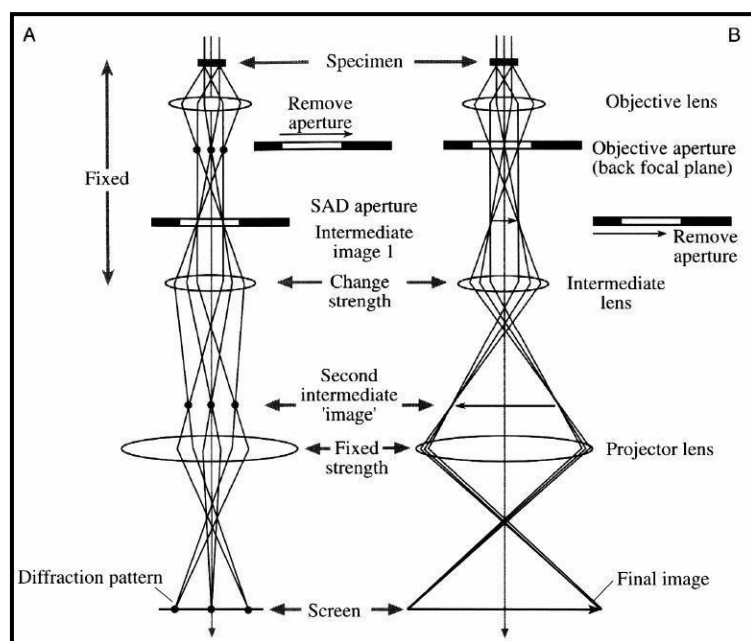


Fig.6.1 Shows two different operations of TEM.

- **Experimental Set Up**

TEM offers two methods of specimen observation as shown in **fig.6.2**

- Image mode
- Diffraction mode

In image mode, the condenser lens and aperture will control electron beam to hit the specimen, the transmitted beam will be focused and enlarged by objective and projector lens and form the image in the screen, with recognizable details related to the sample microstructure. In diffraction mode, an electron diffraction pattern is obtained on the fluorescent screen, originating from the sample area illuminated by the electron beam. The diffraction pattern is entirely equivalent to an X-ray diffraction pattern. A single crystal will produce a spot pattern on the screen and polycrystal will produce a powder or ring pattern. The microstructure, e.g. the grain size, and lattice defects are studied by use of the image mode, while the crystalline structure is studied by the diffraction mode.

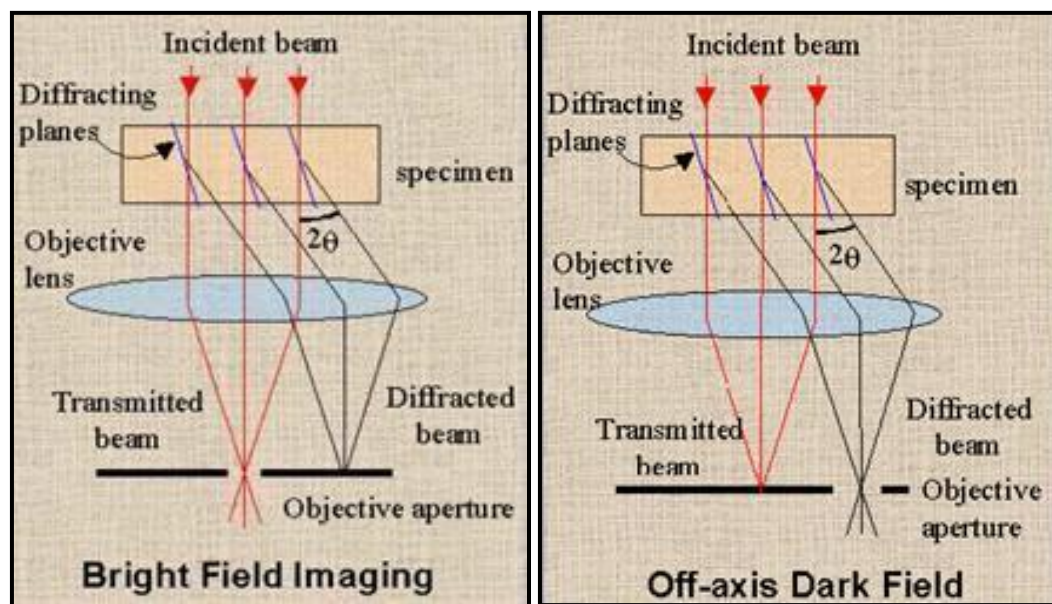


Fig. 6.2 Two image modes of TEM.

Image Modes of TEM

There are two primary image modes in TEM differ in the manner in which way an objective aperture is used as a filter in electric optics system are

1. Bright field microscopy
2. Dark field microscopy

In bright field imaging, the image of a thin sample is formed by the electrons that pass the film without diffraction, the diffracted electrons being stopped by a diaphragm. In the corresponding dark field imaging mode, a diffracted beam is used for imaging. The technique known as bright Field is particularly sensitive to extended crystal lattice defects in an otherwise ordered crystal, such as dislocations. The electron rays corresponding to bright field and dark field imaging are shown in **fig. 2.7** respectively and the experimental set up for transmission electron microscope is shown in **fig. 2.8**.



Fig. 6.3 Experimental set up of Transmission Electron Microscope.

Specifications:

- Model : TEM with CCD camera Philips, Tecnai 20
Electron Source : W emitter and LaB6

Accelerating Voltage	: 200 kV
Point Resolution	: 0.27 nm or better
Line Resolution	: 2.0 nm or better
Magnification	: 25X to 750000X or higher

4.7. X-ray photoelectron spectrometer (XPS)

Chemical Composition of the synthesized nanostructure, charge state of dopants, and purity of sample were analyzed by X-ray photoelectron spectroscopy (XPS, Specs, Germany). In photoelectron spectroscopy, photons are used to eject electrons from the bulk materials. Usually monochromatic, low energy X-rays are used to irradiate the sample which results in photoelectron emission from the atoms of the sample's surface and the kinetic energy distribution of the ejected photoelectrons is directly measured with the help of an electron spectrometer. As each surface atom possesses core-level electrons, the binding energy of each core-level electron is the characteristic of the atom and its specific orbit.

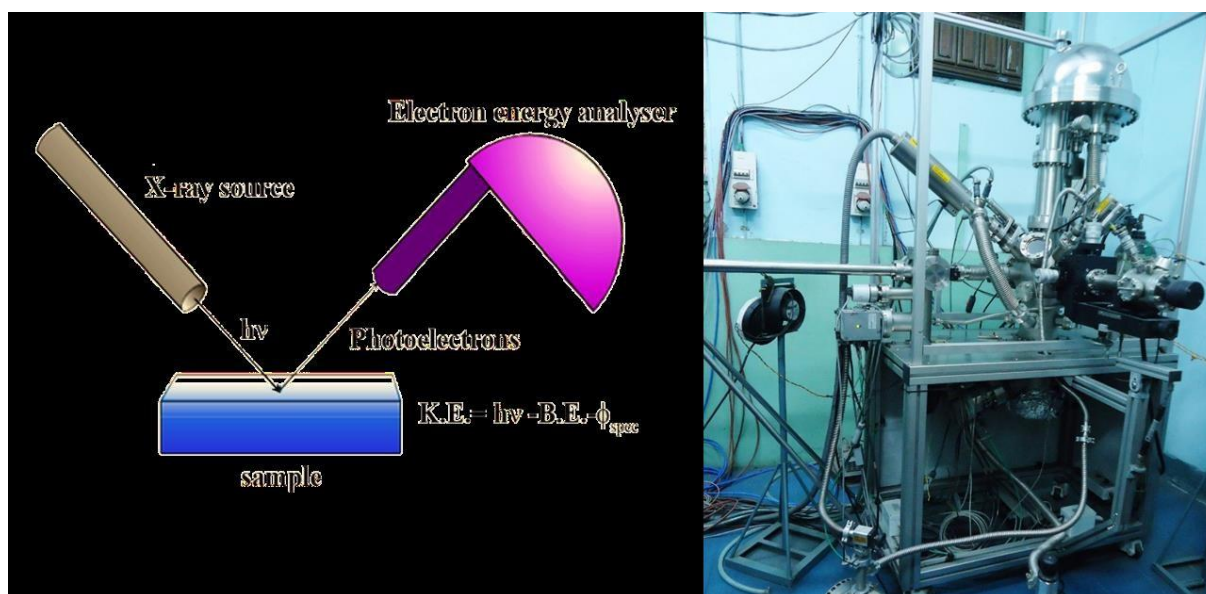


Fig. 4.7 Left: Schematic of the photo-excited electron emission in XPS instrument. Right: SPECS, HAS 3500 XPS instrument

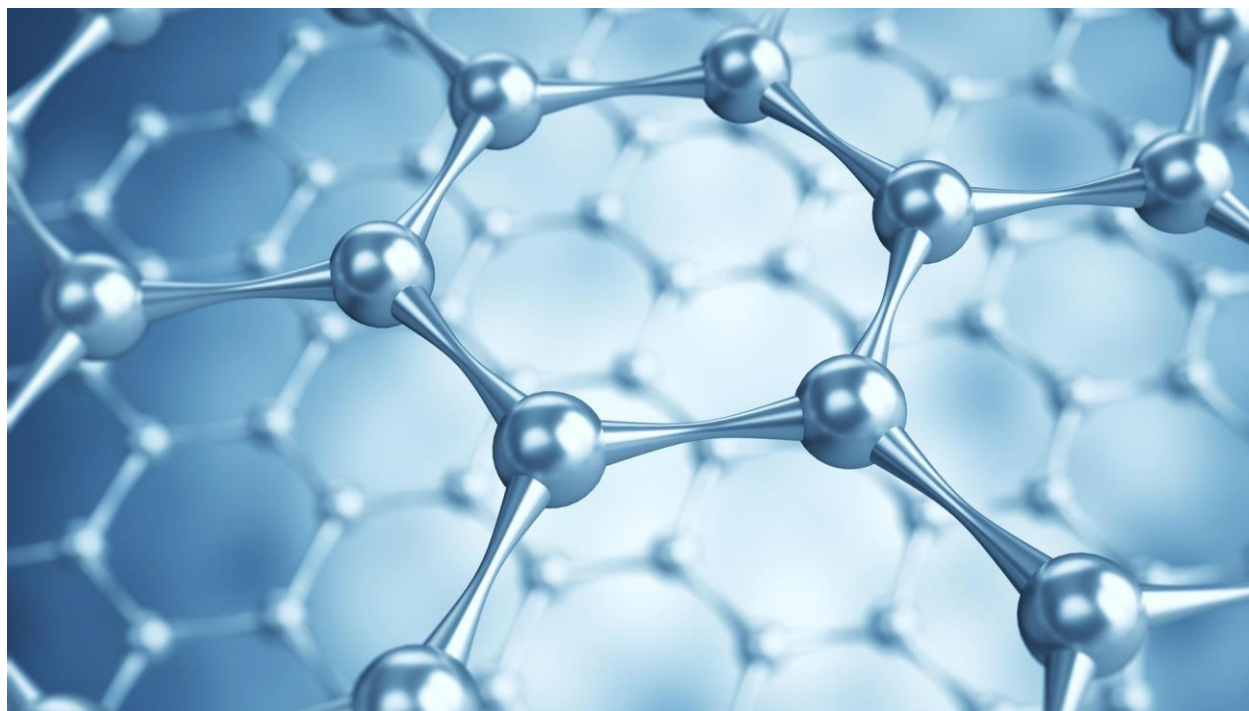
Since the energy of the incident X-rays is known, the measured kinetic energy of a core-level photoelectron peak can be directly assign to its characteristic binding energy. Therefore, XPS provides a means of elemental identification and the use of a standard set of sensitivity factors also provides a surface atomic composition. The kinetic energy (E_k) of these electrons is measured and their binding energy (E_b) can be calculated. The determination of the electron binding energy is the goal of the spectrometer which is found using the following relation:

$$E_b = h\nu - E_k$$

Where, $h\nu$ is the X-ray energy (known) and E_k is the kinetic energy of the photoe

Chapter-5:

Electrochemical study of MOS₂ Nanosheet for Potential Applications in Supercapacitor



5.1) Introduction:

Transition metal sulfide MoS_2 crystal has a sandwich interlayer structure formed by stacking of the (S-Mo-S) layers in [001] direction [1]. These layers are loosely bound to each other only via van der Waals forces, which accounts for easy cleavage of (S-Mo-S) layers in the direction of [001]. Two-dimensional and three-dimensional functional nanostructured materials have received great attention for their inherent physicochemical properties like high specific surface-to-volume ratio, anisotropy, chemical inertness, photo corrosion resistance, and excellent tribological performance [1, 2]. Such materials are applicable in various fields, including lubricants, energy storage, field-effect transistors, and catalysis.

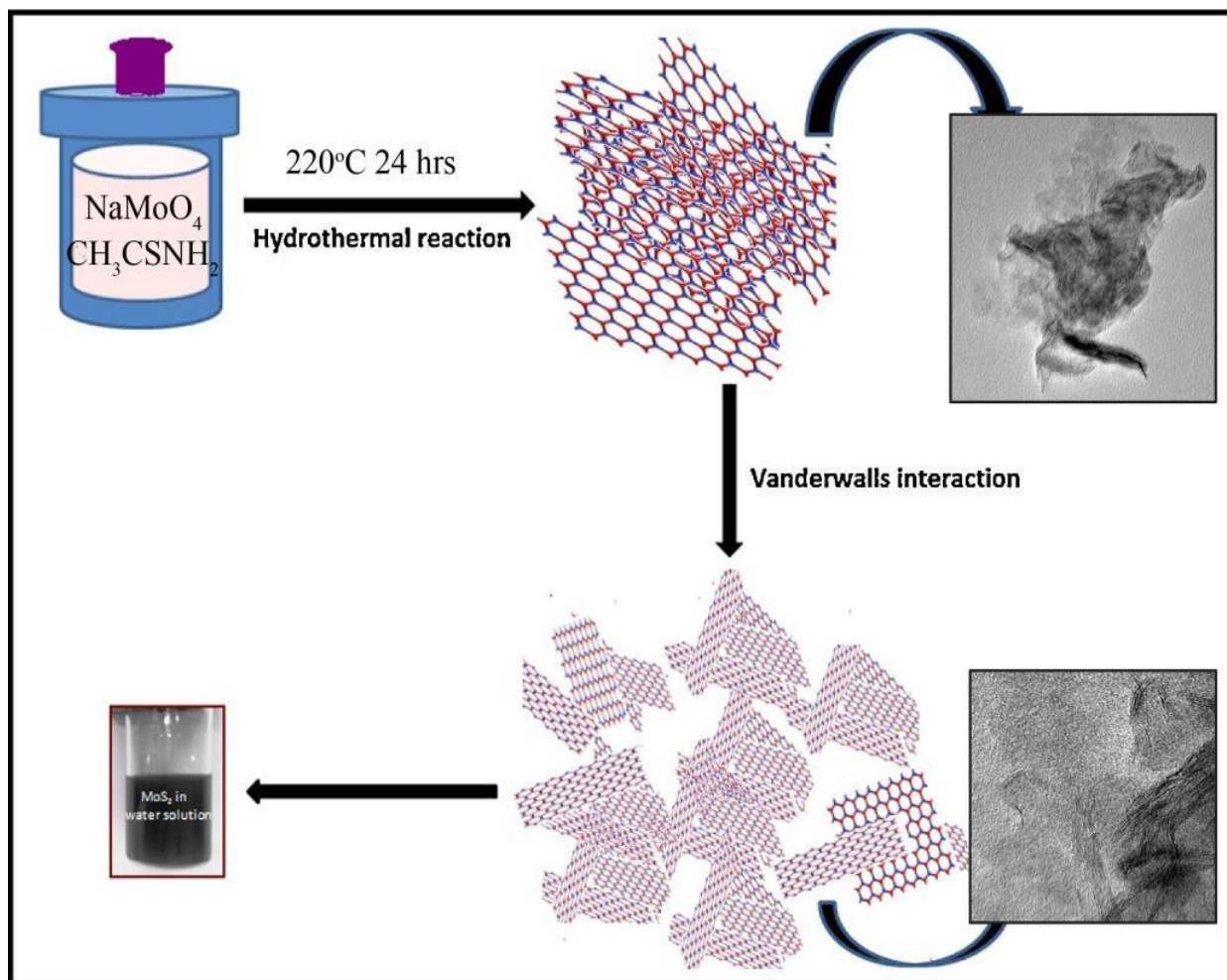
5.2 Preparation:

5.2.1) Materials

Sodium molybdate ($\text{NaMoO}_4 \cdot 2\text{H}_2\text{O}$) and thioacetamide (CH_3CSNH_2) were purchased from Sigma-Aldrich. Ethanol purchased from Analytical Reagent and was used without further purification.

5.2.2) Preparation of MoS_2 nanosheets:

In this synthesis, at first in a 100 mL beaker 0.15 g of $\text{NaMoO}_4 \cdot 2\text{H}_2\text{O}$ and 0.3 g of CH_3CSNH_2 were mixed with 1:2 ratio in 80 mL of deionized water. The mixture solution was stirred 20 minutes to prepare a homogeneous mixture and then transferred into a 100 ML Teflon-lined stainless-steel autoclave. The autoclave was heated at 220°C for 24 h, followed by natural cooling to room temperature. The obtained black product was washed thoroughly with DI and ethanol by centrifugation at 6000 rpm for 10 minutes. After that the final products were dried at 60°C overnight in vacuum oven.



Scheme 1: Synthesis of MoS₂

5.3) Characterization:

The phase purity of the exfoliated nanosheets were confirmed by XRD (Bruker Miniflex Benchtop model). Band gap was measured by UV visible spectroscopy (Shimadzu 3600). RAMAN investigation was carried out by WI-TECH using 532 nm LASER source. The morphological investigation was carried out by FESEM (ZENIS) and HRTEM (JEOL 2100).

5.3.1) XRD Analysis:

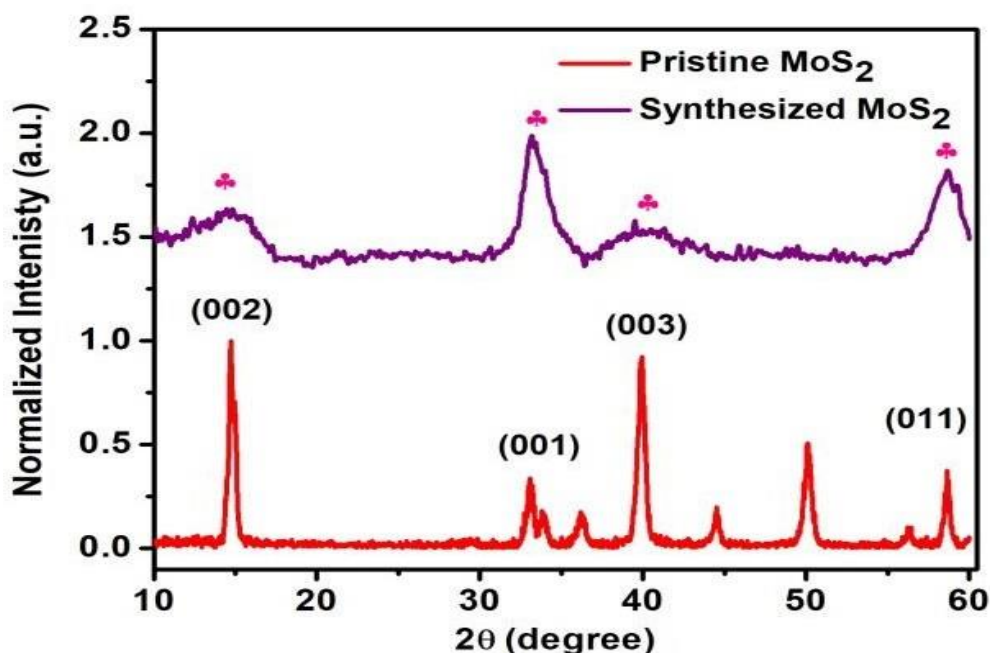


Fig.5.1 XRD peaks of pristine MoS₂ and synthesized MoS₂

The phase purity and crystallinity of the synthesized MoS₂ nanosheets were investigated by XRD. The XRD pattern (Fig.5.1) exhibits four prominent peaks at 2θ values of 14.73° ($d=0.601\text{nm}$), 33.11° ($d=0.270\text{nm}$), 39.92° ($d=0.226\text{nm}$) and 58.64° ($d=0.154\text{nm}$) which can be attributed to the diffraction from (002), (100), (103) and (110) crystallographic planes respectively which corresponds well with JCPDS card no: 17-1508 of MoS₂. The narrow XRD peaks indicate small values of FWHM and hence better crystallinity of the final prepared sample. All the diffraction peaks of the bulk MoS₂ are consistent with the MoS₂ with JCPDS No: 06-0097 (Luo et al., 2014). Compared with bulk MoS₂ powder, a weak diffraction peak at 14.73° corresponding to (002) plane is observed for exfoliated MoS₂.

5.3.2) Raman study:

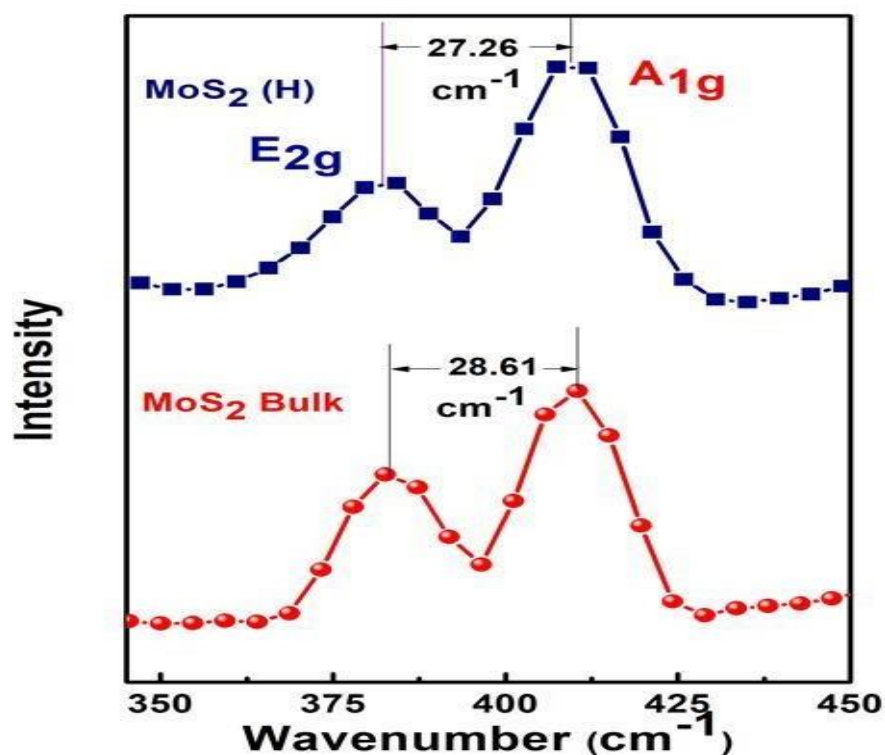


Fig. 5.2: Raman spectra of bulk MoS₂ and hydrothermal MoS₂

The Raman spectrum (Figure 5.2) in the informative range from 350 to 450 cm⁻¹ reveals the characteristic peaks of MoS₂. The two dominant peaks of bulk MoS₂ at 382.88 and 410.49 cm⁻¹ are associated with the in-plane E_{2g} and out-of-plane A_{1g} vibrational modes of the hexagonal MoS₂, respectively (Kong et al. 2013). For the hydrothermal MoS₂, corresponding two peaks are at 382.22 and 409.48 cm⁻¹. It has been reported that the difference between the Raman peak frequencies of E_{2g} and A_{1g} undergoes a stepwise decrease with decreasing number of MoS₂ layers (Lee et al. 2010). Therefore the decrease in the frequency difference for the hydrothermal MoS₂ compared with the bulk MoS₂ confirms that MoS₂ nanosheets are ultrathin with a few layers.

5.3.3) Morphological Investigation:

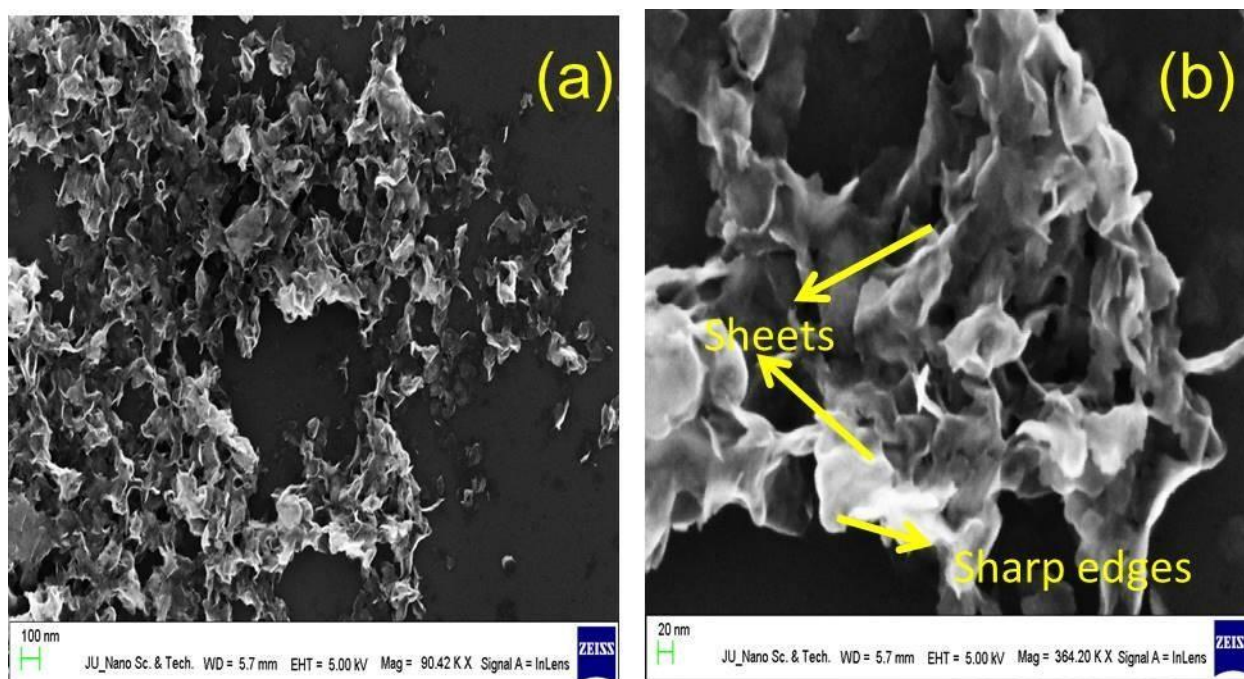


Fig 5.3: FESEM Images of MoS₂ sheets

For FESEM sample preparation a dispersed water solution of synthesized sample was prepared and drop casted on the cleaned Si wafer. Figure 5.3 shows the FESEM images of the synthesized Nanosheets on the Si wafer. The sharp edges of the sheets are clearly visible in the FESEM images (Fig 5.3(b)).

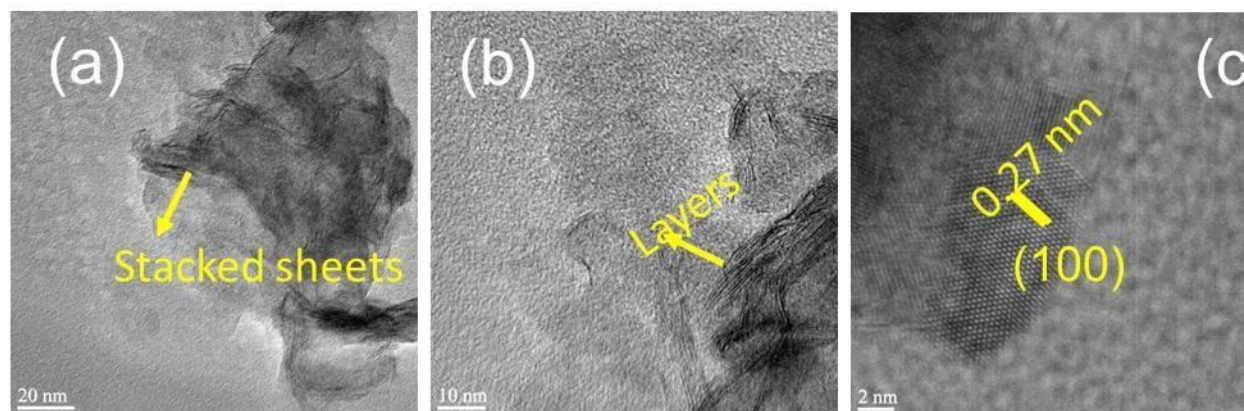


Fig 5.4: TEM image (a); HRTEM images (b) & (c)

An HRTEM image in Fig. 4 clearly shows the MoS₂ layers are well stacked. To get more insight into the crystal structure of MoS₂ sheets synthesized in our method, the HRTEM images were further analyzed as in Fig. 4(b) and (c). The lattice d spacing is estimated to be 0.27 nm, which corresponds to (100) lattice plane of hexagonal MoS₂ phase and is in well agreement with XRD pattern results.

5.3.4) UV spectra analysis:

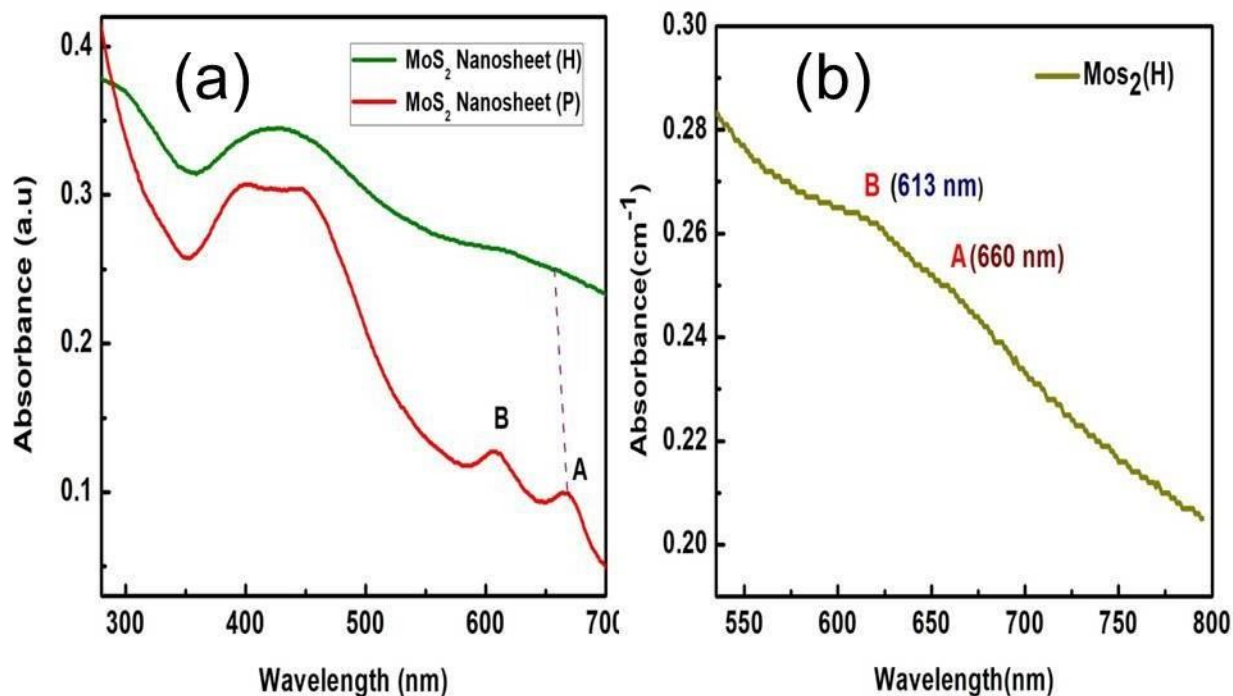


Fig. 5.5: Linear optical absorption spectrum of few-layer MoS₂.

The UV-Vis spectrum of few-layer MoS₂ is shown in Fig.5.5. The characteristics peaks are observed for bulk MoS₂ at (A) 665 nm (B) 614 nm are in very good agreement with the previously reported values (Wilson and Yoffe, 1969; Zhang et al., 2015). Characteristics peaks are observed for hydrothermal few layer mos2 at (A) 660 (B) 613 .The absorption peaks, namely A and B occur due to the direct excitonic transitions orbital. This analysis confirms the presence of few-layer MoS₂ nanosheets.

5.3.5 XPS Analysis:

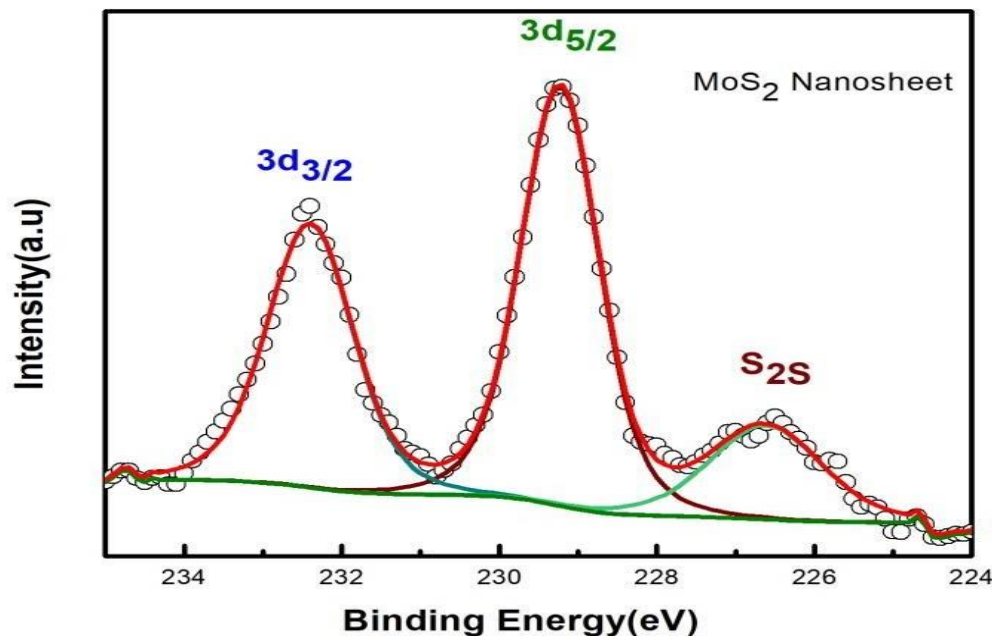


Fig. 5.6: Analysis of X-ray Photo electron spectroscopy (XPS) of few-layer MoS₂.

Typically, 1T and 2H MoS₂ exhibits different position in binding energy which have previously confirmed. Our study reveals Mo has +4 oxidation states with a position of 3d_{3/2} and 3d_{5/2} to a value of 232.35 eV and 229.18 eV respectively which strongly concludes pure 2H hexagonal phase of MoS₂. The deconvoluted spectra consists no peak around 231.4 eV and 228.3 eV for 3d_{3/2} and 3d_{5/2} respectively suggest no formation of 1T phase (mainly observed in single layer) during bottom up synthesis of MoS₂. Moreover, no extra peak was obtained at 229 eV which is mainly due to oxidized state of MoS₂ due to hydrothermal synthesis in open conditions. Previously discussion reveals the position of A band in UV-absorption studies which have directly correlated with layer number per unit nanosheet. From UV-Vis analysis, the peak position of A band corresponds to 660 nm with almost 3 layers per nanosheet which can be correlated with our XPS spectrum having hexagonal phase of MoS₂ with almost nonexistence of 1T phase.

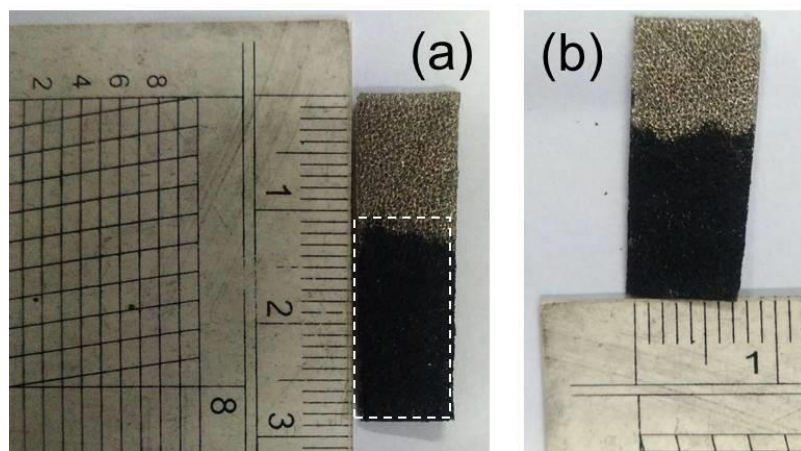
5.4) Results and Discussion:

5.4.1) Details of 3-electrode Set-up:

A three electrode cell was used for all electrochemical measurements for the as prepared supercapacitor electrodes. In the set-up, MoS₂ coated on Ni foam acted as the working electrode, Ag/AgCl electrode was chosen to be as the reference electrode and platinum (Pt) wire acted as the counter electrode of AUTOLAB electrostation. 1M KOH solution was taken as the electrolyte. All measurements were carried out at room temperature. Cyclic voltammetry (CV) was performed at different scan rates varying from 2 to 100 mV s⁻¹. Galvanostatic charge/discharge (GCD) measurements were conducted at various current densities varied from 1 to 5 A g⁻¹ to evaluate the specific capacitance. A potential window in the range from -1 to 0 V was used in the CV measurements.

5.4.2) Working Electrode Preparation:

Firstly nickel foam was used as the substrate for the working electrode. The nickel foams were cleaned with help of dilute HCl, ethanol and deionized water with few minutes in ultrasonication. The electrode for electrochemical study was made in few steps. Firstly the active material that is molybdenum disulfide (mos₂), carbon black and Polyvinylidene fluoride (PVDF) was taken in weight ratio of 8 : 1 :1. All of three were mixed and a slurry mixture was obtained with the help of N Methyl-2-pyrrolidone (NMP) which was added drop by drop when the three powders were stirred to mix up. Moving into the second step, the slurry was coated on the cleaned and dried nickel foam with the dimensions 1 cm x 2 cm. Then the electrodes were vacuum dried at 80°C. After that the final electrode was obtained.



Digital picture of prepared electrode

5.4.3) Cyclic Voltammetry Analysis:

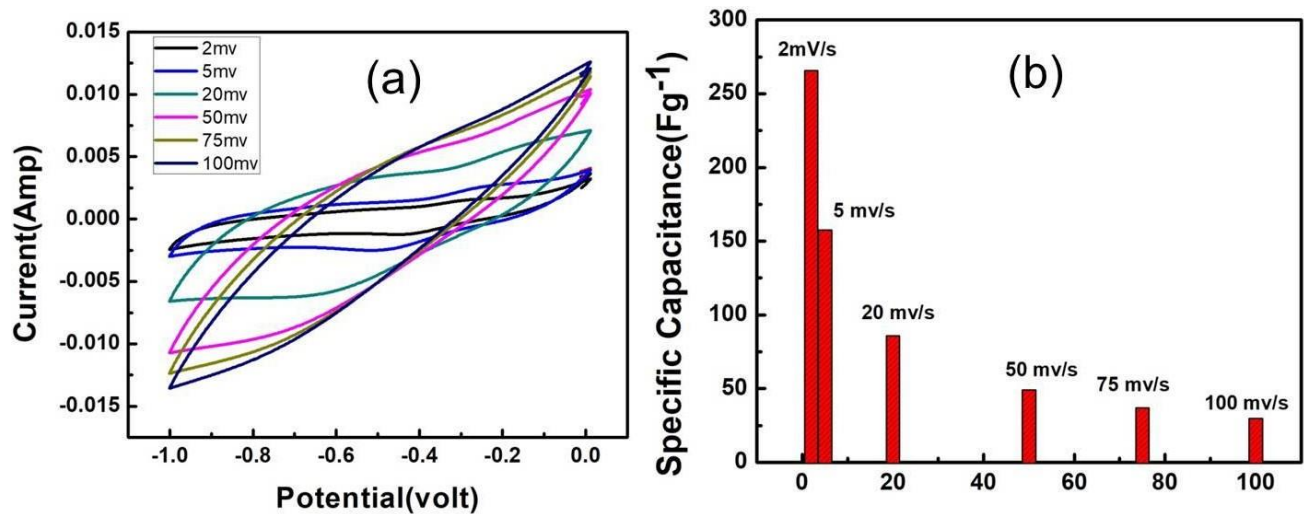


Fig.5.7 (a) Cyclic Voltammetry curves of MoS₂ at different scan rates and (b) shows calculated Specific Capacitance at various scan rates.

As shown in figure 5.7 the cyclic voltammetry was carried out at different scan rates with a fixed voltage window. Here mainly the capacitance of the sample is measured. Redox peaks are visible at lower scan rates more prominently.

The specific capacitances were calculated from the CV curves in accordance to following equation and are shown in the following...

$$C_s = \frac{\int I(v)dv}{m\Delta vV} \dots\dots\dots(i)$$

Where C_s = Specific Capacitance.

Δv = Potential window. \int = Area under CV curve

m = active mass of the electrode material for specific capacitance F/g

In case of areal capacitance m will be replaced by A = area of the active electrode (cm²)

V = Scan rate.

From the table-1 highest capacitance of 265.67 F g^{-1} (968 mF/cm^2) is obtained at 2 mV/s scan rate. C_s decreases as scan rate increases. It is because when the scan rate is very high the electrochemical reaction is so fast that all the ions cannot take part in the redox reaction process and the diffusion of ions is limited. Hence with the increase of scan rate the specific capacitance decreases. Interestingly, with the sweep rates increase, the current density increases and the positions of anodic and cathodic peaks shift to a more anodic and cathodic direction, respectively, indicating that the fast and reversible redox reactions occurring at the electro/electrolyte interface. Figure 5.2 (b) lists the as obtained capacitances in a histogram representation.

Scan rate (mV/s)	Specific Capacitance (F/g)	Areal Capacitance (mF/Cm ²)
2	265.67	968
5	157.45	574
20	85.9	313
50	49	181
75	37.0	135
100	29.67	108

Table 1: Variation of scan rate with the specific capacitance

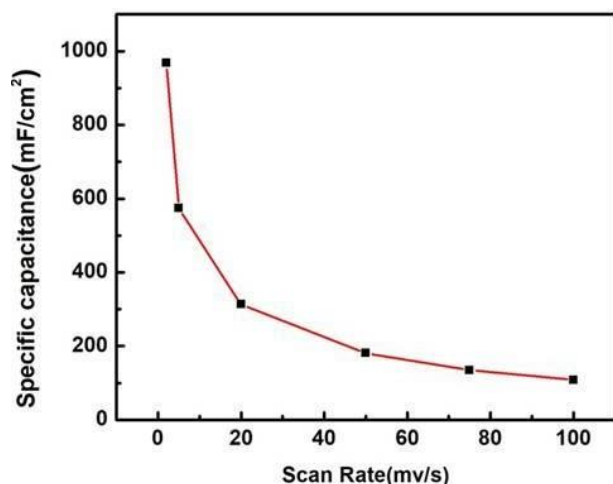


Fig 5.8: Variation of Areal capacitance with scan rate

5.4.4) Galvanostatic Charge Discharge analysis:

In this section, the charge storage capacity of the synthesized MoS_2 was analyzed with the help of charging-discharging measurements carried out at different current densities. The non-linearity in the time trajectory of the potential is attributed to the Faradic redox reaction. However, a small voltage drop indicates a good interfacial contact between the active working electrode and the substrate (Ni Foam) during GCD measurements. It has been observed that the widths of the GCD curves (Figure 5.9 (a)) were expanded at lower current density; while in contrast, the curves were shrinking at higher current densities. Therefore, the specific capacitance follows an inverse relationship with the current density (Fig. 5.9 (b)). The inverse relationship between current density and specific capacitance is due to the redox reaction that takes place at the interface between electrode and electrolyte. In addition, at the lower current density, the electrolyte ions get enough time to react with the active electrode materials and hence specific capacitance increases.

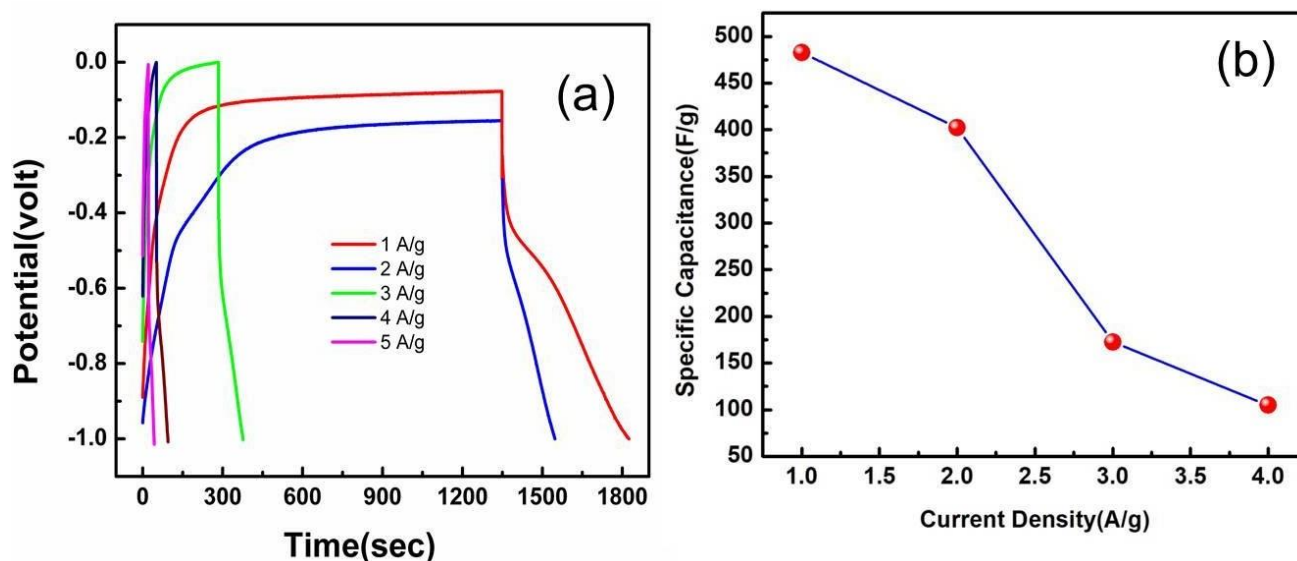


Fig. 5.9:- Galvanostatic Charging-Discharging curves of MoS_2 at different current densities and (b) shows the values of specific capacitance obtained from discharge curve.

The specific capacitance can be calculated from the charging-discharging curves by the following equation .

$$C_s = \frac{I\Delta t}{m\Delta v} \dots\dots\dots(ii)$$

Where ,

C_s = Specific Capacitance

I = Discharge Current

Δt = Discharge time

m = Active mass of the electrode material.

Δv = Potential window

The specific capacitance obtained from the discharging curves were calculated by equation (2) at different current densities is listed below.

Current Density (A g ⁻¹)	1	2	3	4	5
Specific capacitance (F g ⁻¹)	482.43	402.3	272.94	172.52	104.85

Table 2: Details of current densities and the respective Specific capacitance of MoS₂

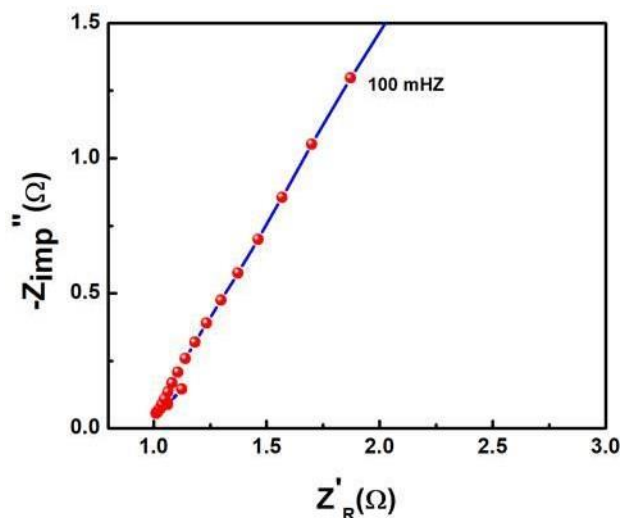


Fig.5.10 Nyquist plot of MoS₂

EIS spectra using the equivalent circuit diagram (inset of Fig. 5.10), the bulk solution resistance (R_s) remained 0.30 Ω for MoS₂ nanosheet. The smaller semicircle indicates low charge transfer resistance between electrode material and electrolyte ions as well reduced contribution of pseudo capacitance due to annealing process.

5.5) Conclusion:

In summary, MoS₂ nanosheets were synthesized by a hydrothermal method. Confirmation of the crystallinity and phase has been done using X-Ray diffraction and Raman Spectroscopy. Morphology and structure were analysed using FESEM analysis revealing the Sheet structure of. The electrode material attains a specific capacitance of 265.67 F/g (968 mF/cm²) at 2 mV/s scan rate and 482.43 F/g at 1 A/g current density. The obtained high value was attributed to the sheet like morphology which enhance the interaction with the electrolyte ions. Especially for MoS₂ have superior electrochemical properties, making them promising electrode materials for practical applications like symmetric/asymmetric supercapacitor devices.

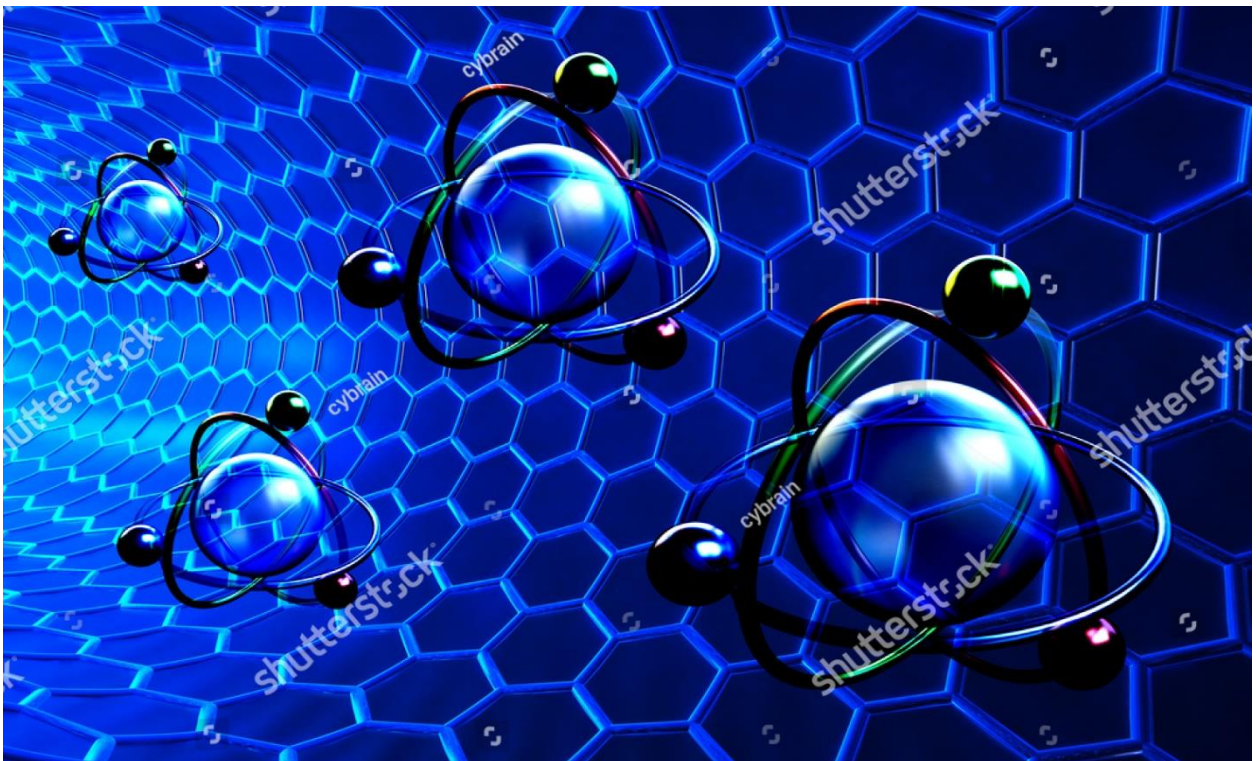
References

1. D. Yu, Q. Qian, L. Wei, W. Jiang, K. Goh, J. Wei, J. Zhang and Y. Chen, Chem. Soc. Rev., 2015, 44, 647–662.
2. (a) Y. Yang, G. Ruan, C. Xiang, G. Wang and J. M. Tour, J. Am. Chem. Soc., 2014, 136, 6187–6190; (b) L. Shen, J. Wang, G. Xu, H. Li, H. Dou and X. Zhang, Adv. Energy Mater., 2015, 5, 1400977.
3. T. H. Murray, Science, 2014, 343, 1208–1210.
4. D. Yu, K. Goh, H. Wang, L. Wei, W. Jiang, Q. Zhang, L. Dai and Y. Chen, Nat. Nanotechnol., 2014, 9, 555–562.
5. L. Qian, X. Tian, L. Yang, J. Mao, H. Yuan and D. Xiao, RSC Adv., 2013, 3, 1703–1708.
6. Ghosh D, Das CK , ACS Appl Matter Interfaces 2015 Jan 21;7(2):1122-31
7. Venkat Srinivasan and John W. Weidner , Journal of Power Sources 108 (2002) 15–20.
8. Meher SK and Rao GR , J Phys Chem C 2011; 115: 25543- 25556.
9. Wang D, Wang Q and Wang T , Inorg Chem 2011 ; 50: 6482- 6492.
10. Yaun C, Yang L, Hou L, et al. , Energy Environ Sci 2012; 5: 7883- 7887.
11. Eyert V, Hock KH and Horn S , J Phys Condens Matter 2000; 12: 4923.
12. Salunkhe RR, Jang K, Lee SW, Ahn H. Aligned nickel-cobalt hydroxide nanorod arrays for electrochemical pseudocapacitor applications. RSC Advances. 2012;2(8):3190-3.

13. Mallick P, Mishra NC. Evolution of structure, microstructure, electrical and magnetic properties of nickel oxide (NiO) with transition metal ion doping. *American Journal of Materials Science*. 2012;2(3):66-71.
14. Ahire DV, Patil GE, Jain GH, Gaikwad VB. Synthesis of nanostructured NiO by hydrothermal route and its gas sensing properties. In *Sensing Technology (ICST), 2012 Sixth International Conference on* 2012 Dec 18 (pp.136-141). IEEE.
15. Kim SI, Lee JS, Ahn HJ, Song HK, Jang JH. Facile route to an efficient NiO supercapacitor with a three-dimensional nanonetwork morphology. *ACS applied materials & interfaces*. 2013 Feb 19;5(5):1596-603.
16. Zang L, Zhu J, Xia Y. Facile synthesis of porous NiO nanofibers for highperformance supercapacitors. *Journal of materials engineering and performance*. 2014 Feb 1;23(2):679-83.
17. Gandhi AC, Pant J, Pandit SD, Dalimbkar SK, Chan TS, Cheng CL, MaYR, Wu SY. Short-range magnon excitation in NiO nanoparticles. *The Journal of Physical Chemistry C*. 2013 Aug 30;117(36):18666-74.
18. Zhu Y, Cao C, Tao S, Chu W, Wu Z, Li Y. Ultrathin nickel hydroxide and oxide nanosheets: synthesis, characterizations and excellent supercapacitor performances. *Scientific reports*. 2014 Aug 29;4.
19. Promita Howli , Swati Das, Samrat Sarkar, Madhupriya Samanta, Karamjyoti Panigrahi, Nirmalya Sankar Das and Kalyan Kumar Chattopadhyay, Co_3O_4 Nanowires on Flexible Carbon Fabric as a Binder-Free Electrode for All Solid-State Symmetric Supercapacitor *ACS Omega* 2017, 2, 4216–4226

Chapter-6

Synthesis and studies of sheet like MOS_2 Nanostructures for Application in nanofluid



6.1 Introduction:

2D molybdenum disulfide (MoS_2) has a structure analogous to graphene, in which two close-packed sulfur atom layers sandwich one molybdenum atom layer and these layers are held together by van der Waals forces. Due to their extremely thin structure, the 2D MoS_2 nanosheets exhibit unique mechanical, electrical, thermal and optical properties, making them significantly different from their bulk counterparts and also resulting in their application in catalysis, electronics, photonics, energy storage, and sensors. Over the past few decades, MoS_2 nanoparticles with various morphologies, such as nanosheets, flower-like structure, sphere-like structure and fullerene-like structure have been used as oil additives. Meanwhile, the lubrication mechanisms of MoS_2 nanoparticle in oils have been extensively studied and suggested as rolling, interlayer sliding and exfoliation–material transferring. In particular, the formation of a tribofilm composed of MoS_2 molecules has been emphasized as the key mechanism for decreasing the friction and wear. In addition, (Chen et al.) recently reported the excellent extreme pressure property of ultrathin MoS_2 nanosheets as oil additives. They suggested that the ultrathin shape of MoS_2 nanosheets could ensure the entrance of the nanosheets into the rubbing interfaces. Therefore, it is desirable to fabricate 2D MoS_2 nanosheets to be used as oil additives, as they could be penetrated into the contact area easily.

6.2 Experimental Details:

6.2.1 Synthesis of MoS_2 Nanosheets:

In this synthesis, at first in a 100 mL beaker 0.15 g of $\text{NaMoO}_4 \cdot 2\text{H}_2\text{O}$ and 0.3 g of CH_3CSNH_2 were mixed with 1:2 ratio in 80 mL of deionized water. The mixture solution was stirred 20 minutes to prepare a homogeneous mixture and then transferred into a 100 ML Teflon-lined stainless-steel autoclave. The autoclave was heated at 220°C for 24 h, followed by natural cooling to room temperature. The obtained black product was washed thoroughly with DI and ethanol by centrifugation at 6000 rpm for 10 minutes. After that the final products were dried at 60°C overnight in vacuum oven.

6.3 Characterizations:

The samples were characterized by X-ray diffraction (XRD, BRUKER D8 Advance) analysis using a $\text{Cu-K}\alpha$ radiation (0.154056 nm) over a scanning angle (2θ). Also field emission scanning electron microscope (FESEM, Hitachi, S-4800) study and transmission electron

microscope (JEOL-JEM 2100, operated at 200 kV) studied the microscopic structure of the samples. Raman study has been done using Raman spectrometer (Witec, kexcitation= 532 nm) to confirm the presence of Molybdenum (Mo) and Sulfer in the sample. The thermal properties were studied by NTPL make 120 KV Automatic Breakdown Voltage Test Setup for breakdown voltage test, ADTR-2k Plus Automatic Dielectric Constant and Resistivity measuring instrument for dielectric constant and resistivity test and KD2 Pro Thermal Property Analyzer for thermal response measurement .

6.4 Results and Discussion:

6.4.1 Nanofluid Preparation:

Between two methods of nanofluid preparation, “two step method” has chosen over “one step method” as it is not expensive and suitable for mass production and also lesser amount of particle is wasted in “two step method” [3]. Here all the nanofluids are prepared by following “two step method”. Transformer oil, is used as the base fluid for our application. Five nanofluids with weight concentrations of 0.00, 0.0025, 0.005, 0.0075, 0.01 wt % has been prepared respectively using said method. Synthesized sample dispersed in transformer oil then stirring for 15 min and finally put in the bath sonicator for ultrasonication for 1 hr. Thus nanofluid is prepared.

6.4.2 Electrical Property Analysis:

6.4.2.1 AC Breakdown Voltages:

The breakdown voltage of an insulator is the minimum voltage that causes a portion of an insulator to become electrically conductive. So from the ac breakdown test we can find out the tolerance level of electrical stress on transformer oil [4]. Here for the experiment we have used spherical copper electrodes with a gap distance of 2.5 mm according to international IEC156 standard [5] and with a ramp voltage of 2kV/s. Before testing, all of the nanofluid samples prepared by the said manner were degassed in vacuum for 4 hours at 100°C to remove any dissolved water during ultrasonication procedure and then normally cooled down to room temperature. To get exact breakdown voltages of the prepared nanofluids, 15 readings were taken at a fixed temperature for every sample and the mean value of the breakdown voltage were calculated and plotted against weight percentage in figure 9. The mean breakdown voltage of bare oil is 25.06 KV, and it increases maximum to 26.38 KV of

initial breakdown voltage at a loading percentage of 0.005wt % and after that the obtained mean value decreases for more weight concentrations. The percentage enhancement of mean breakdown voltages is listed in table 1.

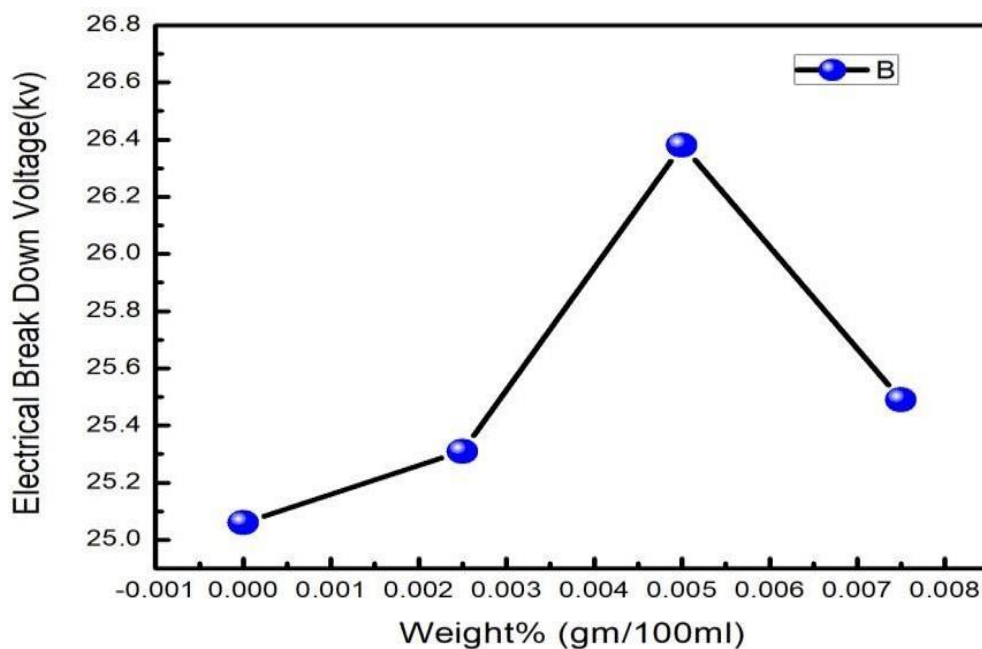


Fig.6.1 breakdown voltage enhancement plot Table-

1 electrical breakdown voltage varies with weight percentage

Sample MoS2 Wt% (gm)	Electrical breakdown voltage in transformer oil (kv)
0.00	25.06
0.0025	25.31
0.005	26.38
0.0075	25.49

Explanation of Breakdown Mechanism:

The breakdown voltage is the voltage in which an insulator becomes electrically conductive. Though breakdown characteristics is a completely electrical property of an insulator, it depends on many other things like temperature, moisture, how many times reading are being taken etc. A single theory cannot explain electrical breakdown mechanism for any insulating liquid because breakdown mechanism has many facets [7-11]. There are different kind of theories based on ionization [12], weak link formation [13], and streamer propagation [14] which can be used for more understanding about the different breakdown behavior.

When a high voltage is applied in the cathode a large number of free electrons has generated in the transformer oil. These free electrons possess fast breakdown of transformer oils [15]. Now introducing of some nanoparticles in the transformer oil can decrease the breakdown event as the free electrons present in the oil trapped by the dispersed nanoparticles [16]. Here the dispersed nanoparticles having high surface area plays the key role because the charge trapping ability of nanoparticles proportionally depends on the surface area. Nanoparticles with high surface area can trap more charge. Nanoparticles of 2D materials contain highest exposure of surface energy among the different kinds of morphological nanoparticles. So maximum number of free electron can be trapped on its surface. Due to sheet like morphology, synthesized MoS₂ has high surface energy. Hence adding them in the transformer oil helps to increase the breakdown voltage. But there is also a demerits of high surface energy. Nanoparticles with high surface energy encourage the agglomeration nature of the nanoparticles [17]. So there is a critical concentration which can increase the breakdown voltage maximum without agglomeration. This critical concentration is important in terms of application. In our experiment, 0.005 wt% is the critical concentration because after this MoS₂ concentration the breakdown voltages starts to decrease due to agglomeration of dispersed sheets at bottom. "Streamer propagation theory" [18] can further confirmed the enhancement of breakdown voltage. Dissolved water present in the transformer oil can excites the streamer formation which can causes the streamer burst in the end that's leading to breakdown of transformer oil at an appreciably low applied voltage [19]. So dissolved water present in the transformer oil should be minimized to avoid the streamer burst. Materials having high water affinity like Carbon black [20], Fullerene [21] can be used to absorb dissolved water in the media. So streamer development takes place at a higher voltage than that of base fluid thereby increasing the breakdown voltage. Here, MoS₂ is found to be super hydrophilic in nature. Hence streamer development is decelerated after addition of the material, resulting in enhancement of the average breakdown voltage. But again, addition

of more nanoparticles above the critical concentration enhances their agglomeration tendency which in-turn increases the mobility of free electrons and ions converting the trapping center to de-trapping center allowing streamer development at relatively lower voltage and decrease the final breakdown voltage.

6.5. Thermal Property Analysis:

5.7.1 Thermal conductivity:

Thermal conductivity is one of the most important parameter which decides the heat transfer performance of the nanofluids. Thermal conductivity is the materials own property which indicates the ability to conduct heat. Fourier's first law gives the heat flux as proportional to the temperature difference, surface area, and length of the sample.

used in transformer performs mainly two functions. (a) The oil transfers the heat by convection method from transformer core and winding to the cooling surface. (b) Oil maintains the insulation of windings and also extinguishes the fire hazard that may occur due to fault of the windings of the transformer. So transformer oil requires to have a good thermal conductivity to conduct the heat generated in the core and windings.

Here from the figure 6.2 we can see the temperature dependency of thermal conductivity increasing and decreaseing percentage of MoS₂/TO (Transformer Oil) and MoS₂/EG (Ethylene Glycol) at 0,0.0025,0.005,0.0075,0.01 weight percentages. This fig only shows the temperature dependency of thermal conductivity of TO and EG at room temperature and 40⁰C temperature. Now variation in temperature dependency of thermal conductivity can be seen by introducing some MoS₂ in TO and EG, which indicating the role of nanoparticles in thermal conductivity [26].For MoS₂/TO nanofluid At 40⁰C temperature Percentage of thermal conductivity increase 17.55 % when weight percentage is 0.005 gm. For MoS₂/EG nanofluid At 40⁰C temperature Percentage of thermal conductivity increase 25.53 % when weight percentage is 0.0075 gm. Percentage of thermal conductivity increase calculated by this following equation.....

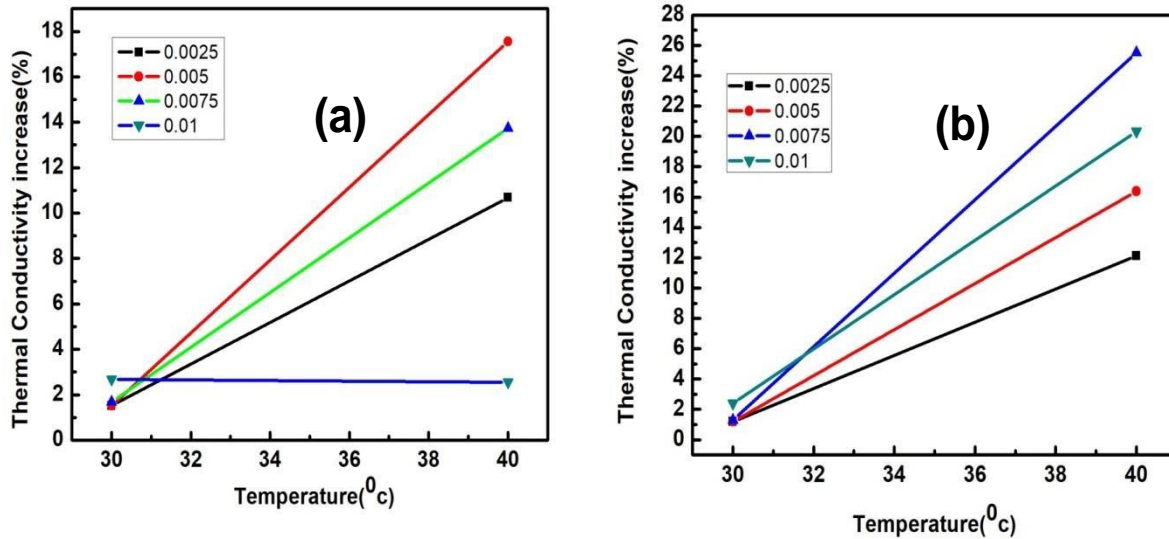


Fig.6.2 Percentage of Thermal conductivity enhancement plot (a)Experimental result In transformer oil (b) Experimental results in ethylene glycol

$$\text{Increase \% of thermal conductivity} = \frac{\lambda - \lambda_0}{\lambda_0} \times 100$$

λ_0 = Thermal conductivity of base oil.

λ = Thermal conductivity of nanofluid.

Table-2 thermal conductivity varies with weight percentage

Sample wt %	Thermal conductivity increase in Transformer oil(%)		Thermal conductivity increase in Ethylene Glycol(%)	
	At 30⁰c	At 40⁰c	At 30⁰c	At 40⁰c
	temp	temp	temp	temp
0.00	0	0	0	0
0.0025	1.52	10.68	1.19	12.10
0.005	1.52	17.55	1.19	16.38
0.0075	1.52	13.74	1.20	25.53
0.01	2.67	8.39	2.40	20.32

6.7 Conclusion:

In this experiment, the synthesized MoS₂ nanosheets used to prepare TO based nanofluids. The calculated breakdown voltage enhancement was around 5.32% in the weight percentage (wt%) 0.005%. It drops down to 1.6 % enhancement when the wt% reaches to 0.0075 due to self- agglomeration among the sheets which increases the charge movement rate leading to reduction of breakdown voltage. Moreover, the thermal conductivity value increases up to 17.55% at 40°C in the same Wt%. 0.005 due to high surface area of the filler. Besides, the efficiency of the sheets is further validated by performance in Ethylene Glycol (EG) which vividly used as coolant. In case of EG the observed enhancement was 25.53% at wt% 0.0075. The above indicated result proves the efficiency of the 2D morphology of layered transition metal dichalcogenide in multifunctional applications.

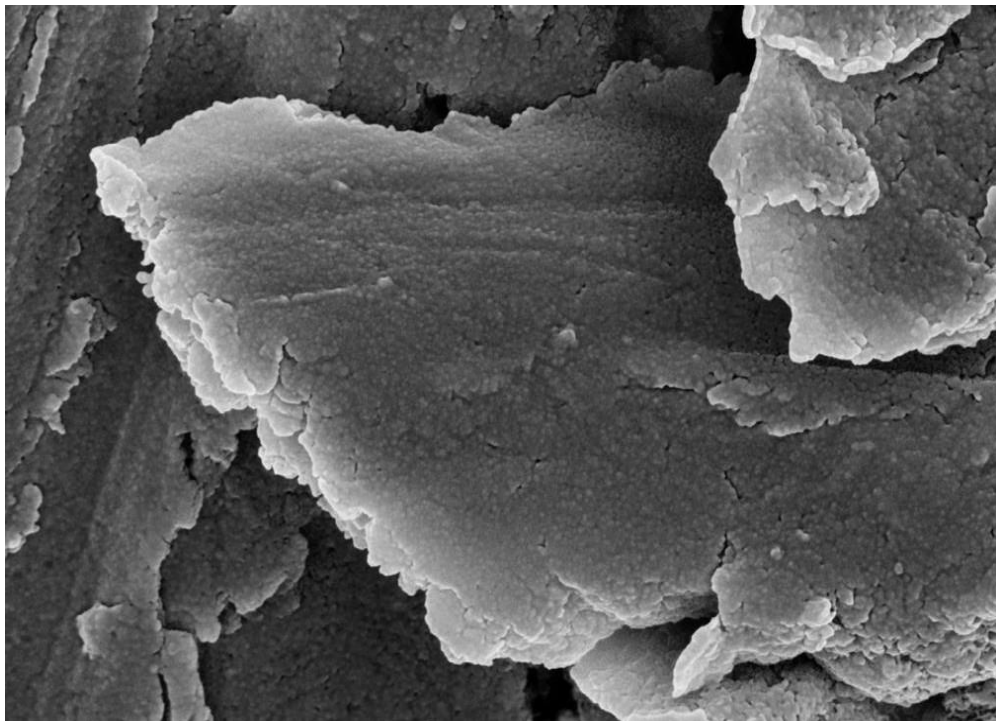
Reference

- [1] S. Sarkar, A. Jha, K. K. Chattopadhyay. Thionyl chloride assisted functionalization of amorphous carbon nanotubes: A better field emitter and stable nanofluid with better thermal conductivity. *Materials Research Bulletin*. 2015; 6; 61-8.
- [2] O. Williams, J. Hees, J. Ieker, W. J. Ger, L. Kirste, . . Nebel. Size-dependent reactivity of diamond nanoparticles. *ACS nano* 2010; 4(8): 4824-4830.
- [3] Y. Xuan, Q. Li, P. Tie, The effect of surfactants on heat transfer feature of nanofluids. *Experimental Thermal and Fluid Science*. 2013; 46: 259-262.
- [4] J. Taha-Tijerina, L. Peña-Parás, D. Maldonado-Cortés. 2D-Based Nanofluids: Materials Evaluation and Performance. *Two-dimensional Materials-Synthesis, Characterization and Potential Applications*. InTech. 2016.
- [5] J. Taha-Tijerina, T.N. Narayanan, G. Gao, M. Rohde, D.A. Tsentalovich, M. Pasquali, et al. Electrically insulating thermal nano-oils using 2D fillers. *Acs Nano* 2012; 6(2): 1214- 1220.
- [6] S. D. Costa, J. E. Weis, O. Frank, and M. Kalbac, "Effect of layer number and layer stacking registry on the formation and quantification of defects in graphene. *Carbon*. 2016; 98: 592-598.
- [7] N. Wang, S. Pandit, L. Ye, M. Edwards, V. Mokkalapati, M. Murugesan, et al. Efficient surface modification of carbon nanotubes for fabricating high performance CNT based hybrid nanostructures. *Carbon*. 2017; 111: 402-410.
- [8] Z. Sun, S. Pöller, X. Huang, D. Guschin, C. Taetz, P. Ebbinghaus, et al. High-yield exfoliation of graphite in acrylate polymers: A stable few-layer graphene nanofluid with enhanced thermal conductivity. *Carbon*. 2013; 64: 288-294.
- [9] A. Abdelmalik, J. Fothergill, S. Dodd. Electrical breakdown strength characteristics of palm kernel oil ester-based dielectric fluids. *Electrical Insulation and Dielectric Phenomena (CEIDP).2011 Annual Report Conference IEEE*. 2011; 183-186.
- [10] J. Miao, M. Dong, M. Ren, X. Wu, L. Shen, H. Wang. Effect of nanoparticle polarization on relative permittivity of transformer oil-based nanofluids. *Journal of Applied Physics*. 2013; 113(20): 204103.
- [11] B. Du, X. Li, J. Li. Thermal conductivity and dielectric characteristics of transformer oil filled with BN and Fe₃O₄ nanoparticles. *IEEE Transactions on Dielectrics and Electrical Insulation*. 2015; 22(5): 2530-2536.
- [12] R.A.R. Prasath, N.K. Roy, S.N. Mahato, P. Thomas. Mineral oil based high permittivity CaCu₃Ti₄O₁₂ (CCTO) nanofluids for power transformer application. *IEEE Transactions on Dielectrics and Electrical Insulation*. 2017; 24(4): 2344-2353.

- [13] S. Li, M. Karlsson, R. Liu, A. Ahniyaz, A. Fornara, E.J. Salazar-Sandoval. The effect of ceria nanoparticles on the breakdown strength of transformer oil. *Properties and Applications of Dielectric Materials (ICPADM).2015 IEEE 11th International Conference*. 2015; 289-292.
- [14] D. Martin, Z. Wang. Statistical analysis of the AC breakdown voltages of ester based transformer oils. *IEEE Transactions on Dielectrics and Electrical Insulation*. 2008; 15(4).
- [15] K. Koo, J. Higham. The effects of hydrostatic pressure, temperature, and voltage duration on the electric strengths of hydrocarbon liquids. *Journal of the Electrochemical Society* 1961; 108(6): 522-528.
- [16] A. Suleiman, N. Muhamad, N. Bashir, N. Murad, Y. Arief, B. Phung. Effect of moisture on breakdown voltage and structure of palm based insulation oils. *IEEE Transactions on Dielectrics and Electrical Insulation*. 2014; 21(5): 2119-2126.
- [17] D.H. Fontes, G. Ribatski, E.P. Bandarra Filho. Experimental evaluation of thermal conductivity, viscosity and breakdown voltage AC of nanofluids of carbon nanotubes and diamond in transformer oil. *Diamond and Related Materials*. 2015; 58: 115-121.
- [18] J. G. Hwang, M. Zahn, F. M. O'Sullivan, L. . Pettersson, O. Hjortstam, and R. Liu. Effects of nanoparticle charging on streamer development in transformer oil-based nanofluids. *Journal of applied physics*. 2010; 107: 014310.
- [19] P. Dhar, A. Katiyar, L. S. Maganti, A. Pattamatta, and S. K. Das. Superior dielectric breakdown strength of graphene and carbon nanotube infused nano-oils. *IEEE Transactions on Dielectrics and Electrical Insulation*. 2016; 23: 943-956.
- [20] K. Wu and L. Dissado. Model for electroluminescence in polymers during the early stage of electrical tree initiation. in *Solid Dielectrics, 2004. ICSD 2004. Proceedings of the 2004 IEEE International Conference*. 2004; 505-508.
- [21] C. Le Gressus and G. Blaise. Breakdown phenomena related to trapping/detrapping processes in wide band gap insulators. *IEEE Transactions on electrical insulation*. 1992; 27: 472-481.
- [22] W. Wiegand, C. Boggs, D. Kitchin. Effect of Carbon Black on Insulating Oils, *Industrial & Engineering Chemistry*. 1931; 23(3): 273-276.
- [23] H. Jin, T. Andritsch, I. A. Tsekmes, R. Kochetov, P. H. F. Morshuis, and J. J. Smit. Properties of Mineral Oil based Silica Nanofluids. *IEEE Transactions on Dielectrics and Electrical Insulation*. 2014; 21: 1100-1108.
- [24] M. A. Brown, A. Goel, and Z. Abbas. Effect of electrolyte concentration on the Stern layer thickness at a charged interface. *Angewandte Chemie International Edition*. 2016; 55: 3790-3794.

- [25] M.M. Bhunia, S. Das, P. Chattopadhyay, S. Das, K.K. Chattopadhyay. Enhancement of thermal conductivity of transformer oil by exfoliated white graphene nanosheets, in: Environment and Electrical Engineering (EEEIC), 2016 IEEE 16th International Conference, IEEE. 2016; 1-5.
- [26] M. Kole, T. Dey. Investigation of thermal conductivity, viscosity, and electrical conductivity of graphene based nanofluids. *Journal of Applied Physics*. 2013; 113(8): 084307.
- [27] M. Pompili and . Mazzetti, “Effect of Reduced Viscosity on the Electrical Characteristics of Transformer and Switchgear oils”, I International Symposium on Electrical Insulation, pp. 363-366, 2002.
- [28] F.M. Lark, “Dielectric Strength of Mineral Oils”, *Transactions of the American Institute of Electrical Engineers*, Vol. 54, pp. 50-55, 1935.
- [29] . Hoi, K. Yatsuzuka and K. sano, “Motion of a Conductive Particle in Viscous Fluid Simulating Liquified Plastic Waste”, I Conference on Industry Applications, vol. 3, pp. 1831-1836, 1999.
- [30] H. Kuirita, O. Usui, T. Hasegawa and H. Fujii, “Effect of Particles on Partial Discharge Inception in Oil Immersed Insulating System”, I International Conference on Dielectric Liquids, pp. 126-131, 1999.
- [31] R. Prasher, D. Song, J. Wang, and P. Phelan, Measurements of nanofluid viscosity and its implications for thermal applications, *Applied Physics Letters*, 2006, vol. 89, pp. 133108.
- [32] T. S. Sreeremya, A. Krishnan, L. N. Satapathy, and S. Ghosh, Facile synthetic strategy of oleophilic zirconia nanoparticles allows preparation of highly stable thermo-conductive coolant, *RSC Advances*, 2014, vol. 4, pp. 28020-28028.
- [33] C.H. Kim, I.E. Kwon, C.H. Park, Y.J. Hwang, H-S. Bae, B.Y. Yu, C.H. Pyun, G.Y. Hong, *J. Alloys Comp.* 311(2000) 33-39.
- [34] Xiaomei Yu, Boseong Kim, and Yu Kwon Kim, Highly Enhanced Photoactivity of Anatase TiO₂ Nanocrystals by Controlled Hydrogenation-Induced Surface Defect
<https://doi.org/10.1021/cs4005776>
-

Chapter-7: **Final Conclusion** **&** **Future aspects**



Conclusion & Future aspects:

In summary, MoS₂ nanosheet were synthesized by a hydrothermal method. Confirmation of the crystallinity and phase has been done using X-Ray diffraction and Raman Spectroscopy. Morphology and structure were analysed using FESEM & HRTEM revealing the thin Sheet morphology of MoS₂. The electrode material attains a specific capacitance of 265.67 F/g at 2 mV/s scan rate and 482.43 F/g at 1 A/g current density. The obtained high value was attributed to the sheet like morphology which enhance the interaction with the electrolyte ions. Especially for MoS₂ having superior electrochemical properties, makes them promising electrode materials for practical applications like symmetric/asymmetric supercapacitor devices. The performance of nanosheets was also investigated in TO based nanofluids which shows 5.32% enhancement in Break down voltage at very low wt% 0.005. Normally, the sheets consist of excess S²⁻ charge in the sharp edges of sheet which may attribute to the charge trapping/de trapping in the base fluid and delays the breakdown occurrence. Further, in coolant base fluid the thermal conductivity enhancement is 25.53% due to large surface area of the synthesized sheets. Those obtained results clearly indicates the scope of the synthesized MoS₂ nanosheets in the supercapacitors applications as well as in nanofluids.

In future, to increase the performance of the MoS₂, halide substitution (i.e. F, Cl) can be carried out which increases the conductivity of the pristine MoS₂ and can improve the performance in nanofluids applications. Additionally, carbon coating on the surface of MoS₂ can be beneficial approach for long term use as electrode material as the carbon coating prevents the rapid ion-accumulation on the MoS₂ surface thus preventing the degradation in long scan. Apart form nanofluids and supercapacitor applications, synthesized MoS₂ can be further used in solar cell as well as field emission applications.